TARGETING FGFR1 IN METASTATIC BREAST CANCER

by

Hang Lin

A Dissertation

Submitted to the Faculty of Purdue University

In Partial Fulfillment of the Requirements for the degree of

Doctor of Philosophy

Department of Medicinal Chemistry and Molecular Pharmacology

West Lafayette, Indiana

May 2022

THE PURDUE UNIVERSITY GRADUATE SCHOOL
STATEMENT OF COMMITTEE APPROVAL

Dr. Michael K. Wendt, Chair

Department of Medicinal Chemistry and Molecular Pharmacology

Dr. Zhong-Yin Zhang

Department of Medicinal Chemistry and Molecular Pharmacology

Dr. Emily Dykhuizen

Department of Medicinal Chemistry and Molecular Pharmacology

Dr. Luis Solorio

Weldon School of Biomedical Engineering

Approved by:

Dr. Zhong-Yin Zhang

Dedicated to my parents, for their constant love and support

ACKNOWLEDGMENTS

Foremost, I would like to express my deepest gratitude to my advisor, Dr. Michael K. Wendt, for his patience and encouraging manner in supervising me with immense knowledge during the last five years as a PhD student. His guidance helped me all the time of my graduate research, including editing of my thesis, journal papers and grant support of funding, and attending the conferences.

I would also like to thank Dr. Zhong-Yin Zhang, Dr. Emily Dhykuizen, and Dr. Luis Solorio, who as the members of my thesis committee, have given insightful comments and significant questions. I have learned much during the preliminary exam and committee meetings. Moreover, I would like to thank Dr. Danzhou Yang and her lab members for all the suggestions and supports for the collaboration.

I thank my fellow labmates and friends at Purdue University: Meng-Ju Wu, Remah Ali, Saeed S. Akhand, and Shiqi Tang for all the supports and assistance in my PhD life; I also would like to thank my current labmates. I really enjoy the time with you in Wendt lab.

Last but not the least, I would like to thank my grandparents and my parents, Eugene Lin and Tina Yang, my younger sister Kylie Lin, my boyfriend Winston Chen and my cute puppy Taffy, for encouraging and inspiring my interests and supporting me spiritually and financially during the youth of my life.

TABLE OF CONTENTS

LIST OF FIGURES

LIST OF ABBREVIATIONS

BC:	Breast cancer
MBC:	Metastatic breast cancer
FGF:	Fibroblast growth factor
FGFR:	Fibroblast growth factor receptor
EMT:	Epithelial mesenchymal transition
MET:	Mesenchymal epithelial transition
TKI:	Tyrosine kinase inhibitor
PROTAC:	Proteolysis targeting chimeras
G4:	G-quadruplex
Her2:	Human epidermal growth factor receptor 2
ER-α:	Estrogen receptor alpha
PR:	Progesterone receptor
PAM50:	Prediction analysis of microarray 50
TF:	Transcription factor
Ig:	Immunoglobulin
FDA:	Food and Drug Administration
TSS:	Transcription start site
Pol I:	RNA polymerase I
PDGFR-β:	Platelet-derived growth factor receptor beta
RTK:	Receptor tyrosine kinase
ICB:	Immune checkpoint blockade
CD:	Circular dichroism
FN:	Fibronectin
TCR:	T cell receptor

ABSTRACT

Metastasis remains the major cause of breast cancer (BC)-related death as developing an effective therapeutic strategy for the treatment of metastatic breast cancer (MBC) is a major clinical challenge. Fibroblast growth factor receptor (FGFR) is an emerging target for MBC as its expression is amplified in metastases and FGFR1 can be upregulated in MBC cells through the process of epithelial-mesenchymal transition (EMT). Inactivation of FGFR by tyrosine kinase inhibitors (TKIs) has achieved great success in various types of cancer. However, FGFR TKI resistance has become a concern in improving MBC patients' outcomes. Therefore, it is critical to develop advanced therapeutic interventions for improving patients' survival. In this dissertation work, we investigated novel therapeutic avenues to target FGFR1 in MBC.

To date, a variety of FGFR TKIs have been evaluated in clinical trials or clinically approved for cancer treatment. However, the efficacies of FGFR TKIs in MBC remain unclear. Herein, we evaluated the efficacies of several experimental and clinically approved FGFR TKIs using 3D culture and *in vivo* model systems. Our results demonstrated that FGFR-targeted kinase inhibitors are completely effective at blocking ligand-induced cell growth but fail to eliminate dormant BC cells. Moreover, animals succumb to disease progression while on therapy. Therefore, we explored broader approaches to inhibit FGFR1 expression in addition to blockade of its kinase activity.

Proteolysis targeting chimeras (PROTACs), heterobifunctional molecules inducing degradation of protein of interest via proteasome machinery, have emerged as a powerful tool for targeted cancer therapies. Together with our collaborators, we developed an array of FGFR PROTACs. Here, we showed that FGFR PROTACs inhibited metastatic and drug-resistant BC cell growth. Furthermore, our results identified potential FGFR PROTACs which induced FGFR1 degradation and blocked FGFR1 downstream signaling. Using 3D culture, FGFR PROTACs are shown to target MBC aggressiveness. Hence, our data suggested that PROTAC-mediated FGFR1 degradation is a promising strategy for MBC therapies.

In addition to the aforementioned approaches, G-quadruplex (G4) is revealed highlighting new possibilities for anticancer therapies. The Examination of the FGFR1 proximal promoter indicated sequences forming potential for G-quadruplex (G4) secondary structures. We found that G4 stabilizing agents are able to block constitutive and EMT-induced expression of FGFR1.

Additionally, G4 stabilizers could effectively block ectopic FGFR1 expression derived from CMV promoter driven constructs. Importantly, use of the clinical G4-targeting compound CX-5461 suppresses FGFR1 promoter activity, targets FGFR1 expression, and inhibited FGFR1 downstream signaling, resulting in eradication of dormant breast cancer cells. Finally, *in vivo* application of CX-5461 reduced FGFR1 expression, blocked pulmonary tumor formation, and prolonged animal survival. Overall, our findings indicated that targeting FGFR1 expression through G4 stabilization may be a potential therapeutic strategy for MBC.

FGFR1 has attracted great attention as a therapeutic target in a variety of tumors. In this dissertation work, we have identified the potential FGFR kinase-independent function which may contribute to TKI resistance. Moreover, we have revealed novel therapeutic options to overcome FGFR TKI resistance and achieve significant antitumor responses in MBC. In the future, our innovative therapeutic strategies can serve as an influential tool to investigate the FGFR1 regulation and kinase-independent function during metastasis.

CHAPTER 1. INTRODUCTION

Cancer is a group of diseases that develop from genetic transformation and involve abnormal cell growth. Due to the complexity of cancer, there are various therapy methods that have been established to cure cancer, such as chemotherapy, hormone therapy, targeted therapy, and immunotherapy. Given that cancer is a systemic disease caused by evolution, heterogeneity and environmental inputs, there are still some challenges to overcome for improving cancer therapies ("The global challenge of cancer," 2020).

1.1 Breast cancer

Breast cancer (BC) is the most common cancer diagnosed in women and the second leading cause of cancer death in women (Sung et al., 2021). BC is a heterogeneous disease which can be categorized via different pathological characteristics, such as tumor size, tumor grade, origins of cancer, and expression of hormone receptors which are human epidermal growth factor receptor 2 (Her2), estrogen receptor alpha (ER-α), and progesterone receptor (PR). In recent years, thousands of BC patients' samples have been extensively investigated through various molecular analyses. The goal is to improve the existing classifications by integrating broad molecular profiling and result in advanced identification of BC patients who can benefit from novel treatments (Russnes, Lingjærde, Børresen-Dale, & Caldas, 2017). For instance, prediction analysis of microarray 50 (PAM50), an approach to define intrinsic molecular subtypes by mRNA expression of 50 genes in BC patients, has been shown to advance the classification of BC patients and lead to a more explicit identification of future recurrence risk and improve treatment decisions (Ohnstad et al., 2017).

BC patients presenting with non-metastatic tumors at the time of diagnosis have 99% of 5-year relative survival rate; however, this percentage drops to less than 28% for patients presenting with disseminated tumors according to American Cancer Society statistics in 2021. Metastasis is a complicated process which includes five key steps: invasion, intravasation, circulation, extravasation, and colonization (Fig. 1.1) (Fares, Fares, Khachfe, Salhab, & Fares, 2020). Epithelial-mesenchymal transition (EMT) is the process that transforms epithelial cells to mesenchymal phenotypes. During this process, epithelial cells develop the ability to invade, resist stress and disseminate (Hanahan & Robert, 2011). Once the cells acquire the ability to penetrate

the neighboring tissue, the process of invasion is initiated while these motile cells pass across the basement membrane and extracellular matrix, proceeding to intravasation when these cells enter the vasculature (Bockhorn, Jain, & Munn, 2007). The metastatic cells then travel in the circulation system and invade the vascular basement membrane and extracellular matrix in the step of extravasation (Reymond, D'Água, & Ridley, 2013). Lastly, these cells will set in the new location, adapt to the environments, and colonize to form a secondary tumor. However, it is challenging for the circulating cells to overcome the harsh conditions once they extravasate at the target site (Valastyan & Robert, 2011).

The metastatic cells have different fates while they get to the secondary site. A group of cells will not survive, some of them are capable to proliferate, and another group of cells would stay dormant, which is an arrested phase in cancer progression (Gomis & Gawrzak, 2017). Efforts to treat metastatic cancer are impeded due to those metastatic cells often staying dormant for many years, or even decades. Furthermore, these dormant cells are thought to be responsible for late relapses (Redig & McAllister, 2013). They are hard to be targeted since they express weak antigens to escape the immune system, which is the main factor in tumor antiproliferation (Fares et al., 2020). Therefore, there is a critical need to develop effective approaches to eradicate dormant cancer cells.

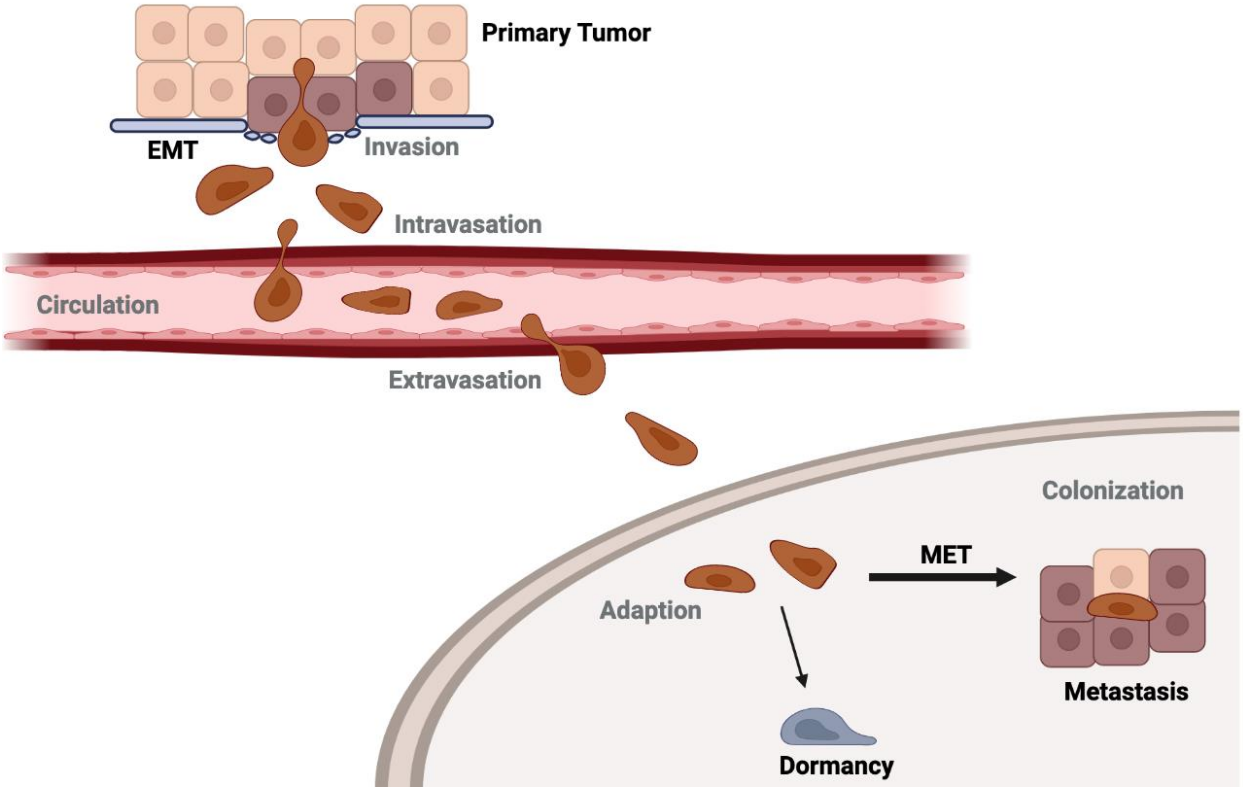

Figure 1.1 Overview of the metastatic cascade. The five key steps consist of invasion, intravasation, circulation, extravasation, and colonization. Epithelial cells acquire mesenchymal-like traits through activation of EMT. Once the cancer cells adapt to the metastatic sites, they will undergo mesenchymal-epithelial transition (MET) and proliferate to form secondary tumors.

1.2 Epithelial-mesenchymal transition (EMT)

EMT controls the reversible biochemical conversion that enables epithelial cells to gain mesenchymal phenotypes and achieve epithelial-mesenchymal plasticity, which is crucial for cancer metastasis (X. Ye & Weinberg, 2015). Recently, EMT has been regarded as a spectrum of transitional phases between epithelial and mesenchymal states, on the contrary to a process which involves a binary option between full-epithelial and full-mesenchymal states (M, Ruby, Rebecca, & Jean, 2016). The activation of EMT is governed by various growth factors and signaling pathways (Fig 1.2) (Redig & McAllister, 2013). Recent findings also indicated that EMT can be initiated via kinase inhibitor treatments and thus promote cancer cell persistence in the presence of these compounds (Sharma et al., 2010). In addition, EMT transcription factors (EMT-TFs) play key roles in regulating EMT. The core EMT-TFs are often co-expressed in varied combinations to coordinate complex EMT programs, and they involve different EMT-TF families, such as Snail, Zeb, and Twist, according to the distinct biological context (Stemmler, Eccles, Brabletz, & Brabletz, 2019). The signaling pathways could mediate the expression and stabilities of EMT-TFs. For instance, AKT-mediated nuclear factor-kB (NF-kB) activation stimulates Snail expression, and thus promotes EMT (Julien et al., 2007). Our lab also identified that phospho-Erk stabilizes the expression of Twist and supports a mesenchymal population (W. S. Brown, S. S. Akhand, & M. K. Wendt, 2016). Tumor cells shift between different intermediate states with different invasive, metastatic, and differentiation features (Pastushenko et al., 2018). It has been shown that tumor cells which present a mix of epithelial and mesenchymal phenotypes are more easily survive in circulation and colonize at the secondary site (Pastushenko et al., 2018).

In breast cancer, EMT has been identified to play a key role in tumor progression. Cells that have undergone EMT increased resistance to chemotherapy and targeted therapies (A. Singh & Settleman, 2010). Moreover, it has been shown that EMT-TFs regulate gene signatures and further promote distant metastasis (Heerboth et al., 2015). However, the mechanism of how EMT contributes to the recurrence of minimal residual disease is not fully clarified. Hence, there is a critical need to investigate the underlying mechanisms how EMT influences metastasis, resistance to drugs, and recurrence of dormant cells which would benefit cancer patients.

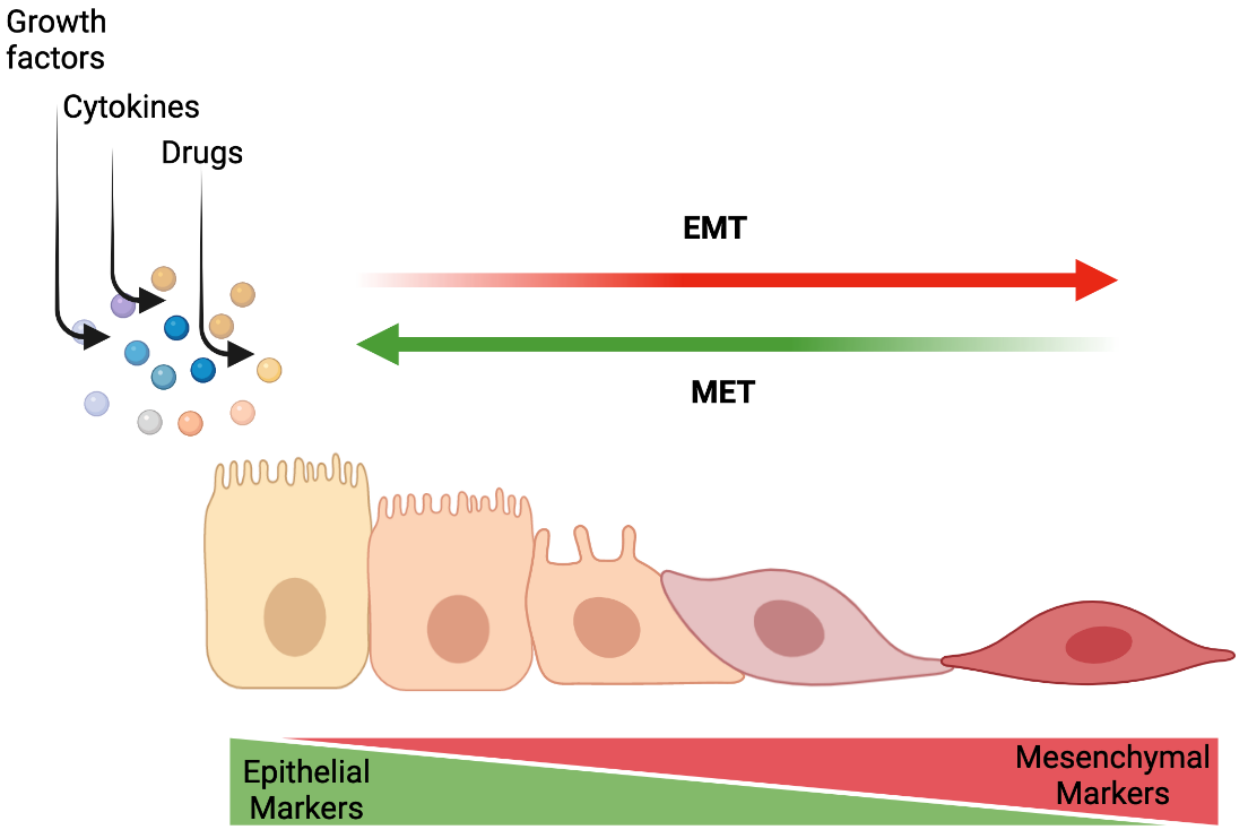

Figure 1.2 Epithelial-mesenchymal transition. Growth factors, cytokines, and some therapies can drive EMT process. The EMT process is modulated through activation of signaling pathways and subsequent mediation of EMT-TF that result in the expression change of various critical genes. During this process, epithelial cells lose the expression of epithelial markers, such as E-cadherin and cytokeratin, and gain the mesenchymal phenotypes, such as increased N-cadherin and vimentin. As a result of these significant gene changes, epithelial cells lose their cell-cell junctions, polarities and become more invasive and migratory phenotypes.

1.3 Fibroblast growth factor receptors (FGFRs)

Fibroblast growth factor receptors (FGFRs) are a family of receptor tyrosine kinases (RTKs) mainly expressed on the cell membrane and regulate developmental and adult cells (Dai, Zhou, Chen, Xu, & Chen, 2019). The FGFR family consists of four members: FGFR1 to FGFR4. FGFR1-4 are located on different chromosomes and encoded by separate genes. However, they show high homology, with their sequence similarity ranging from 56% to 71% (Itoh & Ornitz, 2004). Dysregulation of FGFRs has been identified in various cancers, such as urothelial carcinoma, cholangiocarcinoma, and breast cancer (Drago et al., 2019; Goyal et al., 2019; Loriot et al., 2019). FGFRs are stimulated by extracellular signals, fibroblast growth factors (FGFs). To date, 23 FGFs have been identified (Ornitz & Itoh, 2015). The third (III) extracellular immunoglobulin (III-Ig) domain of FGFR governs the specificity of FGFR binding to different FGFs. For instance, FGF2 has overly high specificity toward IIIc isoform, a splicing FGFR variant. Moreover, FGFR1-IIIc is highly upregulated during EMT in BC (Michael K. Wendt, Taylor, Schiemann, Sossey-Alaoui, & Schiemann, 2014). These results may imply that FGF2:FGFR1-IIIc signaling promotes tumor progression in BC. The binding of FGFs and FGFRs induces FGFRs dimerization; subsequently, activates the intracellular kinase domain, and drives downstream signaling pathways. The classical FGF/FGFR signaling pathways include Ras/Raf/mitogen-activated protein kinase (MAPK)/extracellular-signal-regulated-kinase (Erk), phosphatidylinositol-3kinase/protein kinase B (PI3K/AKT), PLCγ and signal transducer and activator of transcription (STAT) (Xie et al., 2020). Activated FGF/FGFR signaling pathways further promote proliferation, resistance to anticancer agents, and neoangiogenesis (Touat, Ileana, Postel-Vinay, André, & Soria, 2015).

1.4 FGFR1 regulation during EMT in breast cancer

Previous studies by our lab and others have identified that expression FGFR1 is significantly upregulated during EMT which is stimulated by transforming growth factor-beta (TGF-β), a major mediator of EMT (Brown, Tan, Smith, Gray, & Wendt, 2016; Michael K. Wendt et al., 2014). Silencing FGFR1 via shRNA dramatically reduced pulmonary tumor outgrowth in MBC animal models (Michael K. Wendt et al., 2014). Moreover, FGF: Erk signaling stabilizes EMT-TF Twist and thus maintains mesenchymal cell population and sustains drug-resistance

phenotype. (Wells S. Brown, Saeed Salehin Akhand, & Michael K. Wendt, 2016). These results suggest that FGFR1 plays a key role in EMT and MBC. However, the detailed mechanism how FGFR1 expression is increased during EMT remains unknown. Advances in the understanding of the FGFR1 regulation mechanism during metastasis will further facilitate the improvement of FGFR1 targeted therapies.

1.5 Targeting FGFR in cancer

Mutations and amplification in *FGFR* have been implicated in a variety of cancer types. Hence, wide-ranging studies have been performed on the development of FGFR tyrosine kinase inhibitors (TKIs) (Fig 1.3). To date, there are various FGFR TKIs which are evaluated in clinical trials or approved by Food and Drug Administration (FDA). In terms of reversible FGFR TKIs, erdafitnib, an ATP-competitive pan-FGFR inhibitor, is the first FDA FGFR TKI for the treatment of advanced or metastatic urothelial carcinoma (Markham, 2019). Another FDA-approved FGFR TKI is pemigatinib, a selective FGFR TKI against FGFR1-3, for treatment of locally advanced or metastatic cholangiocarcinoma (Hoy, 2020). Whereas covalent inhibitors confer improved binding kinetics and selectivity compared to noncovalent drugs, developing irreversible FGFR TKIs has drawn great academic and pharmaceutical attention recently. Therefore, a group of covalent TKIs have been developed and investigated. The first covalent FGFR TKI is FIIN1(W. Zhou et al., 2010). Together with our collaborator, we have developed FIIN4, a FIIN1 derivative compound, and demonstrated that FIIN4 dramatically suppressed MBC (W. S. Brown, L. Tan, et al., 2016). Moreover, futibatinib, a pan-FGFR covalent TKI, is under evaluation in phase II clinical trial. The FGFR1/futibatinib structure has been revealed by crystal structure (Kalyukina et al., 2019). Besides FGFR TKIs, antibody therapies are also being studied as an approach to target FGFR or FGF ligands. Different from FGFR TKIs, FGFR antibodies are designed to have a high affinity for specific FGFR isoforms or FGF ligands. Some of these antibody therapies have been evaluated in clinical trials, such as Bemarituzumab and R3Mab (MFGR1877S) (Odonnell et al., 2012; Wainberg et al., 2021). Lastly, another therapeutic avenue is the use of FGF traps which are a group of structurally heterogeneous molecules that can bind and sequester FGF2, and thus hinder their interaction with cognate receptors (Presta, Chiodelli, Giacomini, Rusnati, & Ronca, 2017). An example is FP-1039 that selectively binds and neutralizes various FGFs which have a high affinity toward FGFR1, preventing the interaction between FGF-FGFR1 and, consequently

suppressing FGFR1 downstream signaling (Harding et al., 2013). Now FP-1039 is investigated in phase I clinical trial.

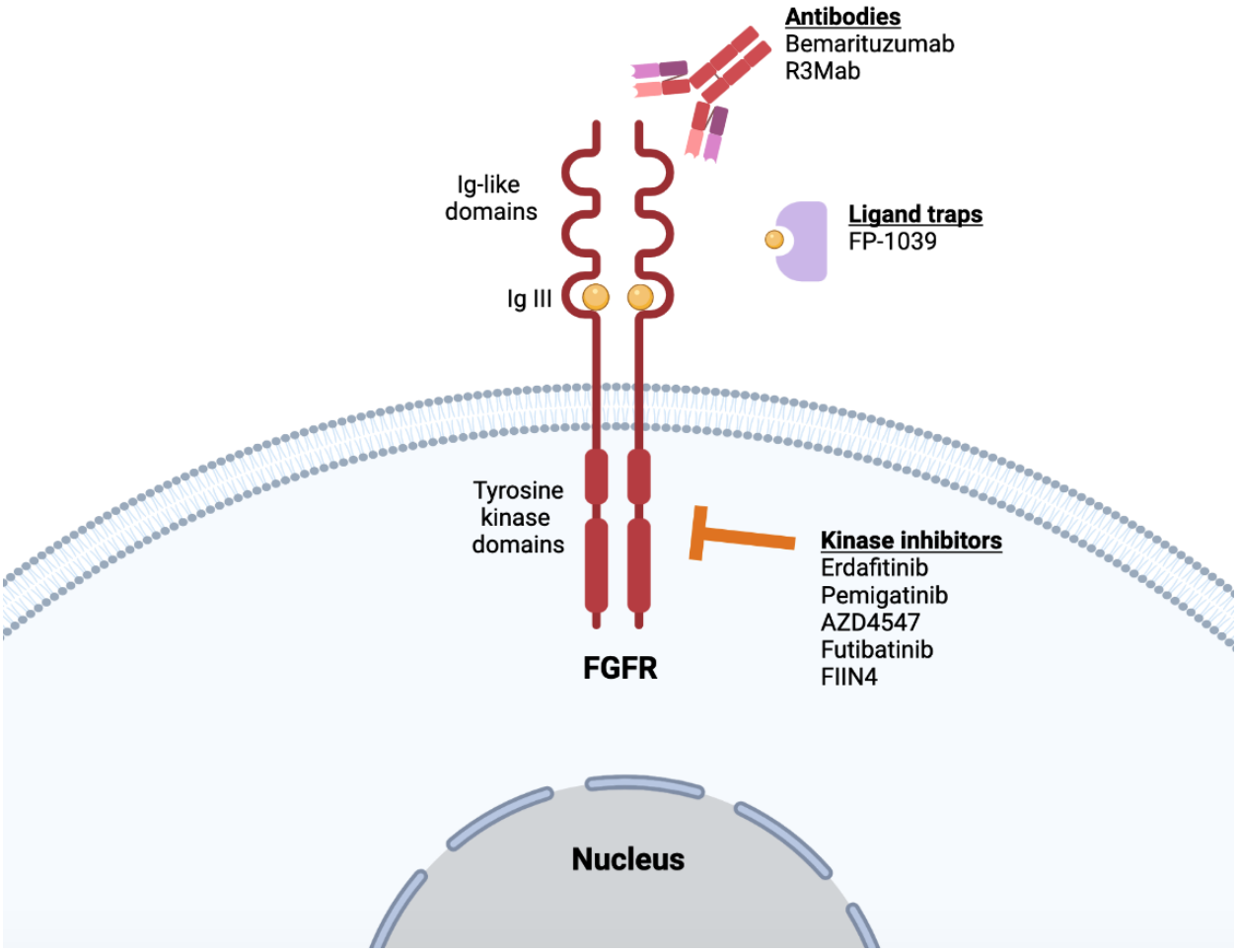

Figure 1.3 Different therapeutic approaches for targeting FGFRs. To date, there are various options to target FGFRs in cancer. FGFR TKIs including reversible and irreversible (covalent) inhibitors have been widely investigated. Erdafitinib and pemigatinib are two FDA-approved FGFR reversible TKIs. Moreover, covalent FGFR TKIs, futibatinib and FIIN4, have attracted attention due to their ability of more sustained inhibition. In terms of antibody therapies like bemarituzumab and R3Mb, target the extracellular domains of the kinase receptors. Moreover, a variety of IgG are also developed to trap ligands, prevent the ligands to interact with receptors, and thus suppress downstream signaling.

1.6 FGFR kinase-independent function

Our recent studies suggest that when cells undergo EMT FGFR1 exits the cell membrane and localizes throughout the cytoplasm and nucleus. Furthermore, co-immunoprecipitation experiments coupled with mass spectrometry indicate that FGFR1 interacts with several nuclear and mitochondrial proteins (W. S. Brown, L. Tan, et al., 2016). Consistent with these data, it is reported that FGFR1 nuclear translocation regulates MBC cell migration and invasion in a kinase-independent fashion (Chioni & Grose, 2012). Moreover, it has been demonstrated that nuclear FGFR1 leads to endocrine resistance through regulating gene transcription in ER^+ BC. Nuclear FGFR1 was not inhibited by FGFR TKIs (Servetto et al., 2021). In conclusion, these results support the development of treatment approaches to target FGFR kinase-independent function.

1.7 G-quadruplexes regulation in oncogene

DNA and RNA can fold into various alternative secondary structures. Recently, G-quadruplexes (G4s), the particular DNA and RNA secondary structures, were discussed to play key roles in cancer progression (Asamitsu, Obata, Yu, Bando, & Sugiyama, 2019). In a G4 structure, four guanines form a G-quartet via Hoogsteen hydrogen bonds. G4s are formed via stacks of G-quartets which are stabilized by central cations with the stabilizing preference for monovalent cations in the order $K^+ > Na^+ > Li^+$ (Fig 1.4) (Sen & Gilbert, 1990). According to biophysical studies on a variety of G4 structures, algorithms utilizing sequence motifs such as $G_{\geq 3}N_xG_{\geq 3}N_xG_{\geq 3}N_xG_{\geq 3}$ were developed to predict putative G4 structures (Todd, 2005). However, experimental data shows that G4 structures can form within sequences which have less than 3 guanines per repeat, such as the G4 in PDGFR-β promoter (Chen et al., 2012). To date, the identification of a G4 motif via computational analyses does not prove the formation of G4 structures at these regions *in vivo*, but simply shows the potential to form a G4. G4 formation still needs to be experimentally validated (Kosiol, Juranek, Brossart, Heine, & Paeschke, 2021).

G4 structures are not randomly presented throughout the genome but are enriched in certain regions, such as promoters, telomeres, and transcription factor binding sites (Chambers et al., 2015; Eddy & Maizels, 2008). Especially the promoter regions which are 1kb upstream of the transcription start site (TSS) of gene are highly enriched in G4 compared to the rest of the genome. It has been shown that more than 40% of human promoter regions contain at least one G4 (Huppert

& Balasubramanian, 2007). The localization of G4s at regions which modulate genome function has implied G4s in a range of biological roles (Fig 1.5). The finding that G4-rich telomeric sequences form G4 structures implicated a mechanistic connection with the telomerase-mediated extension of telomeres, leading to a search of G4 stabilizing ligands that might suppress the growth of cancer cells via hindering telomere maintenance (Fouquerel, Parikh, & Opresko, 2016; Sen & Gilbert, 1988). Furthermore, a variety of models have been proposed for the biological roles of G4s in DNA replication (Valton & Prioleau, 2016). G4 structures constitute an impediment to fork progression while helicases are disrupted (Lopes et al., 2011; Paeschke et al., 2013). According to the same mechanism, G4 stabilizers induced replication-dependent loss of epigenetic information indicating that G4s can hinder the replication machinery (Guilbaud et al., 2017). Additionally, treatment with G4 stabilizers caused decreased transcripts levels at genes containing G4 sequences in their respective promoters, such as the oncogene *MYC* (Siddiqui-Jain, Grand, Bearss, & Hurley, 2002) and *KRAS* (Cogoi & Xodo, 2006), validating the hypothesis that G4s can act an obstacle to the transcription machinery.

To date, small molecules which can stabilize G4s structures have been regarded as a promising therapeutic avenue for targeting oncogene (Kosiol et al., 2021). Around 1000 G4 stabilizers have been reported in the G-Quadruplex Ligands Database (Qian Li et al., 2013). TMPyP4, a cationic porphyrin, has been shown to inhibit telomerase (Han, Wheelhouse, & Hurley, 1999) and transcription of oncogene *MYC* via a mechanism to involve a G4 target in the nuclease hypersensitivity element (NHE) in the *MYC* promoter (Siddiqui-Jain et al., 2002). Its related compound, TMPyP2, has the similar structure with TMPyP4 but has a much lower affinity to G4s. Hence, the use of TMPyP4 and TMPyP2 could be an identification for G4 structures (Grand et al., 2002). Furthermore, quarfloxin (CX-3543) is the first G4 ligand to enter human clinical trials. It binds to DNA G4 and has been shown to selectively hinder the interaction of rDNA G4 with the nucleolin protein, thus suppressing RNA polymerase I (Pol I) transcription and causing apoptosis in cancer cells (Drygin et al., 2009). Another small molecule possessing a similar mechanism is CX-5461which suppresses Pol I-driven transcription DNA replication. Moreover, CX-5461 demonstrates *in vivo* anti-tumor activity against human solid tumors in murine xenograft models (Drygin et al., 2011). Further mechanism study clearly showed that CX-5461 acts as a G4 stabilizer, stalls replication forks, and induces DNA damage which needs the BRCA and NHEJ pathways for repair (Xu et al., 2017). Now this compound is in advanced phase I clinical trial in patients with

solid tumor and BRCA1/2, PALB2, or homologous recombination deficiency (HRD) tumor (NCT04890613).

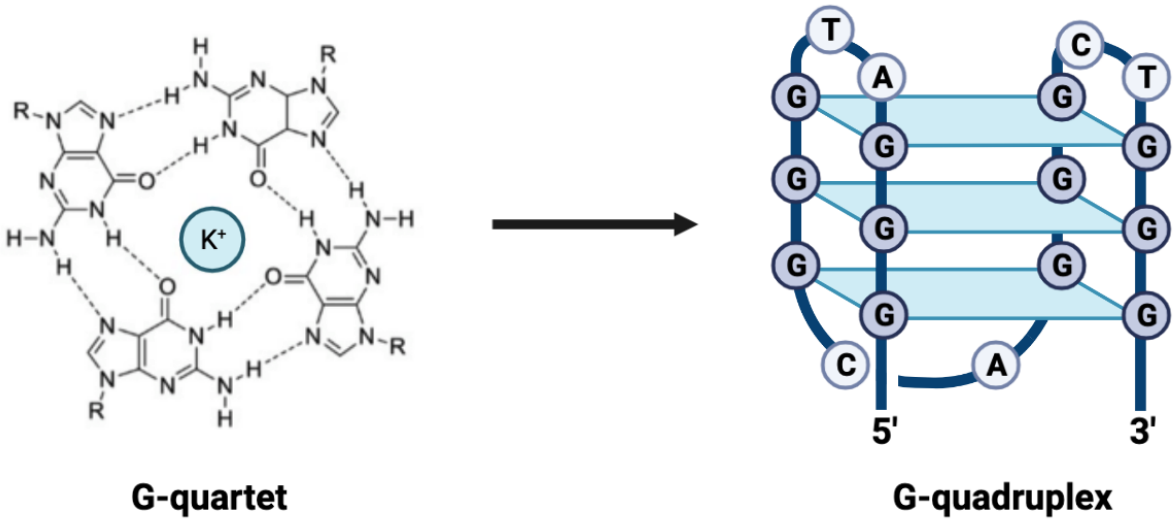

Figure 1.4 The structure of G-quadruplex. Four guanines form a G-quartet through Hoosteen hydrogen bonds. G-quartets stack to construct a G-quadruplex structure. Monovalent metal cations (Na^+ or K^+) locate in the central channel to stabilize the structure.

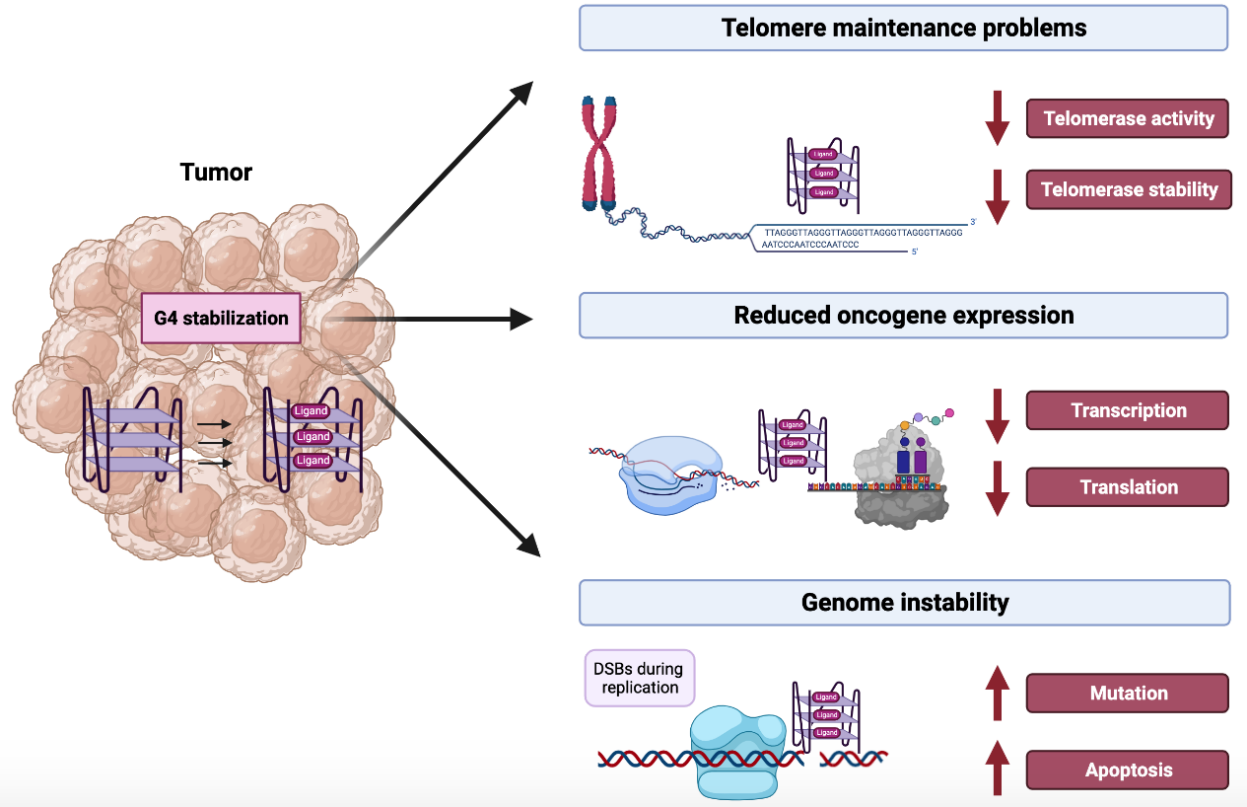

Figure 1.5 Overview of the influences of G4 ligand on cancer cells. Most G4 ligands lead to reduced cell viabilities. These growth changes are due to alteration of biological processes. Depending on the G4 stabilizers and cell type, G4 stabilization cause changes in telomere maintenance, gene expression of oncogene, and increased genome instability (Kosiol et al., 2021).

1.8 Proteolysis targeting chimeras (PROTACs)

Proteolysis targeting chimeras (PROTACs) have been shown that they effectively targeted Focal adhesion kinase (Fak) and receptor tyrosine kinases (RTKs) in BC (Burslem et al., 2018; Cromm, Samarasinghe, Hines, & Crews, 2018). PROTACs are molecules that consist of a ligand attracting E3 ligase, another ligand binding to the protein of interest, and a linker tethering these two ligands (Fig. 1.6) (Gu, Cui, Chen, Xiong, & Zhao, 2018). Therefore, PROTACs can recruit E3 ligase for targeted protein degradation via ubiquitin-proteasome system (Smith et al., 2019). Furthermore, PROTACs are comparable with kinase inhibitors which are able to adjust dosages and provide temporal control to attain the desired level of signal suppression, but they do not require any gene-editing of cells (Raina et al., 2016). There are four PROTACs have entered clinical trials. For instance, ARV-110 is an androgen receptor degrader and in phase II clinical trial for treatment of metastatic prostate cancer (NCT03888612). Furthermore, ARV-471 is a PROTAC targeting estrogen receptor and in phase II clinical trial for advanced or metastatic ER^+/HER^- breast cancer (NCT04072952).

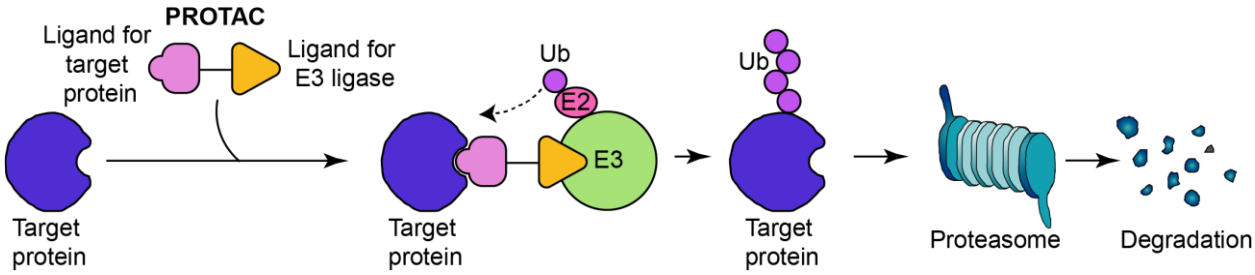

Figure 1.6 Proteolysis-targeting chimera (PROTAC) mechanism. PROTAC recruits E3 ligase to the target protein, induces ubiquitination and following degradation of the target protein by the proteasome.

CHAPTER 2. KINASE INHIBITION OF FGFR IN METASTATIC BREAST CANCER

The material in this chapter has been prepared for submission to a journal for publication as a manuscript.

2.1 Introduction

Metastatic breast cancer (MBC) is the most advanced stage of the disease leading to the majority of breast cancer-related death (Dillekås, Rogers, & Straume, 2019). However, the mechanisms that govern MBC progression remain unclear, hindering development of effective treatments. Receptor tyrosine kinases (RTKs) can become constitutively activated through mutation, and in this setting, targeting RTK signaling with active-site binding kinase inhibitors has become a mainstay of cancer therapy (Pottier et al., 2020). Wild type RTKs still play key roles in tumor progression and metastasis through the integration of signals from the tumor microenvironment, but therapeutic inhibition of ligand-dependent, wild type RTKs has not been well established yet (Huang & Fu, 2015; Park et al., 2016; Qian et al., 2015; Wise & Zolkiewska, 2017).

Thirteen percent of BC patients have genomic amplification of the RTK fibroblast growth factor receptor 1 (FGFR1*)*, and this event correlates with decreased patient survival (Razavi et al., 2018). Furthermore, MBC patients show higher FGFR1 amplification percentage (26%)(Q. Li et al., 2021). FGFR1 expression is also upregulated during epithelial-mesenchymal transition (EMT), which is a key driver of cancer metastasis (Wells S. Brown et al., 2016; Michael K. Wendt et al., 2014). Additionally, FGFR1 signaling can stabilize Twist, an EMT-related transcription factor (TF), and propagate drug-resistant, mesenchymal subpopulations (W. S. Brown, S. S. Akhand, et al., 2016; W. S. Brown, L. Tan, et al., 2016). Previous findings by our lab and others demonstrated that genetic depletion of FGFR1 or enzymatic inhibition of FGFR kinase activity hinders pulmonary metastasis (Liu et al., 2014; Wang et al., 2017; Michael K. Wendt et al., 2014).

Suppression of the FGF/FGFR signaling axis by tyrosine kinase inhibitor (TKI) is a successful therapeutic avenue in various cancer types (Dai et al., 2019). Erdafitinib is the first FDA-approved FGFR kinase inhibitor for treatment of metastatic urothelial carcinoma due to its potent antitumor activity in phase II clinical trials (Loriot et al., 2019). Afterward, Pemigatinib, a

selective FGFR1-3 kinase inhibitor, has been FDA authorized as the first targeted therapy for cholangiocarcinoma (Abou-Alfa et al., 2021). Besides these two FDA-approved FGFR kinase inhibitors, there are other FGFR kinase inhibitors evaluated in clinical trials. For instance, AZD4547 is in phase II clinical trial for treatment of refractory solid tumors, lymphomas, or multiple myeloma with FGFR1/2/3 alterations (Yue et al., 2021). Furthermore, there are some covalent FGFR kinase inhibitors have been developed, such as futibatinib and FIIN4. These covalent inhibitors exert their function via forming a covalent bond with a cysteine residue in the phosphate-binding loop (P-loop) of FGFR (Kalyukina et al., 2019; Tan et al., 2014). Futibatinib now is under phase II clinical trial for treatment of advanced or metastatic unresectable intrahepatic cholangiocarcinoma (Yue et al., 2021). Together with our collaborator, we developed FIIN4 which was synthesized with the same synthetic route as FIIN2 (Tan et al., 2014). Recently, we identified that the combination of FIIN4 and immune checkpoint blockade (ICB) significantly restricted pulmonary tumor growth and prolonged overall survival (Akhand et al., 2020). However, unlike urothelial and bile duct carcinomas where FGFRs become mutationally activated, FGFR1 expression changes in MBC remain ligand dependent. Indeed, recent clinical studies demonstrated minimal response to FGFR kinase inhibitors in BC patients (Chae et al., 2017).

In the current study, we investigated the efficacies of various FGFR TKIs in our MBC animal and 3D spheroid models. The use of *in vivo* and *in vitro* models indicated that FGFR kinase inhibition suppresses ligand-induced MBC spheroid growth, limits pulmonary tumor growth, and increases overall survival. However, treatment of FGFR kinase inhibitors fails to eliminate dormant MBC cells. These results revealed that FGFR1 kinase-independent function may contribute to this FGFR-TKI resistance. Hence, there is a critical need to explore other approaches which not only can target FGFR1 kinase activity but also FGFR1 kinase-independent function.

2.2 Methods and materials

2.2.1 Cell cultures and reagents

D2-HAN (D2.A1 and D2.OR) and 4T1 derivatives (4T1 and 4T07) were obtained from Fred Miller (Wayne State University, Detroit, MI) and cultured in DMEM containing 10% fetal bovine serum (FBS) and 1% Pen/Strep at 37 °C in a humidified atmosphere in a 5% CO2 incubator.

Bioluminescent D2-HAN derivates, 4T1 derivatives were engineered to stably express luciferase by transfection with pNifty-CMV-luciferase. All cell lines are regularly tested for mycoplasma contamination trough PCR. The development and synthesis of FIIN4, the covalent FGFR inhibitor, were described previously (Brown et al., 2016c). AZD4547 and futibatinib were purchased from MedKoo. Erdafitinib was purchased from AdooQ

2.2.2 Cell viability assays

Cancer cells were plated in the 96-white wall clear bottom plate (Corning) and with 3-days drug treatment. CellTiter-Glo assay (Promega) was used to measure cell viability according to the manufacture's protocol.

2.2.3 Immunoblot analyses

Immunoblot assays were performed on cell lysates prepared by lysing the samples with 3D RIPA lysis buffer containing 50 mM Tris, 150mM NaCl, 0.25% Sodium Deoxycholate, 1.0% NP40 and 0.1% SDS supplemented with protease inhibitor cocktails (Sigma), 10 mM Sodium Orthovanadate, 40 mM b-glycerolphosphate, and 20 mM Sodium Fluoride. Total Erk, phospho-Erk and FGFR1 antibodies were purchased from Cell Signaling Technology. Tubulin antibody was purchased from Developmental Studies Hybridoma Bank (DSHB). Immunoblot results were obtained from X-ray films and LI-COR systems (LI-XOR biosciences).

2.2.4 Animal studies and drug treatments

4T07 (5x105) were delivered into the lateral tail vein of 4-6-week-old BALB/c mice purchased from Jackson Laboratories. FGFR kinase inhibitors were administered through oral gavage with the indicated concentrations once a day. The gavage formulation of AZD4547 and Erdafitinib was in 0.5% hydroxypropyl methylcellulose. The gavage formulation of FIIN4 and futibatinib was in 0.5% Carboxymethylcellulose. Pulmonary tumor formation was monitored via bioluminescent imaging after intraperitoneal injection of luciferin through AMI HT (Spectral Instruments). The lungs were fixed overnight by 10% formaldehyde (Fisher) after sacrificing the mice and then stored in 80% ethanol. Paraffin sectioning at 5μm thickness and H&E staining were conducted by AML laboratories, Inc. (Jacksonville, FL). The images of lung sections were

obtained by Cytation 5 cell imaging multi-mode reader with Gen5 software (BioTek Instruments, Inc.). All in vivo assays were conducted under IACUC approval from Purdue University. No randomization or blinding was done.

2.2.5 Three-dimensional (3D) spheroid assay

Breast cancer cells (4x103) were plated in 96-well, ultra-low attachment and round bottom plates (Corning) in full growth media and cultured for a week. Afterwards, the spheroids were transferred with 50µl residual media to 96-well flat clear bottom white wall plates with a bed of 50µl growth factor reduced basement membrane hydrogel and 150µl fresh media containing 5% basement membrane hydrogel with FGF2 or FGFR inhibitors. The luminescence of spheroids is detected every three days and media is replenished every three days. The D2.OR spheroids are trypsinized and transferred to 100mm 2D culture dishes. Lastly, Colony formation assay is performed after culture for 14 days.

2.2.6 Statistical analysis

A two-tail student's t test was used for comparing the difference between two groups of data in in vitro assays. Error bars identify the standard error of the mean. For in vivo experiments, the measurements were compared with a Mann-Whitney non-parametric test. Survival analysis was performed via GraphPad Prism 9 software, and the distributions of survival were compared by a log-rank test.

2.3 Results

2.3.1 Pulse treatment of FGFR kinase inhibitor represses FGFR downstream signaling

FGFR kinase inhibitors have been proved as an effective therapy for various cancer types (Dai et al., 2019). However, the tumor reduction response of FGFR kinase inhibitors in patients harboring FGFR mutation is more effective than patients with FGFR amplification (Nogova et al., 2017). According to CBioPotal data, MBC patients show a higher FGFR1 amplification percentage (26%) than patients with primary breast tumors (13%) (Q. Li et al., 2021; Razavi et al., 2018). Herein, we investigated the efficacies of different FGFR kinase inhibitors in MBC cell line,

D2.A1, which has high endogenous FGFR1 expression and could be a great model for studying FGFR1 amplification (Michael K. Wendt et al., 2014). To compare the residence time of different FGFR inhibitors, we performed FGFR kinase inhibitor 1hr pulse treatment, washed off the inhibitors, serum-starved the cells, and then stimulated the cells with FGF2 which is the FGFR1 ligand (Belov & Mohammadi, 2013). The results indicated that the pulse treatments of covalent FGFR kinase inhibitors, FIIN4 and futibatinib, are not as effective as reversible inhibitors to suppress FGFR1 downstream signaling (Figure 2.1). That covalent inhibitors need more reaction time to covalently bind to the ATP binding pocket compared to reversible kinase inhibitors could be the reason, since it has been shown that irreversible inhibitors react with their targets in a time-dependent fashion (J. Singh, Petter, Baillie, & Whitty, 2011).

2.3.2 FGFR kinase inhibitors reduce tumor growth and prolong survival in breast cancer

We further tested the efficacies of FGFR kinase inhibitors in 4T07 tail-vein injection model which is established to form robust pulmonary tumors (Akhand et al., 2020). The high dose treatment (100mg/kg) everyday successfully reduces pulmonary tumor growth (Figure 2.2 A, 2.2 B, 2.2 C). However, the reversible FGFR kinase inhibitors, AZD4547 and erdafitinib, cause weight loss in mice (Figure 2.2 D). Therefore, we continued to conduct lower dose treatment (50mg/kg everyday) of the FDA-approved FGFR kinase inhibitor, erdafitinib, in the 4T07 tail vein inoculation model. Low dose treatment of erdafitinib reduces pulmonary growth (Figure 2.3 A, 2.3 B) and prolongs the survival rate (Figure 2.3 C). Moreover, we evaluated the efficacies of the covalent FGFR inhibitors, FIIN4, and futibatinib, in the highly metastatic 4T1 model of breast cancer (Figure 2.4 A). While these two covalent inhibitors led to a dramatic inhibition of 4T1 primary tumor growth, but complete tumor regression could not be achieved due to dose-limiting toxicity (Figure 2.4C, 2.4D).

2.3.3 FGFR kinase inhibition suppresses 3D spheroid growth but fails to eliminate dormant breast cancer cells

In addition to this *in vivo* approach, we also compared the efficacies of three small molecule inhibitors of FGFR kinase activity, AZD4547, FIIN4, and futibatinib, using the 4T07 cell model growing in a 3D spheroid assay. This 3D culture approach combines tumor spheroid formation in a non-adherent round bottom dish followed by placement of the spheroid onto a bed of matrix

(Figure 2.5A) (Ali, Brown, Purdy, Davisson, & Wendt, 2018). Our results demonstrated that 100 nM of these compounds are highly effective against 4T07 3D spheroid growth (Figure 2.5B, 2.5C). We also utilized the 3D spheroid approach to evaluate these compounds against the D2.A1 cells, another murine model of MBC. Unlike the 4T07 cells, addition of exogenous FGF2 significantly stimulated growth of D2.A1 spheroids, and the FGFR kinase inhibitors could effectively return spheroid growth back to control levels (Figure 2.5D, 2.5G). These data suggested complete and on-target inhibition of ligand-induced cell growth at these concentrations. To further illuminate potential the efficacies of FGFR kinase inhibitors, we tested the different FGFR inhibitors using the D2.OR cell model. The D2.OR cells stop growing when placed on soft matrices and thus serve as a model of tumor dormancy (Rao, Kondapaneni, & Narkhede, 2019). This approach demonstrated two findings. The first was that FGF2 stimulation was capable of breaking the D2.OR dormancy phenotype and inducing growth of the D2.OR spheroids (Figure 2.5F, 2.5G). As expected, addition FGFR kinase inhibitors prevented ligand-induced cell growth, but trypsinization of these spheroids and return to 2D culture resulted in similar colony formation, irrespective of FGFR inhibition (Figure 2.5I). These data indicated that targeted inhibition of FGFR kinase activity effectively blocks ligand-induced cell growth but fails to eliminate MBC cells, resulting in emergence of resistance.

2.4 Figures

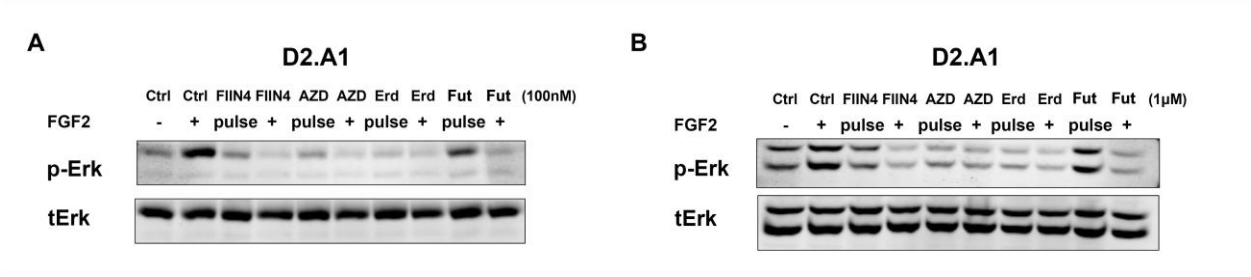

Figure 2.1 FGFR inhibitors suppress FGFR1 downstream signaling. A. The pulse treatment is that we serum starved the cells overnight, treated the cells with 100 nM indicted FGFR inhibitors, AZD4547 (AZD), erdafitinib (Erd), futibatinib (Fut) or FIIN4, for 1 hour, washed off the inhibitors, starved the cells overnight again and then stimulated the cells with 20 ng/ml FGF2 for 10 minutes. This assay can compare the residence time of different FGFR inhibitors. The FGFR inhibitors with FGF2 stimulation treatments which serve as positive controls. These cells were serum starved overnight, treated with 100 nM indicted FGFR inhibitors for an hour and stimulated with 20 ng/ml FGF2. Immunoblot analyses indicating phospho-Erk was induced with 20 ng/ml FGF2 stimulation for 10 minutes. The pulse treatment of 100 nM FGFR inhibitors hindered FGF2-induced phosphorylation of Erk. Covalent inhibitors may take longer to react with ATP pocket of FGFR kinase domain. B. Immunoblot analyses indicating that the pulse treatment of 1 μM FGFR inhibitors abrogated FGF2-induced phosphorylation of Erk.

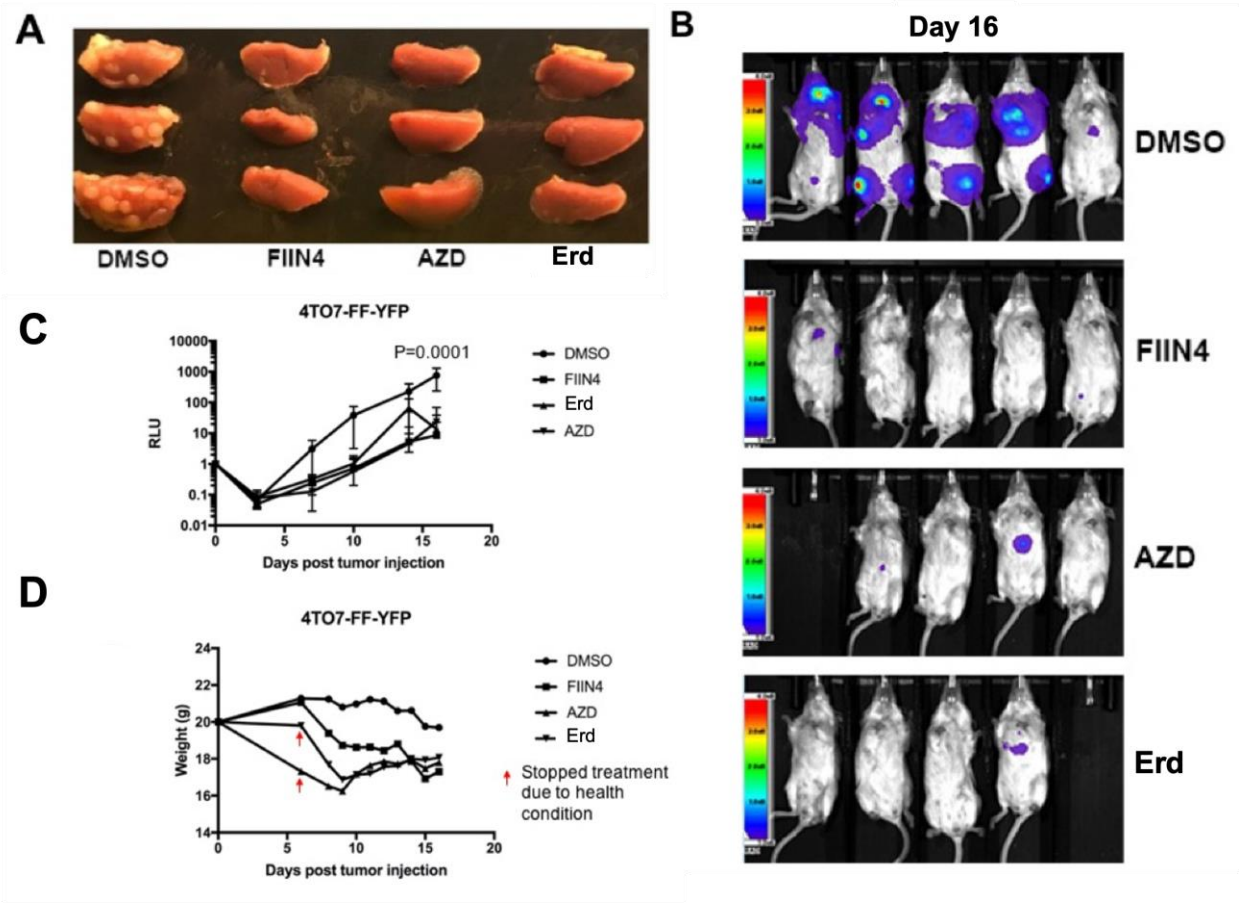

Figure 2.2 High dose treatment of FGFR kinase inhibitors suppresses pulmonary tumor growth but causes weight loss of mice. A. 4T07 cells (5x105) were delivered to the lungs of BALB/c mice (n=5 mice per group) via tail vein injections. Mice were treated with either vehicle (DMSO) or the indicated FGFR inhibitor, AZD4547 (AZD), Erdafitinib, or FIIN4, at 100 mg/kg; po, qd starting 2 days after tumor cell engraftment. Shown are fixed right pulmonary lobes of three representative mice from each group, 17 days after tumor cell engraftment. B. Bioluminescent images of mice at 16 days post engraftment. C. The mean (±SD) of bioluminescent values from each group taken at the indicated time points; two-way ANOVA test was performed resulting in the indicated P value, comparing FGFR inhibitor groups to control. D. The average weights (mean) of the individual groups were measured at the indicated time points.

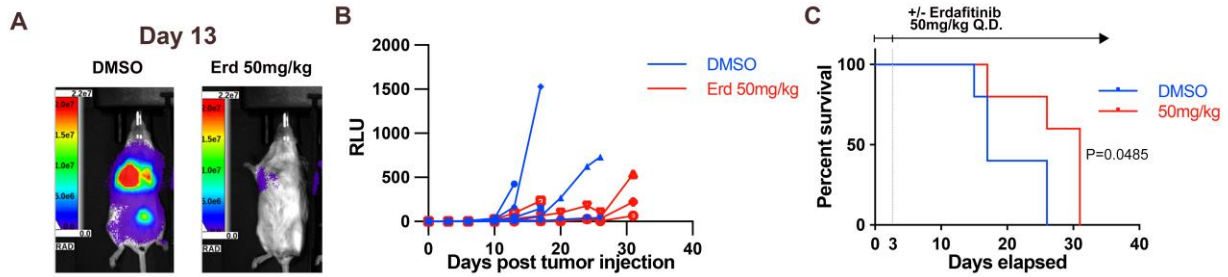

Figure 2.3 Low dose treatment of erdafitinib prolongs the survival rate of mice. A. Representative bioluminescence imaging (BLI) images of control and erdafitinib treated (50 mg/kg) mice bearing 4T07 pulmonary tumors monitored by bioluminescence 13 days following tail vein inoculation. B. Bioluminescent values from pulmonary regions of interest (ROI) were normalized to the values at the initial day of injection. Data are the individual values each mouse (n=5) per treatment group. C. Kaplan-Meier analyses of control and erdafitinib treated mice, bearing 4T07 pulmonary tumors, resulting in the indicated P value.

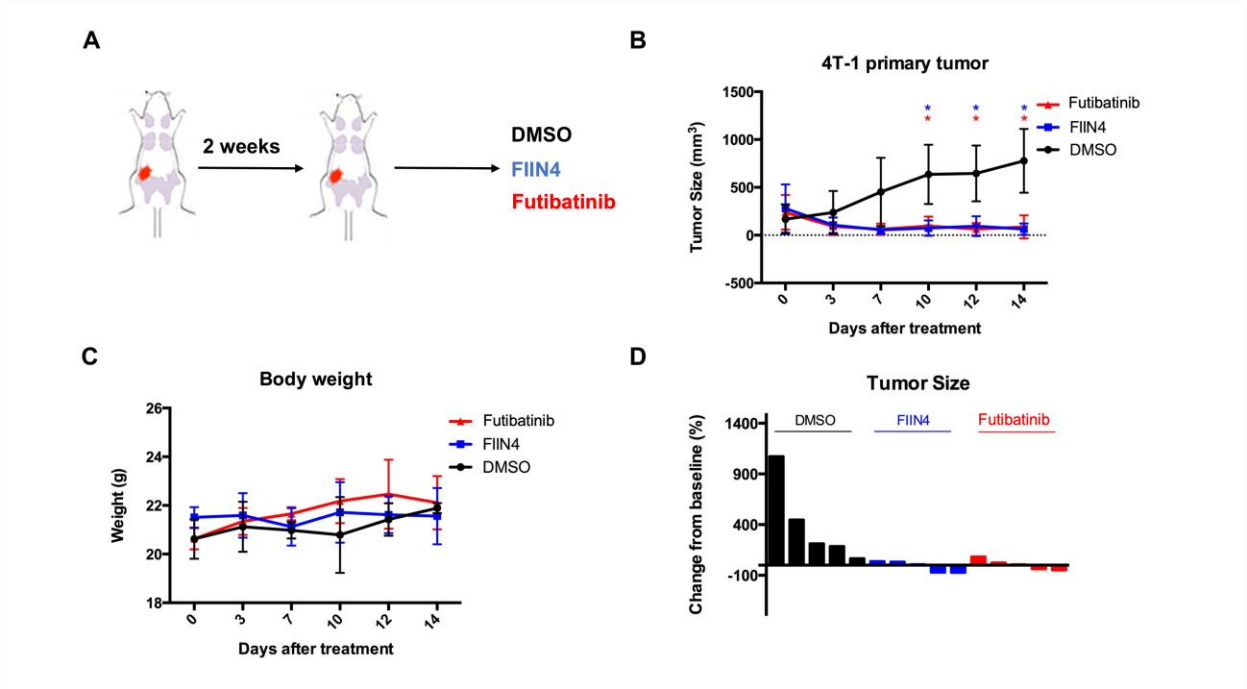

Figure 2.4 Covalent inhibition of FGFR kinase activity leads to tumor growth inhibition but not tumor regression. A. The 4T1 (50K cells) were engrafted onto the mammary fat pad via an intraductal injection in BALB/c mice (n=5 mice per group). Mice were treated with either vehicle (DMSO) or the indicated covalent FGFR inhibitors, FIIN4 and futibatinib, at 50 mg/kg every other day starting 3 weeks after tumor cell engraftment. B. Tumor sizes of 4T-1 primary tumor. Data are the mean ± s.e.m. (n=5) were *p<0.05. C. Mouse weight were taken at the indicated time points. Data are the mean of each group (n=5 mice), ± s.e.m. D. Waterfall plot of tumor size changes of each mouse. The results are the percentages of the ratios between tumor sizes between day 10 post treatment and day 3 post treatment.

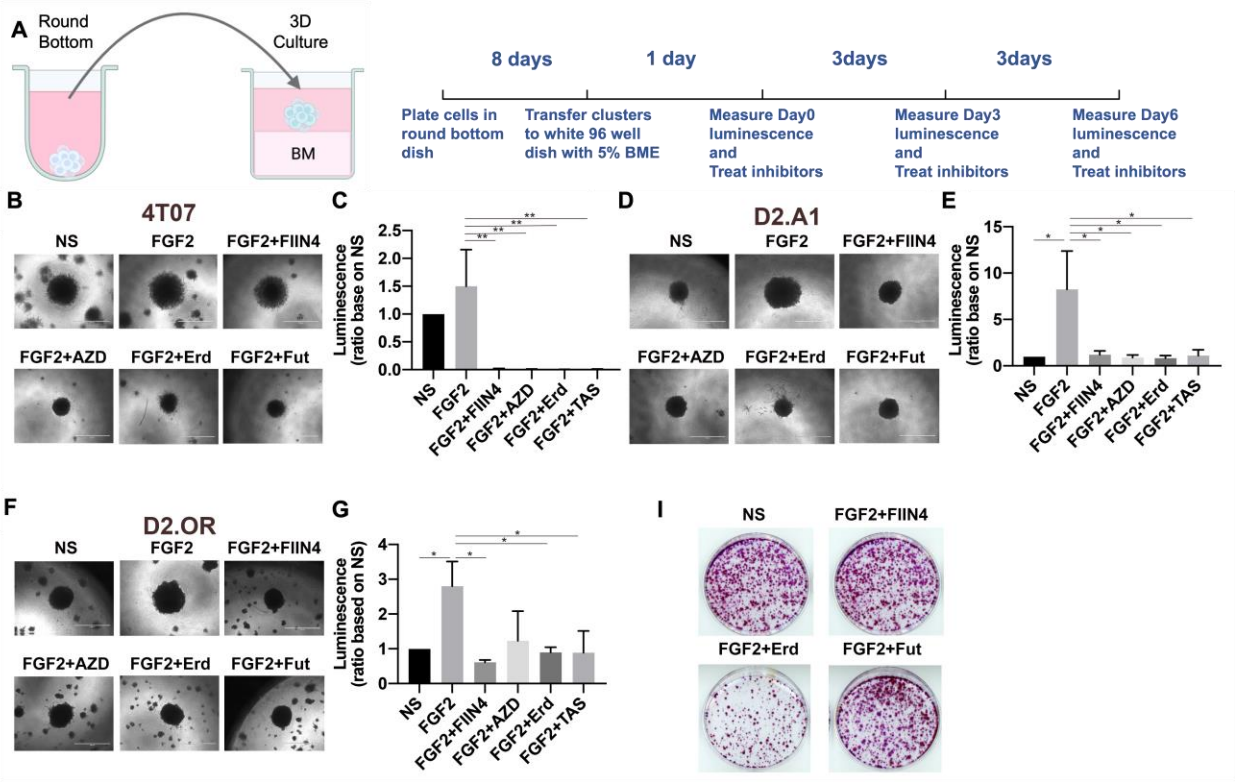

Figure 2.5 FGFR kinase inhibitors suppress 3D spheroid growth but fail to eradicate dormant breast cancer cells. A. 3D spheroid assay procedure. B-C. 4T07 spheroids expressing luciferase were formed in a non-adherent round bottom plate and then plated onto a bed of matrix in the presence or absence of FGF2 (20 ng/ml) or the indicated FGFR inhibitor (100 nM). Luminescence values at day 6 were normalized to the control conditions. Data are the mean ± s.e.m. (n=3) were *p<0.05. D-E. D2.A1 cells expressing luciferase were similarly used in spheroid culture, treated, and analyzed as in panels B and C. F-H. D2.OR cells expressing luciferase were similarly used in spheroid culture, treated, and analyzed as in panels B and C. I. Following 3D culture, spheroids were trypsinized and single cells were plated on tissue culture plastic. Colony formation was visualized by crystal violet staining 14 days later.

2.5 Conclusion

FGFR1 amplification occurs in 13% of patients with breast primary tumors and 26% in metastatic breast cancer patients (Q. Li et al., 2021; Razavi et al., 2018). The TCGA and METABRIC databases have confirmed that the FGFR1 amplification percentage is the highest among the FGFR family members (Santolla et al., 2019). FGFR1 amplification correlated with poor prognosis in ER-positive cancers and lead to the resistance of endocrine therapy in breast cancer (Elbauomy Elsheikh et al., 2007; Turner et al., 2010). Moreover, FGFR1 expression is an independent prognostic factor of triple-negative breast cancer (TNBC) (Cheng et al., 2015). In terms of metastatic breast cancer, FGFR1 is upregulated during EMT, the initiation process of metastasis (Michael K. Wendt et al., 2014). Though FGFR TKIs have been evaluated in breast cancer clinical trials, the efficacies of FGFR TKIs in MBC are not fully determined (Santolla & Maggiolini, 2020). Here, we presented data showing FGFR TKIs reduced pulmonary tumor growth, increased survival rate but not succeeded in eliminating dormant breast cancer cells.

In this study, we first determined if FGFR TKIs can suppress FGFR1 downstream signaling, phosphor-Erk. To compare the residence time of different FGFR TKIs, we performed the pulse treatment, which is to treat FGFR TKI for an hour, wash-off the inhibitors, stay overnight, stimulate the cells with FGF2 and investigate the phospho-Erk expression via immunoblot analyses. The data indicated that reversible TKIs, AZD4547 and erdafitinib, cause more sustained inhibition of phospho-Erk compared to covalent and irreversible TKIs which are FIIN4 and futibatinib. This result suggested that covalent FGFR TKIs need more reaction time to form covalent binding with the targets. We next sought to evaluate these FGFR TKIs in our MBC animal model. Using the 4T07 cancer model, we found that these FGFR TKIs greatly suppress pulmonary tumor growth but also cause weight loss in mice with high dose treatment (100mg/kg). Lower dose treatment (50mg/kg) reduces lung metastasis and prolongs survival. Besides the animal model, we also evaluated FGFR TKIs in 3D spheroid models. The 4T07 is a murine breast cancer line which grows robustly in 3D culture without the ligand, FGF2, stimulation. Our results demonstrated that 4T07 spheroids are sensitive to FGFR TKIs. We also evaluated these compounds in D2.A1 3D spheroid assay. Different from 4T07 cells, FGF2 stimulation dramatically induces D2.A1 spheroid growth, and FGFR TKIs potently reduce the growth of these spheroids treated with FGF2. The data indicated on-target suppression of ligand-induced growth with these FGFR TKIs treatments. To further identify the FGFR TKIs in breast cancer, we tested these compounds in the dormant

breast cancer cells 3D spheroid model, D2.OR cells. The dormancy of D2.OR cells, murine metastatic breast cancer cells, occurs in the 3D soft matrix environment (Rao et al., 2019). Here we showed that FGF2 is able to break the dormancy of D2.OR in 3D culture. Similar to the data in other cell lines, FGFR TKIs suppress the ligand-induced spheroid growth. However, FGFR TKIs fail to eradicate dormant breast cancer cells according to the colony formation assay. This finding suggested that FGFR kinase-independent function may contribute to the resistance.

Overall, in this chapter, we presented that FGFR TKIs inhibit pulmonary tumor growth and suppress BC spheroid viability. However, AZD4547 and erdafitinib lead to weight loss with high-dose treatment. In terms of targeting BC cells in the quiescent state, FGFR TKIs are unable to eliminate dormant breast cancer cells. These results revealed that there is still room for improvement in targeting FGFR1 in MBC.

CHAPTER 3. TARGETING FGFR1 EXPRESSION VIA PROTAC IN BREAST CANCER

The material in this chapter has been prepared for submission to a journal for publication as a manuscript.

3.1 Introduction

MBC is the most advanced stage of BC. However, our understanding of the molecular mechanisms which drive MBC remains incomplete. Therefore, this project will provide significant clinical benefits, since it will mechanistically illustrate FGFR1 as a valid target and its kinase-independent function toward MBC, giving a full rationale for degradation of FGFR1 to advance a novel strategy for impeding MBC.

FGFR1, a druggable tyrosine kinase target, has been shown amplified in invasive BC patients and as a prognostic factor for poor survival (Jang et al., 2012). In our preliminary studies, we have found that depletion FGFR1 dramatically inhibits tumor growth in lungs, a common metastatic site of BC (Michael K. Wendt et al., 2014). Therefore, optimizing FGFR inhibitors is crucial for therapeutic targeting of late-stage BC. However, in current clinical trials, FGFR inhibitors show limited responses in cancer patients (Chae et al., 2017). Since not only activation of FGFR1 signaling promotes invasion but also nuclear trafficking of the receptor is critical in BC and pancreatic cancer (Chioni & Grose, 2012; Coleman et al., 2014). Moreover, through overexpressing FGFR1 fused eGFP followed by immunoprecipitation, our lab has identified that FGFR1 disassociates from E-cadherin which is a cell membrane protein, translocate from cell membrane to nuclei and further interacts with nuclear proteins during EMT. Hence, there is a critical need to develop a therapy which can target FGFR1 kinase-independent function.

Proteolysis targeting chimeras (PROTACs) have emerged as a powerful tool for targeted degradation of endogenous proteins, focal adhesion kinase (Fak) and tyrosine kinases (RTKs) in BC (Burslem et al., 2018; Cromm et al., 2018). PROTACs are molecules that consist of a ligand of the protein of interest and covalently linked ligand of an E3 ligase (Gu et al., 2018). Upon binding to the protein of interest, PROTACs can recruit E3 ligase for targeted protein ubiquitination, which is subject to proteasome-mediated degradation (Smith et al., 2019). Moreover, PROTACs achieve targeted protein reduction like gene knockdown/out technologies

and also could mimic pharmacological protein inhibition (Raina et al., 2016). In consideration of reference indicated that FGFR1 kinase-independent function could be the cause of MBC, we propose that FGFR PROTACs would be a potent tool for targeting MBC.

3.2 Methods and materials

3.2.1 Cell cultures and reagents

D2-HAN (D2.A1 and D2.OR) and 4T07 were obtained from Fred Miller (Wayne State University, Detroit, MI) and cultured in DMEM containing 10% fetal bovine serum (FBS) and 1% Pen/Strep. Her2 transformed and Lapatinib resistant HMLE cell line (HME2-LapR) is developed as described (M. K. Wendt, Taylor, Schiemann, & Schiemann, 2011) and cultured in DMEM supplemented with 10% FBS, 1% Pen/Strep and 10μg/ml of insulin at 37 °C in a humidified atmosphere in a 5% CO_2 incubator.

3.2.2 Cell viability assays

Cancer cells were plated in the 96-white wall clear bottom plate (Corning) and with 3-days drug treatment. CellTiter-Glo assay (Promega) was used to measure cell viability according to the manufacture's protocol.

3.2.3 Immunoblot analyses

Immunoblot assays were performed on cell lysates prepared by lysing the samples with 3D RIPA lysis buffer containing 50 mM Tris, 150mM NaCl, 0.25% Sodium Deoxycholate, 1.0% NP40 and 0.1% SDS supplemented with protease inhibitor cocktails (Sigma), 10 mM Sodium Orthovanadate, 40 mM b-glycerolphosphate, and 20 mM Sodium Fluoride. Total Erk, phospho-Erk and FGFR1 antibodies were purchased from Cell Signaling Technology. Tubulin antibody was purchased from Developmental Studies Hybridoma Bank (DSHB). Immunoblot results were obtained from X-ray films and LI-COR systems (LI-XOR biosciences).

3.2.4 Three-dimensional (3D) spheroid assay

Breast cancer cells (4x103) were plated in 96-well, ultra-low attachment and round bottom plates (Corning) in full growth media and cultured for a week. Afterwards, the spheroids were transferred with 50µl residual media to 96-well flat clear bottom white wall plates with a bed of 50µl growth factor reduced basement membrane hydrogel and 150µl fresh media containing 5% basement membrane hydrogel with FGF2, FGFR TKIs or FGFR inhibitors. The luminescence of spheroids is detected every three days and media is replenished every three days.

3.2.5 Statistical analysis

A two-tail student's t test was used for comparing the difference between two groups of data in in vitro assays. Error bars identify the standard error of the mean.

3.3 Results

3.3.1 FGFR PROTACs inhibit cell viabilities, induce FGFR1 degradation and suppress FGFR1 downstream signaling in MBC cells

To identify whether these FGFR PROTACs are amenable to target MBC, together with our collaborator, we have developed an array of FGFR PROTACs consisting of two FGFR engaging kinase inhibitors, dovitinib (Dov) and erdatifinib (Erd), differentially linked to the E3 recruiting moieties for VHL or cereblon (Figure 3.1B). We conducted cell viabilities assays in 4T1 and 4TO7 metastatic murine mammary cancer cells (Figure 3.1A). Besides, we also examined the efficacies of the FGFR PROTACs in Her2 transformed HMLE Lapatinib resistant cells (HME2-LapR), proliferative cells with high expression of FGFR1 and highly mesenchymal morphology. The data indicated that FGFR PROTACs inhibit MBC cells dramatically (Figure 3.1A). To examine whether the FGFR PROTACs can target FGFR1 degradation in MBC cells, we treated the HME2-LapR cells, an MBC cell line, with 1 µM FGFR PROTACs for 24 hours. The data showed that there are at least three FGFR PROTACs induce PROTAC-mediated FGFR1 degradation significantly (Figure 3.1B). Moreover, we determined that FGFR PROTACs impede FGFR1 downstream phospho-Erk after FGF2 stimulation (Figure 3.1C). These results indicate that FGFR PROTAC is a potential approach to suppress MBC via blocking FGFR1 signaling.

3.3.2 FGFR PROTACs target MBC aggressiveness in 3D spheroid assay

To evaluate if FGFR PROTACs can abolish MBC aggressiveness, we tested MBC 3D spheroid with FGFR PROTACs. This 3D culture approach combines tumor spheroid formation in a non-adherent round bottom dish followed by placement on a bed of matrix. The goal of this approach is to recapitulate a group of aggressive cancer cells leaving primary mammary tumors which can survive in a non-adherent blood vessel environment. Furthermore, we monitor the growth of spheroids through detecting bioluminescence in luciferase labeled 4T07 and D2.A1 spheroids (Figure 3.2B, 3.2D). Our results showed that FGFR PROTACs are highly effective against 3D spheroid growth in 4T07 (Figure 3.2A, 3.2B). In metastatic D2.A1 cells, FGF2 stimulates D2.A1spheroids growth, and these FGFR PROTACs have potent anti-proliferative activities in the 3D culture (Figure 3.2C, 3.2D).

3.4 Figures

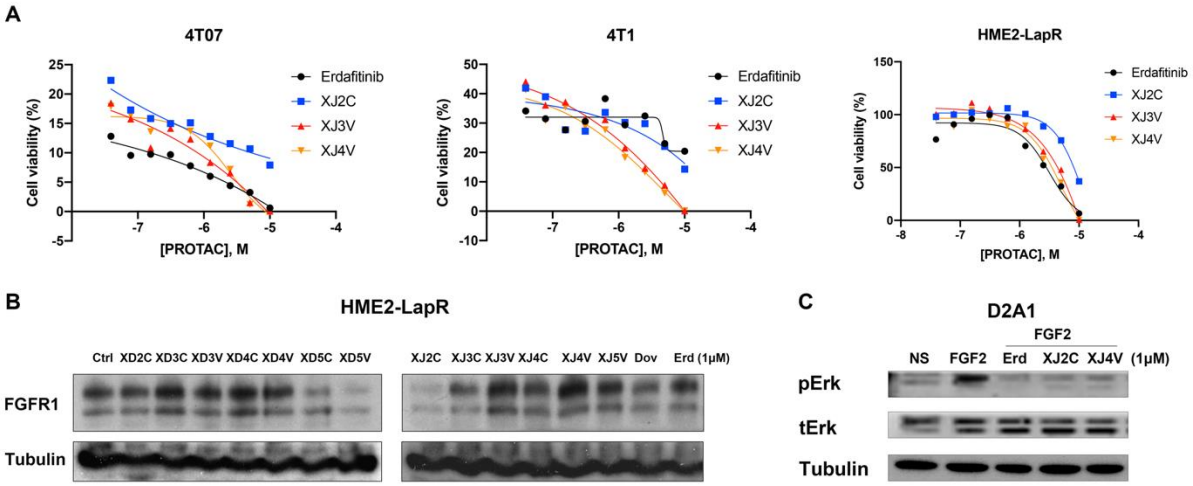

Figure 3.1 FGFR PROTACs suppress FGFR1 expression, downstream signaling and MBC cell viabilities. A. Cell viabilities of 4T07, 4T1 and HME2-LapR in the presence of FGFR PROTACs developed from Erdafitinib. The results show PROTACs inhibit the viabilities of metastatic breast cancer cells dramatically. B. Immunoblotting of PROTAC-mediated FGFR1 degradation in HME2-LapR cells. The data shows at least three PROTACs induce FGFR1 degradation significantly. C. FGFR PROTACs can inhibit phosphor-Erk which is FGFR1 downstream signaling.

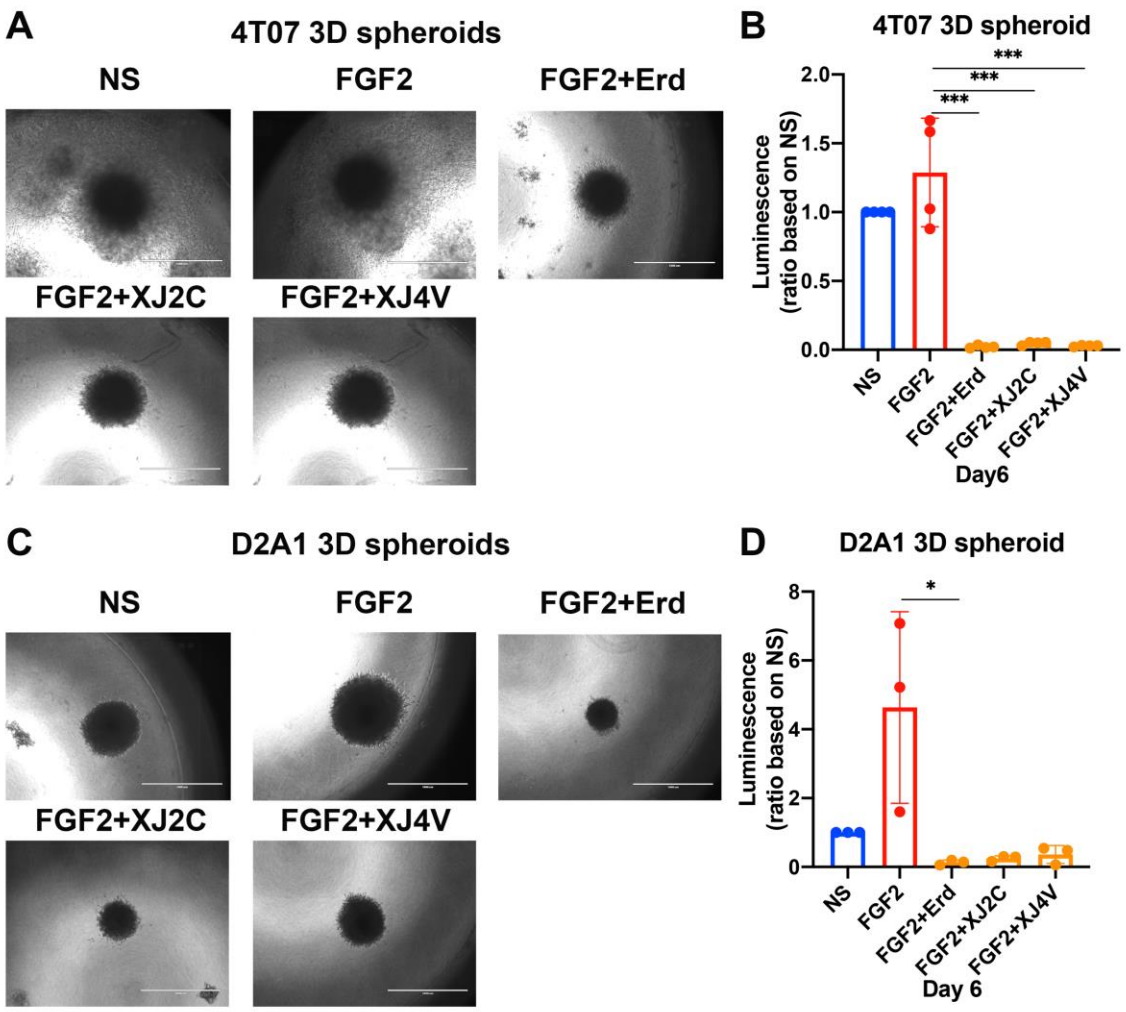

Figure 3.2 FGFR PROTACs suppress MBC 3D spheroid growth. A, C. 4T07 and D2A1 spheroids have been cultured on top of a bed of matrix in the presence or absence of FGF2, Erdafitinib (Erd) or FGFR PROTACs for 6 days. B. The luminescence of spheroid which as an indicator of spheroid growth shows Erdafitinib and FGFR PROTACs inhibit 4T07 spheroid growth. D. The luminescence result shows that FGF2 induces D2A1 spheroids growth. Erdafitinib and FGFR PROTACs abrogate the FGF2-induced growth in D2A1 spheroids.

3.5 Conclusion

According to clinical trials of FGFR TKIs, MBC patients showed limited response to these small molecules (Chae et al., 2017). Hence, overcoming the intrinsic resistance of MBC to FGFR TKIs is critical for developing effective therapies to cure MBC patients. Here, we identified potential FGFR PROTACs which are able to cause the reduction of FGFR1 protein expression. Furthermore, these FGFR PROTACs suppressed metastatic and drug-resistant BC cell growth and inhibited FGFR1 downstream signaling. Lastly, FGFR PROTACs significantly hindered 3D spheroid growth in BC cell lines which suggests FGFR PROTACs against aggressiveness in MBC. In short, our data indicated that PROTAC-mediated FGFR1 degradation is a promising strategy for MBC therapies.

CHAPTER 4. FGFR1 G-QUADRUPLEX REGULATION IN BREAST CANCER METASTASIS

The material in this chapter has been prepared for submission to a journal for publication as a manuscript.

4.1 Introduction

Metastasis is the cause of 90% breast-cancer-related deaths as an effective treatment for metastatic breast cancer (MBC) has not yet been developed. Hence, there is a critical need to identify potential therapeutic targets for abrogating MBC(Hanahan & Weinberg, 2000). Thirteen percent of breast cancer patients have genomic amplification of fibroblast growth factor receptor 1 (FGFR1*)* and this event correlates with poor prognosis (Razavi et al., 2018). We have found that silencing FGFR1 via genetic manipulation prevents metastasis (Michael K. Wendt et al., 2014). These findings suggest FGFR1 as a promising therapeutic target in MBC. Inhibition of FGFR kinase activity with FDA-approved small molecules also inhibits mouse models of metastasis, but animals succumb to disease progression while on therapy. Consistent with these findings, clinical trials of FGFR kinase inhibitors have failed to improve MBC patient outcomes (Chae et al., 2017).

Therefore, there remains a mechanistic gap in knowledge concerning the intrinsic resistance of MBC to FGFR kinase inhibitors. Our recent studies suggest that when cells undergo epithelial-mesenchymal transition (EMT) FGFR1 exits the cell membrane and localizes throughout the cytoplasm and nucleus. Furthermore, co-immunoprecipitation experiments coupled with mass spectrometry indicate that FGFR1 interacts with several nuclear and mitochondrial proteins. Consistent with these data, it is reported that FGFR1 nuclear translocation regulates MBC cell migration and invasion in a kinase-independent fashion (Chioni & Grose, 2012).

To explore different approaches to target FGFR1 kinase-independent function, we investigate the G-quadruplex (G4) regulation of FGFR1 expression in MBC. G4 structures are noncanonical, four-stranded secondary structures of DNA or RNA consisting of multiple planar platforms of four guanines linked together via Hoogsteen hydrogen bonding (Fay, Lyons, & Ivanov, 2017; Q. Li et al., 2009). Given their potential to broadly affect DNA damage repair and oncogenic gene expression, G4s have attracted significant attention as promising therapeutic targets in cancer (Amato et al., 2020; Asamitsu et al., 2019; Grand et al., 2005; Song, Perreault,

Topisirovic, & Richard, 2016; Y. Wang et al., 2019). For instance, G4s must be resolved for maximum transcription of known oncogenes, such as *MYC* and *PDGFR-β*. Therefore, numerous small molecule ligands have been developed that are capable of binding to and stabilizing G4 as means to diminish oncogene expression (Montoya et al., 2019; K.-B. Wang et al., 2019). Some of these molecules have progressed to clinical evaluation, representing a new category of epigenetic therapies (Grand et al., 2002; Muench et al., 2019). The putative proximal promoter of FGFR1 contains sequences with G4 forming potential. Therefore, we sought to address the hypothesis that G4 stabilization would diminish FGFR1 expression and thus act as an effective strategy for the treatment of MBC.

4.2 Methods and materials

4.2.1 Cell cultures and reagents

D2-HAN (D2.A1 and D2.OR) and 4T1 derivatives (4T1 and 4T07) were obtained from Fred Miller (Wayne State University, Detroit, MI) and cultured in DMEM containing 10% fetal bovine serum (FBS) and 1% Pen/Strep. Her2 transformed and Lapatinib resistant HMLE cell line (HME2-LapR) is developed as described (M. K. Wendt et al., 2011). NMuMG and HME2 series cell lines were cultured in DMEM supplemented with 10% FBS, 1% Pen/Strep and 10μg/ml of insulin. BT549 cells were cultured in RPMI-1460 supplemented with 10% FBS, 1% Pen/Strep and 10μg/ml of insulin. MCF10A cells were cultured in 1:1 DMEM (Corning Mediatech, Inc.) and F12 (Corning Mediatech, Inc.) supplemented with 29 mM Hepes (Amresco, LLC), 10 mM Sodium Bicarbonate (Macron), 5% Horse serum (Sigma), 10 μM/mL Insulin, 10ng/mL Epidermal Growth Factor (EGF) (Gold Biotechnology), 0.5 μg/mL hydrocortisone (Sigma), 100 ng/mL cholera toxin (Sigma), and 1% antibiotics (100 units/ml penicillin and 100 g/ml streptomycin; Corning Mediatech) at 37 °C in a humidified atmosphere in a 5% CO_2 incubator.

NMuMG and MCF10A cells expressing YFP and Twist were constructed through stable transduction using pBabe and pMSCV viral particles (W. S. Brown, L. Tan, et al., 2016). Plasmids encoding FGFR1-α-IIIc (NM_023110.2) or FGFR1-β-IIIc (NM_023105.2) were purchased from Cyagen Biosciences (Santa Clara, CA, USA). These constructs were used to construct lentiviral particles, and stable transduction was selected under Hygromycin selection. Bioluminescent D2-HAN derivates, 4T1 derivatives and HME2 series cell lines were engineered to stably express

luciferase by transfection with pNifty-CMV-luciferase. NMuMG cells were stimulated with TGF-β1 for seven days. All cell lines are regularly tested for mycoplasma contamination trough PCR.

4.2.2 Cell viability assays

Cancer cells were plated in the 96-white wall clear bottom plate (Corning) and with 3-days drug treatment. CellTiter-Glo assay (Promega) was used to measure cell viability according to the manufacture's protocol.

4.2.3 Immunoblot analyses

Immunoblot assays were performed on cell lysates prepared by lysing the samples with 3D RIPA lysis buffer containing 50 mM Tris, 150mM NaCl, 0.25% Sodium Deoxycholate, 1.0% NP40 and 0.1% SDS supplemented with protease inhibitor cocktails (Sigma), 10 mM Sodium Orthovanadate, 40 mM b-glycerolphosphate, and 20 mM Sodium Fluoride. Total Erk and p-Erk antibodies were purchased from Cell Signaling Technology. Tubulin antibody was purchased from Developmental Studies Hybridoma Bank (DSHB). Immunoblot results were obtained from X-ray films and LI-COR systems (LI-XOR biosciences).

4.2.4 Luciferase reporter assay

The proximal promoter regions of the human FGFR1 gene relative to the transcriptional initiation site were cloned from BT549 genomic DNA by PCR and inserted into pGL4.2 vector (Promega, Madison, MA). The primers used for cloning were listed in supplementary table 2. The predicted G-quadruplex formation sequences were analyzed via web-based server QGRS Mapper.(Marcel et al., 2011) MCF10A-YFP, MCF10A-Twist and HEK293T cells were transiently transfected overnight with LT1 liposomes (Mirus, Madison, WT) which contained 2.3μg/well of pGL4.2-hFGFR1 Promoter-Luciferase vector and 0.2μg/well pcDNA3.1 Hygro-Renilla vector. Afterward, the cells were treated with TMPyP2 or TMPyP4 for 24hr and 48hr and subsequently harvested and assayed for firefly and *Renilla* luciferase using the Dual-glo Assay System (Promega).

4.2.5 Quantitative PCR analyses

For real-time PCR analysis, metastatic breast cancer cells were treated with G-quadruplex stabilizers at indicated different time points. Afterward, total RNA was isolated using the E.Z.N.A HP total RNA kit (Omega). Total RNA was subsequently transcribed using the Verso cDNA synthesis kit (Thermo Scientific), and semiquantitative real-time PCR was performed via Maxima SYBR Green (Thermo Scientific) as described previously(Michael K. Wendt et al., 2014).

4.2.6 Three-dimensional (3D) spheroid assay

Breast cancer cells (4x103) were plated in 96-well, ultra-low attachment and round bottom plates (Corning) in full growth media and cultured for a week. Afterwards, the spheroids were transferred with 50 µl residual media to 96-well flat clear bottom white wall plates with a bed of 50 µl growth factor reduced basement membrane hydrogel and 150µl fresh media containing 5 % basement membrane hydrogel with FGF2, FGFR inhibitors or G4 stabilizers. The luminescence of spheroids is detected every three days and media is replenished every three days. The D2.OR spheroids are trypsinized and transferred to 100 mm 2D culture dishes. Lastly, Colony formation assay is performed after culture for 14 days.

4.2.7 Animal studies and drug treatments

D2.A1 ($1x10^6$) were delivered into the lateral tail vein of 4-6-week-old BALB/c mice purchased from Jackson Laboratories. FGFR kinase inhibitors were administered through oral gavage with the indicated concentrations once a day. CX-5461 was administered with 50 mM NaH_2PO_4 orally every 3 days. Pulmonary tumor formation was monitored via bioluminescent imaging after intraperitoneal injection of luciferin through AMI HT (Spectral Instruments). The lungs were fixed overnight by 10 % formaldehyde (Fisher) after sacrificing the mice and then stored in 80% ethanol. Paraffin sectioning at 5 µm thickness and H&E staining were conducted by AML laboratories, Inc. (Jacksonville, FL). The images of lung sections were obtained by Cytation 5 cell imaging multi-mode reader with Gen5 software (BioTek Instruments, Inc.). All in vivo assays were conducted under IACUC approval from Purdue University. No randomization or blinding was done.

4.2.8 Circular dichroism (CD) analyses

CD experiments were run on a Jasco J-1100 spectropolarimeter (JASCO Inc.) equipped with a temperature-controlled cell holder and stirrer. DNA (Sigma-Aldrich) was dissolved in 10 mM K+ buffer (2.5 mM potassium phosphate, 7.5 mM KCl, pH 7) to obtain 3-5 μM samples and annealed by heating to 95°C for 5 minutes, followed by overnight cooling at room temperature. CD spectra were measured at 25°C over a spectral range of 230 to 330 nm with a 10 mm quartz cuvette. The spectral parameters were: a scanning rate of 50 nm/min, 1.0 nm data pitch, 1.0 nm bandwidth, a response time of 1 second, and 5 accumulations. The spectra were blank corrected by subtracting a spectrum of the buffer. CD melting experiments were performed by monitoring the ellipticity at 264 nm over a temperature range of 20 - 95°C. The heating rate was 1°C/min and data points were recorded every 0.5°C, while the samples were continuously stirred at 200 rpm. Melting temperatures, Tm, were determined by locating the intersection of the median line between the upper and lower baseline and the melting curve. CD melting experiments were run in duplicate. Spectra and melting curves were also obtained in the presence of CX-5461(AdooQ BioScience) with a 5:1 ligand: DNA ratio.

4.2.9 Statistical analysis

A two-tail student's t test was used for comparing the difference between two groups of data in in vitro assays. Error bars identify the standard error of the mean. For in vivo experiments, the measurements were compared with a Mann-Whitney non-parametric test. Survival analysis was performed via GraphPad Prism 9 software, and the distributions of survival were compared by a log-rank test.

4.3 Results

4.3.1 Putative G4 sequences from FGFR1 promoter fold into G4 sequences in vitro

Given the limitations of targeting only FGFR kinase activity and the established kinase-independent functions of FGFR, we sought to evaluate alternate means of targeting this important oncogenic system (Huang & Fu, 2015; Meric et al., 2002; Templeton et al., 2014). The G4 forming sequences located near the transcription start site (TSS) have been shown to negatively regulate

oncogene expression (Kim, 2019). To investigate if the potential G4 forming sequences fold into G4 structures, we performed circular dichroism (CD) analysis to determine the folding topology and stabilities of these putative G4 forming sequences within 1.5 kb FGFR1 promoter region (Figure 4.1 A). CD plots showing that the formation of parallel G4 structures (a positive peak at 264nm and a negative peak at 245nm) was observed for four of five sequences tested and one sequence folded into a hybrid G4 structure (a negative peak at 245nm and a positive peak at 260nm with a shoulder at 295nm) (Figure 4.1 C) (Del Villar-Guerra, Trent, & Chaires, 2018). CD-melting experiments indicated that three of five putative sequences form stable G4 structures (Figure 4.1 B). S1 and S2 are the sequences at the same position but with different lengths (Figure 4.1 A.) The melting temperatures of S1 and S2 are similar which suggests that the shorter sequence S2 is able to form stable a G4 motif without the additional portion of S1 (Figure 4.1 B). S4 and S5 also are the sequences at the identical position with different lengths (Figure 4.1 A). However, the longer sequence S4 has a much higher melting temperature than S5, which means that the additional portion in S4 is essential to form a stable G4 structure (Figure 4.1 B). Hence, these results imply that S2 and S4 in FGFR1 proximal promoter region form G4 sequences.

4.3.2 G-quadruplex stabilization decreases constitutive and EMT-induced FGFR1 protein levels

To investigate the role of G4 in FGFR1 expression we implemented four stabilizers in two cell lines that express high levels of FGFR1, the murine metastatic D2.A1 cells and HME2-LapR cells, which are HER2 transformed cells that underwent EMT upon spontaneous acquisition of resistance to the HER2/EGFR inhibitor, lapatinib (W. S. Brown, S. S. Akhand, et al., 2016). This approach resulted in a marked downregulation of FGFR1 at the protein level after treatment with the G-quadruplex stabilizers, TMPyP4 and berberine (Figure 4.2 B, 4.2D). The Berberine concentration we treated here is much higher than the IC50 of Berberine in D2.A1 and HME2-LapR cells. On the other hand, the TMPyP4 concentration we applied in this experiment is the IC50 concentration (Figure 4.3C). However, we observed that TMPyP4 hindered the FGFR1 expression more dramatically than Berberine. In terms of mRNA levels, surprisingly, no significant differences in transcript levels were observed suggesting an alternate mechanism of protein diminution other than transcriptional inhibition (Figure 4.2A, 4.2C). To confirm this, we further investigated FGFR1 transcript and protein at various time points after TMPyP4 treatment.

The results indicated that TMPyP4 impeded FGFR1 protein levels within 3 hours in both D2.A1 and HME2-LapR cells with no effect on mRNA levels (Figure 4.2E-H). These findings suggested that TMPyP4 abrogates FGFR1 expression independent of transcriptional inhibition.

To further investigate a potential role of G-quadruplex in the regulation of FGFR1 expression we examined the putative proximal promoter region (-887/+60) which includes the possible G4 forming sequence S4 (Figure 4.1; Figure 4.4A). To define transcriptional regulatory elements of this putative promoter we cloned this sequence upstream of luciferase. We and others have identified that endogenous FGFR1 expression is dramatically enhanced during EMT (W. S. Brown, L. Tan, et al., 2016; Razavi et al., 2018; Michael K. Wendt et al., 2014). Therefore, we overexpressed Twist, a master regulator of EMT, in MCF-10A human mammary epithelial cells (W. S. Brown, L. Tan, et al., 2016). Consistent with a robust regulation of the EMT markers E-cadherin, N-cadherin and endogenous FGFR1, constitutive expression of Twist resulted in activation of the FGFR1 proximal promoter sequence as detected by luciferase activity (Figure 4.4B, 4.4C). Importantly, addition of TMPyP4 had no effect on Twist-induced FGFR1 promoter activity even after 48 hours of treatment (Figure 4.4B). To verify that TMPyP4 regulates endogenous FGFR1 induced by Twist expression, we performed quantitative PCR (qPCR) and western blot. In MCF10A-Twist cells, FGFR1 protein, but not mRNA, expression was again quickly diminished by TMPyP4 reaching maximal loss at 12 hours after addition of the compound (Figure 4.4D, 4.4E).

We also induced endogenous FGFR1 expression in normal murine mammary gland (NMuMG) gland cells by directed overexpression of Twist (Figure 4.4F) (W. S. Brown, L. Tan, et al., 2016). In these studies, we also utilized TMPyP2, a compound with a similar structure as TMPyP4 that fails to bind G4 (Ruggiero & Richter, 2018). Again, Twist-driven FGFR1 protein expression was impeded by TMPyP4, but not TMPyP2, after 3 hours of treatment (Figure 4.4H). To further understand the role of TMPyP4 in EMT-induced FGFR1 expression, we investigated the influence of TMPyP4 on TGFβ-induced FGFR1 upregulation. Stimulation of NMuMG cells with TGFβ for 7 days causes dramatic induction of EMT that includes pronounced upregulation of FGFR1 (Figure 4.4I, 4.4K) (Michael K. Wendt, Allington, & Schiemann, 2009). Addition of TMPyP4 reduced FGFR1 protein expression after 3 hours but again had minimal effects on mRNA levels. Addition of TMPyP2 did diminish FGFR1 levels but to a much lesser extend as compared

to TMPyP4 (Figure 4.4K). Overall, these data suggest that abrogation of FGFR1 expression caused by TMPyP4 is not due to impeded transcription.

4.3.3 TMPyP4 impedes ectopic FGFR1 expression

In addition to formation of DNA G4 in promoters, RNA can also form G4 in the open reading frame (ORF) causing altered splicing and inhibition of translation, leading to suppression of protein expression (Endoh, Kawasaki, & Sugimoto, 2013). Given that our results indicated that TMPyP4 causes FGFR1 protein loss with no effect on FGFR1 transcript levels, we further investigated if TMPyP4 targets RNA G-quadruplexes forming in the FGFR1 ORF. To do this we assessed HME2 cells constructed to constitutively express the full length (α) and truncated (β) isoforms of FGFR1 driven by a CMV promoter (Zhao, Zhuo, Zheng, Su, & Meric-Bernstam, 2019). Furthermore, using QGRS mapper we identified 17 and 20 possible G-quadruplex forming sequences in FGFR1α and β isoforms respectively (Figure 4.5A, 4.5B). Our results revealed that TMPyP4, but not TMPyP2, diminished protein levels of FGFR1α and β isoforms, without affecting transcript levels (Figure 4.6A-D). Here, we also found that TMPyP4 didn't affect the expression of HER2 and EGFR two other highly expressed RTKs in the HME2 cells. We further investigated the influence of TMPyP4 on ectopic expression of FGFR1 when fused to GFP. Again, TMPyP4, but not TMPyP2, diminished FGFR1-GFP protein expression, while having no effect on expression of GFP alone (Figure 4.5E-H). Taken together, these results suggest that stabilization of RNA G4 in the ORF of FGFR1 is capable of blocking expression of the protein.

4.3.4 CX-5461 reduces FGFR1 proximal promoter activity

Although the similar structures but differential ability of TMPyP4 and TMPyP2 to bind and stabilize G4 make them excellent tool compounds for determining the role of G4 in regulating gene expression, TMPyP4 doesn't regulate FGFR1 expression via transcriptional events. Furthermore, it has been shown that TMPyP4 is not ideal for animal studies (Fujiwara, Mazzola, Cai, Wang, & Cave, 2015). Hence, we next sought to expand our observations to the clinically used G4 stabilizers, CX-5461 (Onel, Lin, & Yang, 2014; Xu et al., 2017). To examine the regulatory G4 in FGFR1 proximal promoter region, a series of truncated FGFR1 promoter sequences containing possible G4 sequences S2 and S4 identified previously were cloned to

luciferase reporter vector and transfected into HEK293T cells (Figure 4.1 and Figure 4.7 A). The result indicates that these truncated FGFR1 promoter regions were activated compared to empty vector (Figure 4.7 B). The reporter construct (-1500/+60) with both S2 and S4 shows lower promoter activity which implies that S2 might form G4 structure and lead to suppression of promoter activity (Figure 4.7 B). According to the evaluation of different truncated FGFR1 promoter activities with CX-5461 treatment, CX-5461 reduces all truncated FGFR1 proximal promoter regions with S4 (-1231/+60, -887/+60 and -1500/+60). Interestingly, the reporter including S2 and S4 (-1500/+60) shows slightly lower promoter activity (Figure 4.7 C). This finding suggests that CX-5461 potentially stabilizes both S2 and S4 G4 forming sequences and hinders FGFR1 transcription. According to CD melting curve of S2 and S4 in the presence or absence of CX-5461, CX-5461 shows strong stabilization of both S2 and S4 (Figure 4.8 A, 4.8B).

4.3.5 G-quadruplex stabilization can block FGF-induced growth and eliminate dormant cells

After we identified that CX-5461 suppresses FGFR1 promoter activity, we next investigated if CX-5461 and its related compound, Quarfloxin, regulate FGFR1 expression (Onel et al., 2014; Xu et al., 2017). TMPyP4, quarfloxin, and CX-4561 are all capable of reducing FGFR1 protein expression in the BT549 cells, a human triple-negative breast cancer (TNBC) cell line (Figure 4.9 A-C). Similar to what is observed using FGFR-targeted kinase inhibitors pretreatment of cells with G4 stabilizers also demonstrated reduced downstream signaling in response to exogenous stimulation with FGF2, as determined by phosphorylation of ERK1/2 (Figure 2.1). Furthermore, quarfloxin and CX-5461 downregulates FGFR1 transcript level (Figure 4.9E, 4.9F). On the other hand, TMPyP4 has no effect on FGFR1 transcription (Fig. 4.9D). These results further demonstrates that TMPyP4 and CX-5461 modulate FGFR1 expression through different mechanisms. Besides human TNBC cell line, we also investigated if CX-5461 targets FGFR1 expression in mouse metastatic breast cancer cell line, D2.A1 cells. Since D2.A1 is sensitive to CX-5461 in 2D culture (Figure 4.10C), we utilized the 3D fibronectin (FN)-coated scaffold culture to maintain the D2.A1 cell proliferation upon CX-5461 treatment (Figure 4.10B). Previously we have identified that fibrillar FN can promote proliferation of metastatic breast cancer cells (Shinde et al., 2018). Here, the result also showed that metastatic breast cancer cells D2.A1 maintain proliferative with CX-5461 treatment in 3D FN-coated scaffold culture compared

to 2D cell culture (Figure 4.10C). Furthermore, D2.A1 cells growing on FN-coated scaffold culture present mesenchymal phenotype (Figure 4.10A). The FGFR1 expression is reduced with CX-5461 treatment in FN-coated scaffold culture. These data indicated that CX-5461 targets FGFR1 expression in both human and mouse breast cancer cell lines. To quantitatively interrogate the functional importance of reducing FGFR1 expression levels we again utilized our 3D spheroid assay where growth of D2.A1 3D spheroids can be specifically driven through addition of exogenous FGF2. Concomitant treatment with either the FGFR kinase inhibitor erdafitinib or CX-5461 completely blocked FGF2-induced spheroid growth (Figure 4.10E, 4.10F). Use of the D2.OR dormancy model similarly demonstrated the ability to erdafitinib and CX-5461 to block FGF2-induced spheroid growth (Figure 4.10G, 4.10H). However, unlike erdafitinib, CX-5461 also eliminated dormant cell survival as determined by colony formation after the spheroids were plated back to 2D Cell culture (Figure 4.10). Besides, TMPyP4 also suppressed FGF2-induced spheroid growth (Figure 4.11A, 4.11B) and abolished dormant cell survival in D2.OR dormancy model (Figure 4.11C). These results demonstrate that G4 stabilizers effectively decrease the survival of dormant BC cells.

4.3.6 In vivo application of CX-5461 stabilization reduces FGFR1 expression and blocks pulmonary tumor formation

We next sought to determine if *in vivo* application of a G4 stabilizing agent could reduce FGFR1 expression and block tumor growth in a metastatic site. Metastatic breast cancer patients have been shown to have notably FGFR1 amplification rate compared to patients with primary breast cancer (Q. Li et al., 2021; Razavi et al., 2018). However, patients with FGFR1 amplification present limited response to FGFR kinase inhibitors (Nogova et al., 2017). Metastatic D2.A1 breast cancer cells with high endogenous FGFR1 expression is an ideal animal model representing FGFR1 amplification (Michael K. Wendt et al., 2014). To compare the efficacies of G4 stabilizer and FGFR kinase inhibitor in FGFR1 amplified animal model, we inoculated mice with D2.A1 cells via lateral tail vein injection to allow for pulmonary seeding (Figure 4.12A). Three days after cells were injected, mice were given transient treatment for a period of 10 days and subsequently monitored for survival. The short time treatment with CX-5461 effectively blocked pulmonary growth as compared to the control group. However, the FDA-approved FGFR kinase inhibitor erdafitinib fails to suppress lung metastasis (Figure 4.12B, 4.12C). Furthermore, this approach

demonstrated that even transient treatment with CX-5461 treatment significantly prolonged survival without causing weight loss of mice (Figure 4.12D, 4.12E). On the contrary, Erdafitinib leads to shorter survival rate (Figure 4.12D). Besides the transient treatment, we also performed CX-5461 long time treatment for 22 days in D2.A1 animal model (Figure 4.13A). Treatment with CX-5461 did not cause significant weight loss but did result in a significant reduction in pulmonary tumor nodules (Figure 4.13D-F). Consistent with our *in vitro* data, both immunohistochemistry (IHC) and immunoblot demonstrated a marked reduction in FGFR1 protein levels in tumors derived from CX-5461 treated mice (Figure 4.13H, 4.13I). Interestingly, we also identified that there are more infiltrated $CD8^+$ T cells in nodules from mice with CX-5461 treatment (Figure 4.13H). This result revealed the potential combination therapy of G4 stabilizers and immune checkpoint blockade. Taken together, these findings clearly demonstrate that CX-5461 effectively blocked breast cancer growth in the pulmonary microenvironment.

4.4 Figures

A

```
3700  CGGGTTCAAG CGATTCCTCT GCCGCAGCCT CCCCAGTAGC TGGGATTACA GGCAAGCGCC ACCATGCCTG GCTAATTTTT TTGTATTTTA GTAGAGACGG
3800  GGTTTCACCT TGTTGGCAAG GATAGTCTCG ATCTCCCGAC CTCGTGATCC ACCCGCCTCG GCCTCCCAAA GTGCTGGGAT TACAGGCATA AGCCACCGCA
3900  CCCGGCCAAC TCTTTTCTTA AATTAGCCAG GGAGGCGTGG GTGGGTTGGG TGAGGAGTTG GGTGGGGGGA TCTCATTCAG TATTCAAACT TCTACAAGTT
4000  TCGGGGTTGA GGTGGGTGAT GGTAAGGGAA CAGGCCCTGC CACTACCTTT CATAGTGACT TCCATTTGTG TAATATTTTT GGTCCACTGA GAGCTATTAT
4100  TTTATTTGAT TCTTATGACC ATCTTGTGAA GGAGTATCAA CAGATACCCC GTTTTGATTT TATCAGATGC ATGATTTGTC CTACATCAAA CTTCATAAAT
4200  GATGGACAGA ATGGAGGAAT CCTTCAGACC AAGTGCTGCC TACTTCCCAC CCCAATGGTG GCCTCAGCCT GGGCTCACAT CACACGCCCC AAGGAGCCTT
4300  GGAAAAAATA AAGGCTCTTG GCTCCTTCCT GGGACAGCGT GATTCCTCAT GTCTGAGCAG GCCCATGAAC TTGTATTTTT CAGACGTTCC CTAGGACCCG
4400  TGTCCATCTG GATTAGGGAA CCACTACATT ATACCACTTC GCGGGAAGAC TCAGGGGGAA GCATTTTAGC CACTTTCCTG TGTTCCACAG TACTGGAGGG
4500  TGTTCTGAGT GGGCTGTGAT TAATTTCCAA ACCAACCACA CGTCTCCCCT CAACTCCCAC TGCTTACTCT TTGCTTCCTA GACATTCACT GCAGGCTGGA
4600  GACTTCTGGA AGCCAACAGC ATCGCTGTAG AATTTACAGG GTCCAGTTCC CGGTGGACCA CAAAACCTAA ATTATGTGGC TGGGGAAAGC TGAAATCCAA
4700  GGGAAGGGTT TGAGGAGGGG CTGACCTTAT AATAAAACCG GCTTGTATTT ACTAAGTGTT AACTATGCGC TAGGCCCTCG TTGACGCCTC AACTCTATGT
4800  GAAAAGCACT ATTATCCCCC ATTTACAGAT GGGAAAACAG AGATTTAGAG CGCGAAAATC ATTTCCCCAA GGCGCACAGA CTCCAAAGCC CACGCTACCA
4900  GGTACAACCT CAAGGCTGCG GCGTCTCTTC ACCTGCCCCC TAGCCCCCAA ACCGCTGCTA TGTCTAGGGC CTGACATTCC GGCGCCCTCT GGGACGTGCT
5000  CAGATGCAGG GGCGCAAACG CCAAAGGAGA CCAGGCTGTA GGAAGAGAAG GGCAGAGCGC CGGACAGCTC GGCCCGCTCC CCGTCCTTTG GGGCCGCGGC
5100  TGGGGAACTA CAAGGCCCAG CAGGCAGCTG CAGGGGGCGG AGGCGGAGGA GGGACCAGCG CGGGTGGGAG TGAGAGAGCG AGCCCTCGCG CCCCGCCGGC
5200  GCATAGCGCT CGGAGCGCTC TTGCGGCCAC AGGCGCGGCG TCCTCGGCGG CGGGCGGCAG C
```

TSS

B

	Sequences	Topology	Melting Temperature (°C)
S1	5'- CA **GGG** A **GG** CGT **GGG** T **GGG** TT **GGG** TGA **GG** AGTT **GGG** T **GGGGGG** AT-3'	Parallel	65.01
S2	5'- CA **GGG** A **GG** CGT **GGG** T **GGG** TT **GGG** TGA **GG** AGTT-3'	Parallel	64.54
S3	5'- AA **GGG** AA **GGG** TTTGA **GG** A **GGGG** CT-3'	Hybrid	47.45
S4	5'- CA **GGGGG** C **GG** A **GG** C **GG** A **GG** A **GGG** ACCAGCGC **GGG** T **GGG** AGT-3'	Parallel	60.29
S5	5'- CA **GGGGG** C **GG** A **GG** C **GG** A **GG** A **GGG** ACCA-3'	Parallel	43.88

C

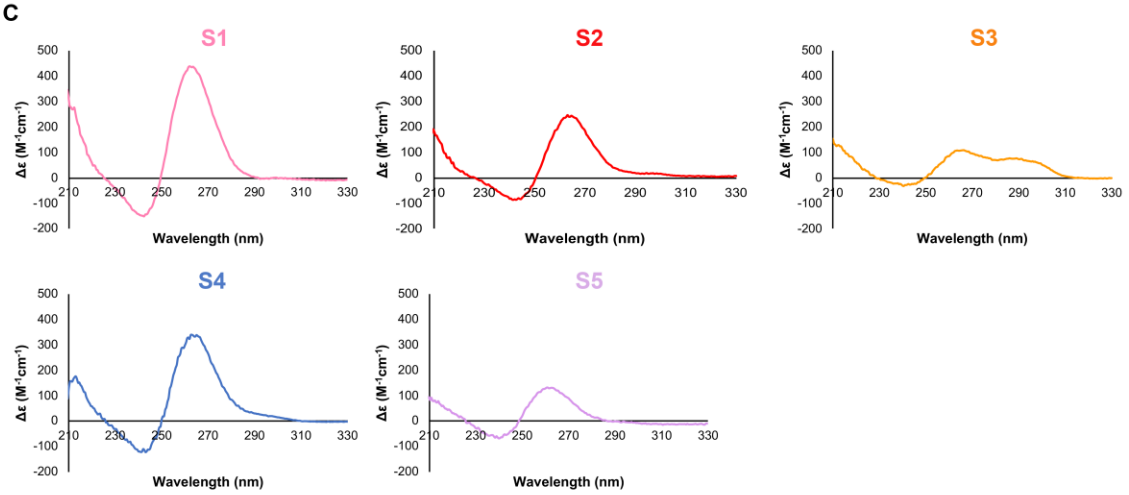

Figure 4.1 Putative G4 sequences in FGFR1 promoter region form stable G4 structures. A. -1500/+60 FGFR1 promoter region with potential G4 forming sequences B. Sequences of putative G4 forming sequences with their topologies and melting temperatures. C. CD spectra of these G4 forming sequences in the presence of K^+.

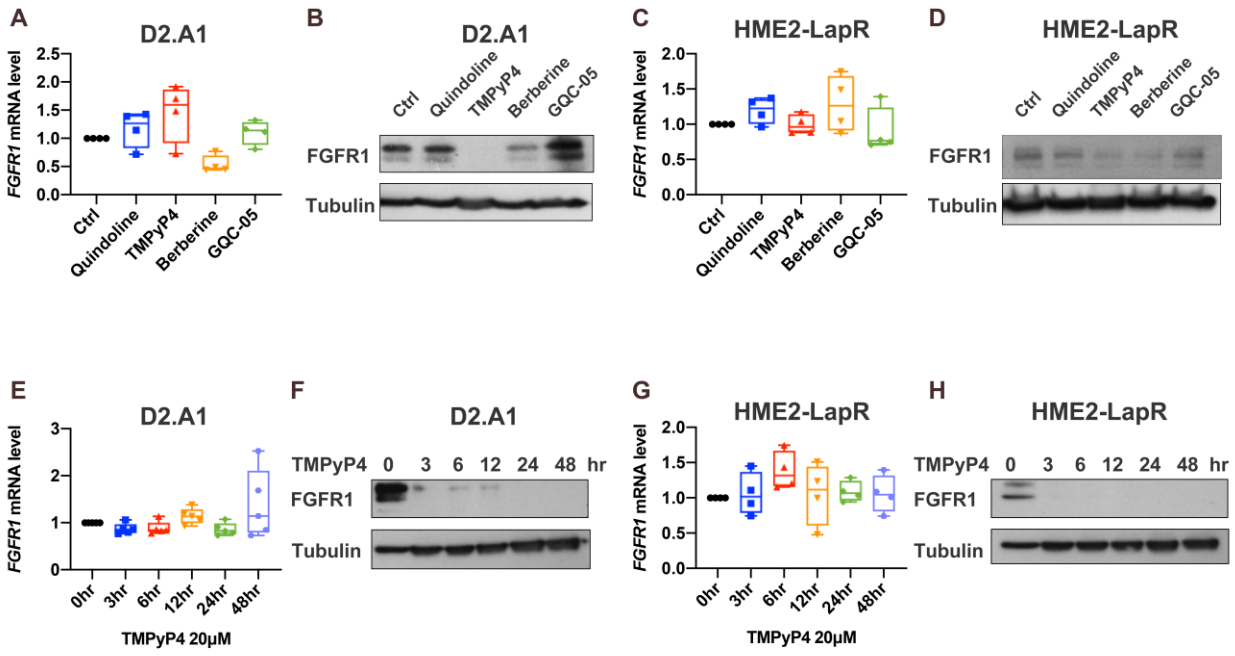

Figure 4.2 TMPyP4 suppresses FGFR1 protein expression metastatic and drug-resistant cell lines. A, C. RT-PCR for FGFR1 transcript levels after treatment with the indicated G4 stabilizers in D2.A1 (A) and lapatinib resistant (HME2-LapR) cells (D). Data are normalized to FGFR1 levels in the control cells for each treatment and are the mean ± s.e.m. of four independent experiments. G4 stabilizer conditions were Quinodline (1 μM), TMPyP4 (20 μM), Berberine (20 μM), and GQC-5 (1 μM) for 24 hours. B, D. Immunoblot analyses showing the FGFR1 protein levels after treatment with G4 stabilizers as described in panel A. E, G. RT-PCR for FGFR1 transcript levels after TMPyP4 treatments for the indicated amounts of time. Data are normalized to FGFR1 levels in the control (0 hour) cells for each treatment and are the mean ± s.e.m. (n=4). F, H. Immunoblot analyses for FGFR1 protein levels following TMPyP4 treatment for the indicated amounts of time. Data in B, D, F, and H are representative of at least three independent experiments.

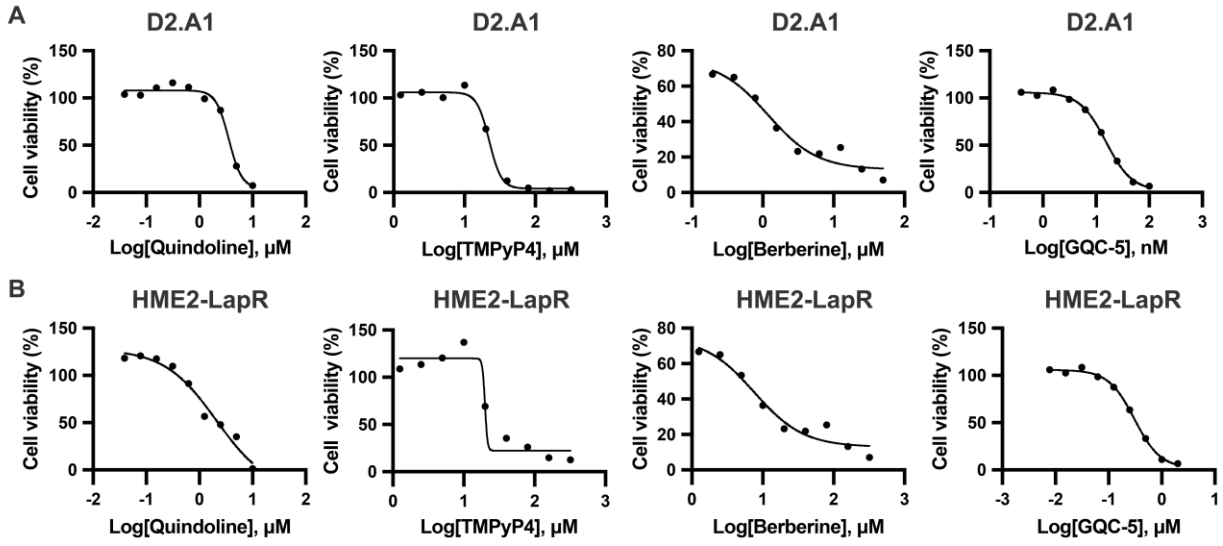

C

IC 50 values (μM)

Cell line	Quindoline	TMPyP4	Berberine	GQC-5
D2.A1	3.5	22.29	1.182	0.0153
HME2-LapR	2.076	19.94	7.565	0.3068

Figure 4.3 G4 stabilizers reduce cell viabilities of metastatic and drug-resistant breast cancer cells. A, B. CellTiter-Glo analyses of G4 stabilizers treatments for 3 days in D2.A1 and HME2-LapR cells. C. The IC_{50} values of G4 ligands in D2.A1 and HME2-LapR cells.

Figure 4.4 TMPyP4 can block EMT-induced expression of FGFR1. A. Schematic representation of the FGFR1 proximal promoter reporter construct. The potential G4 forming sequence S4 is highlighted in yellow. B. Dual-Glo luciferase assay showing FGFR1 proximal promoter activity in control and Twist overexpressing MCF10A cells in the presence or absence of TMPyP4. Data are normalized to the ratio of firefly luciferase to renilla luciferase in MCF10A-YFP cells and are the mean ± s.e.m. (n=4), where $*p<0.05$. C. Immunoblot analyses for FGFR1, N-cadherin, E-cadherin demonstrating induction of EMT upon directed overexpression of Twist in the MCF10A cells. D. Immunoblot analyses for FGFR1 protein levels upon TMPyP4 treatment of MCF10A-Twist cells. E. RT-PCR for FGFR1 transcript levels upon TMPyP4 treatment of MCF10A-Twist cells for the indicated amounts of time. Data are normalized to FGFR1 levels in the control (0 hour) cells for each treatment and are the mean ± s.e.m. (n=4). F. RT-PCR showing that FGFR1 was upregulated in NMuMG cells upon directed overexpression of Twist. Data are normalized to FGFR1 levels in the control (YFP) cells and are the mean ± s.e.m. (n=4). G. RT-PCR for FGFR1 transcript levels upon treatment with TMPyP2 or TMPyP4. Data are normalized to FGFR1 levels in the control (0 hour) cells for each treatment and are the mean ± s.e.m. (n=4). H. Immunoblot analyses for FGFR1 in NMuMG-Twist cells compared to YFP expressing control cells. FGFR1 is not detectable by immunoblot in control NMuMG cells, a lysate from NMuMG-Twist cells was used as a positive control (P). Twist-driven FGFR1 upon treatment with TMPyP2 and TMPyP4 at the indicated time points. I. RT-PCR for FGFR1 mRNA in NMuMG cells following TGF- β1 stimulation (7 days) as compared to non-stimulated NMuMG cells. Data are normalized to FGFR1 levels in the non-stimulated (NS) cells and are the mean ± s.e.m. (n=4). J. RT-PCR for TGF- β1-induced FGFR1 expression upon TMPyP2 and TMPyP4 treatments at the indicated time points. Data are normalized to FGFR1 levels in the control (0hour) cells for each treatment and are the mean ± s.e.m. (n=4). K. Immunoblot analyses for TGF- β1 induced FGFR1 expression upon treatment with TMPyP2 and TMPyP4. All immunoblots are representative of at least 3 independent experiments.

Figure 4.4 continued

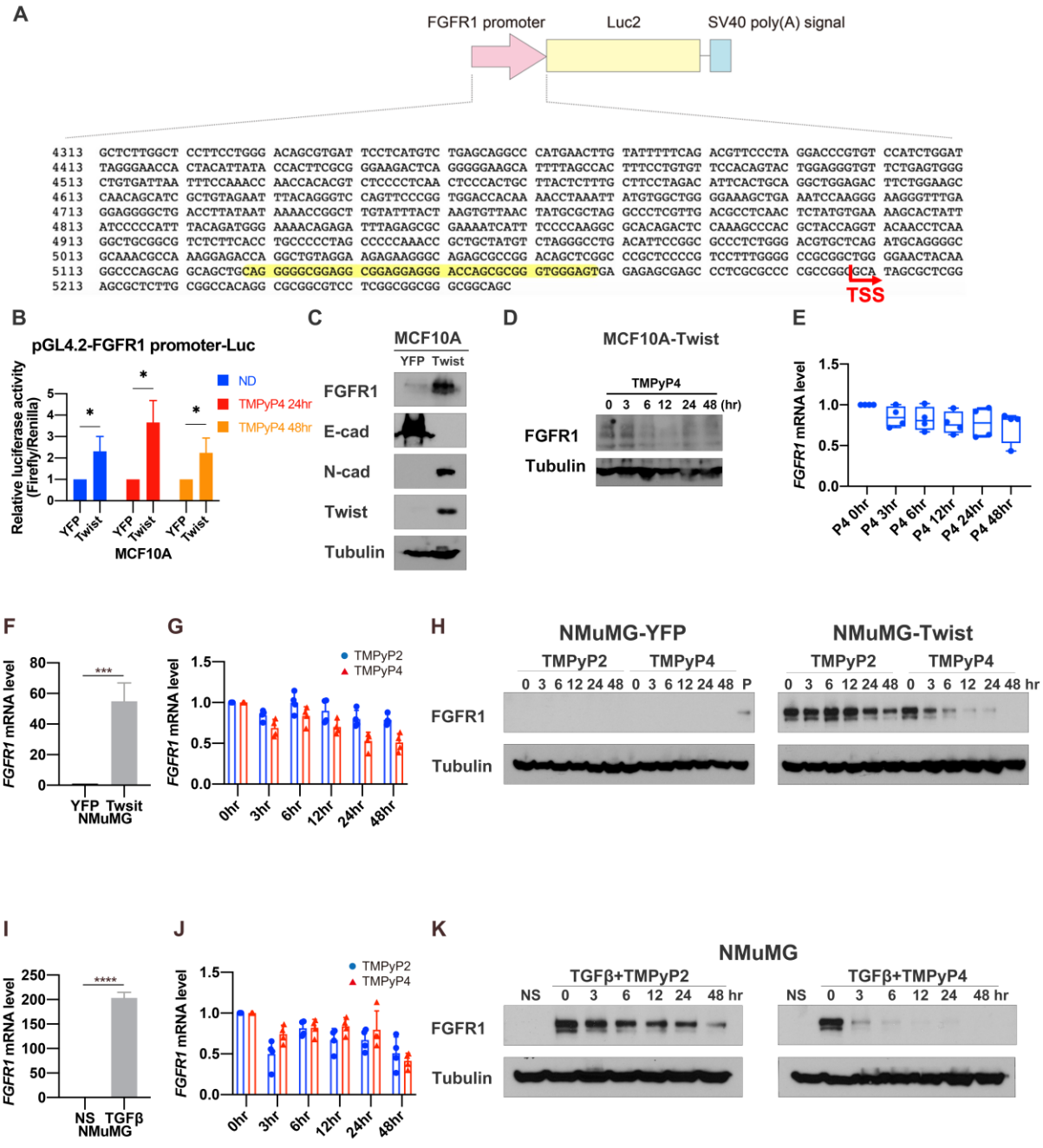

A

FGFR1α mRNA

Gene Information	
Gene ID:	**Number of Products:** 1
Gene Symbol:	**Number of poly A Signals:**
Gene Size: 2469 nt.	**QGRS found:** 20
	QGRS found (including overlaps): 260

```
000001 AUGUGGAGCU GGAAGUGCCU CCUCUUCUGG GCUGUGCUGG UCACAGCCAC ACUCUGCACC GCUAGGCCGU CCCCGACCUU GCCUGAACAA GCCCAGCCCU
000101 GGGGAGCCCC UGUGGAAGUG GAGUCCUUCC UGGUCCACCC CGGUGACCUG CUGCAGCUUC GCUGUCGGCU GCGGGACGAU GUGCAGAGCA UCAACUGGCU
000201 GCGGGACGGG GUGCAGCUGG CGGAAAGCAA CCGCACCCGC AUCACAGGGG AGGAGGUGGA GGUGCAGGAC UCCGUGCCCG CAGACUCCGG CCUCUAUGCU
000301 UGCGUAACCA GCAGCCCCUC GGGCAGUGAC ACCACCUACU UCUCCGUCAA UGUUUCAGAU GCUCUCCCCU CCUCGGAGGA UGAUGAUGAU GAUGAUGACU
000401 CCUCUUCAGA GGAGAAAGAA ACAGAUAACA CCAAACCAAA CCGUAUGCCC GUAGCUCCAU AUUGGACAUC CCCAGAAAAG AUGGAAAAGA AAUUGCAUGC
000501 AGUGCCGGCU GCCAAGACAG UGAAGUUCAA AUGCCCUUCC AGUGGGACCC CAAACCCCAC ACUGCGCUGG UUGAAAAAUG GCAAAGAAUU CAAACCUGAC
000601 CACAGAAUUG GAGGCUACAA GGUCCGUUAU GCCACCUGGA GCAUCAUAAU GGACUCUGUG GUGCCCUCUG ACAAGGGCAA CUACACCUGC AUUGUGGAGA
000701 AUGAGUACGG CAGCAUCAAC CACACAUACC AGCUGGAUGU CGUGGAGCGG UCCCCUCACC GGCCCAUCCU GCAAGCAGGG UUGCCCGCCA ACAAACACAGU
000801 GGCCCUGGGU AGCAACGUGG AGUUCAUGUG UAAGGUGUAC AGUGACCCGC AGCCGCACAU CCAGUGGCUA AAGCACAUCG AGGUGAAUGG GAGCAAGAUU
000901 GGCCCAGACA ACCUGCCUUA UGUCCAGAUC UUGAAGACUG CUGGAGUUAA UACCACCGAC AAAGAGAUGG AGGUGCUUCA CUUAAGAAAU GUCUCCUUUG
001001 AGGACGCAGG GGAGUAUACG UGCUUGGCGG GUAACUCUAU CGGACUCUCC CAUCACUCUG CAUGGUUGAC CGUUCUGGAA GCCCUGGAAG AGAGGCCGGC
001101 AGUGAUGACC UCGCCCCUGU ACCUGGAGAU CAUCAUCUAU UGCACAGGGG CCUUCCUCAU CUCCUGCAUG GUGGGGUCGG UCAUCGUCUA CAAGAUGAAG
001201 AGUGGUACCA AGAAGAGUGA CUUCCACAGC CAGAUGGCUG UGCACAAGCU GGCCAAGAGC AUCCCUCUGC GCAGACAGGU AACAGUGUCU GCUGACUCCA
001301 GUGCAUCCAU GAACUCUGGG GUUCUUCUGG UUCGGCCAUC ACGGCUCUCC UCCAGUGGGA CUCCCAUGCU AGCAGGGGUC UCUGAGUAUG AGCUUCCCGA
001401 AGACCCUCGC UGGGAGCUGC CUCGGGACAG ACUGGUCUUA GGCAAACCCC UGGGAGAGGG CUGCUUUGGG CAGGUGGUGU UGGCAGAGGC UAUCGGGCUG
001501 GACAAGGACA AACCCAACCG UGUGACCAAA GUGGCUGUGA AGAUGUUGAA GUCGGACGCA ACAGAGAAAG ACUUGUCAGA CCUGAUCUCA GAAAUGGAGA
001601 UGAUGAAGAU GAUCGGGAAG CAUAAGAAUA UCAUCAACCU GCUGGGGCCC UGCACGCAGG AUGGUCCCUU GUAUGUCAUC GUGGAGUAUG CCUCCAAGGG
001701 CAACCUGCGG GAGUACCUGC AGGCCCGGAG GCCCCCAGGG CUGGAAUACU GCUACAACCC CAGCCACAAC CCAGAGGAGC AGCUCUCCUC CAAGGACCUG
001801 GUGUCCUGCG CCUACCAGGU GGCCCGAGGC AUGGAGUAUC UGGCCUCCAA GAAGUGCAUA CACCGAGACC UGGCAGCCAG GAAUGUCCUG GUGACAGAGG
001901 ACAAUGUGAU GAAGAUAGCA GACUUUGGCC UCGCACGGGA CAUUCACCAC AUCGACUACU AUAAAAAGAC AACCAACGGC CGACUGCCUG UGAAGUGGAU
002001 GGCACCCGAG GCAUUAUUUG ACCGGAUCUA CACCCACCAG AGUGAUGUGU GGUCUUUCGG GGUGCUCCUG UGGGAGAUCU UCACUCUGGG CGGCUCCCCA
002101 UACCCCGGUG UGCCUGUGGA GGAACUUUUC AAGCUGCUGA AGGAGGGUCA CCGCAUGGAC AAGCCCAGUA ACUGCACCAA CGAGCUGUAC AUGAUGAUGC
002201 GGGACUGCUG GCAUGCAGUG CCCUCACAGA GACCCACCUU CAAGCAGCUG GUGGAAGACC UGGACCGCAU CGUGGCCUUG ACCUCCAACC AGGAGUACCU
002301 GGACCUGUCC AUGCCCCUGG ACCAGUACUC CCCCAGCUUU CCCGACACCC GGAGCUCUAC GUGCUCCUCA GGGGAGGAUU CCGUCUUCUC UCAUGAGCCG
002401 CUGCCCGAGG AGCCCUGCCU GCCCCGACAC CCAGCCCAGC UUGCCAAUGG CGGACUCAAA CGCCGCUGA
```

B

FGFR1β mRNA

Gene Information	
Gene ID:	**Number of Products:** 1
Gene Symbol:	**Number of poly A Signals:**
Gene Size: 2202 nt.	**QGRS found:** 17
	QGRS found (including overlaps): 181

```
000001 AUGUGGAGCU GGAAGUGCCU CCUCUUCUGG GCUGUGCUGG UCACAGCCAC ACUCUGCACC GCUAGGCCGU CCCCGACCUU GCCUGAACAA GAUGCUCUCC
000101 CCUCCUCGGA GGAUGAUGAU GAUGAUGAUG ACUCCUCUUC AGAGGAGAAA GAAACAGAUA ACACCAAACC AAACCGUAUG CCCGUAGCUC CAUAUUGGAC
000201 AUCCCCAGAA AAGAUGGAAA AGAAAUUGCA UGCAGUGCCG GCUGCCAAGA CAGUGAAGUU CAAAUGCCCU UCCAGUGGGA CCCCAAACCC CACACUGCGC
000301 UGGUUGAAAA AUGGCAAAGA AUUCAAACCU GACCACAGAA UUGGAGGCUA CAAGGUCCGU UAUGCCACCU GGAGCAUCAU AAUGGACUCU GUGGUGCCCU
000401 CUGACAAGGG CAACUACACC UGCAUUGUGG AGAAUGAGUA CGGCAGCAUC AACCACACAU ACCAGCUGGA UGUCGUGGAG CGGUCCCCUC ACCGGCCCAU
000501 CCUGCAAGCA GGGUUGCCCG CCAACAAAAC AGUGGCCCUG GGUAGCAACG UGGAGUUCAU GUGUAAGGUG UACAGUGACC CGCAGCCGCA CAUCCAGUGG
000601 CUAAAGCACA UCGAGGUGAA UGGGAGCAAG AUUGGCCCAG ACAACCUGCC UUAUGUCCAG AUCUUGAAGA CUGCUGGAGU UAAUACCACC GACAAAGAGA
000701 UGGAGGUGCU UCACUUAAGA AAUGUCUCCU UUGAGGACGC AGGGGAGUAU ACGUGCUUGG CGGUAACUC UAUCGGACUC UCCCAUCACU CUGCAUGGUU
000801 GACCGUUCUG GAAGCCCUGG AAGAGAGGCC GGCAGUGAUG ACCUCGCCCC UGUACCUGGA GAUCAUCAUC UAUUGCACAG GGGCCUUCCU CAUCUCCUGC
000901 AUGGUGGGGU CGGUCAUCGU CUACAAGAUG AAGAGUGGUA CCAAGAAGAG UGACUUCCAC AGCCAGAUGG CUGUGCACAA GCUGGCCAAG AGCAUCCCUC
001001 UGCGCAGACA GGUAACAGUG UCUGCUGACU CCAGUGCAUC CAUGAACUCU GGGGUUCUUC UGGUUCGGCC AUCACGGCUC UCCUCCAGUG GGACUCCCAU
001101 GCUAGCAGGG GUCUCUGAGU AUGAGCUUCC CGAAGACCCU CGCUGGGAGC UGCCUCGGGA CAGACUGGUC UUAGGCAAAC CCCUGGGAGA GGGCUGCUUU
001201 GGGCAGGUGG UGUUGGCAGA GGCUAUCGGG CUGGACAAGG ACAAACCCAA CCGUGUGACC AAAGUGGCUG UGAAGAUGUU GAAGUCGGAC GCAACAGAGA
001301 AAGACUUGUC AGACCUGAUC UCAGAAAUGG AGAUGAUGAA GAUGAUCGGG AAGCAUAAGA AUAUCAUCAA CCUGCUGGGG GCCUGCACGC AGGAUGGUCC
001401 CUUGUAUGUC AUCGUGGAGU AUGCCUCCAA GGGCAACCUG CGGGAGUACC UGCAGGCCCG GAGGCCCCCA GGGCUGGAAU ACUGCUACAA CCCCAGCCAC
001501 AACCCAGAGG AGCAGCUCUC CUCCAAGGAC CUGGUGUCCU GCGCCUACCA GGUGGCCCGA GGCAUGGAGU AUCUGGCCUC CAAGAAGUGC AUACACCGAG
001601 ACCUGGCAGC CAGGAAUGUC CUGGUGACAG AGGACAAUGU GAUGAAGAUA GCAGACUUUG GCCUCGCACG GGACAUUCAC CACAUCGACU ACUAUAAAAA
001701 GACAACCAAC GGCCGACUGC CUGUGAAGUG GAUGGCACCC GAGGCAUUAU UUGACCGGAU CUACACCCAC CAGAGUGAUG UGUGGUCUUU CGGGGUGCUC
001801 CUGUGGGAGA UCUUCACUCU GGGCGGCUCC CCAUACCCCG GUGUGCCUGU GGAGGAACUU UUCAAGCUGC UGAAGGAGGG UCACCGCAUG GACAAGCCCA
001901 GUAACUGCAC CAACGAGCUG UACAUGAUGA UGCGGGACUG CUGGCAUGCA GUGCCCUCAC AGAGACCCAC CUUCAAGCAG CUGGUGGAAG ACCUGGACCG
002001 CAUCGUGGCC UUGACCUCCA ACCAGGAGUA CCUGGACCUG UCCAUGCCCC UGGACCAGUA CUCCCCCAGC UUUCCCGACA CCCGGAGCUC UACGUGCUCC
002101 UCAGGGGAGG AUUCCGUCUU CUCUCAUGAG CCGCUGCCCG AGGAGCCCUG CCUGCCCCGA CACCCAGCCC AGCUUGCCAA UGGCGGACUC AAACGCCGCU
002201 GA
```

Figure 4.5 Potential G4 forming sequences in FGFR1α and β isoforms mRNA sequences. A, B The mRNA sequences of FGFR1α and β isoforms were analyzed via QGRS mapper. Potential G4 sequences were highlighted with yellow color.

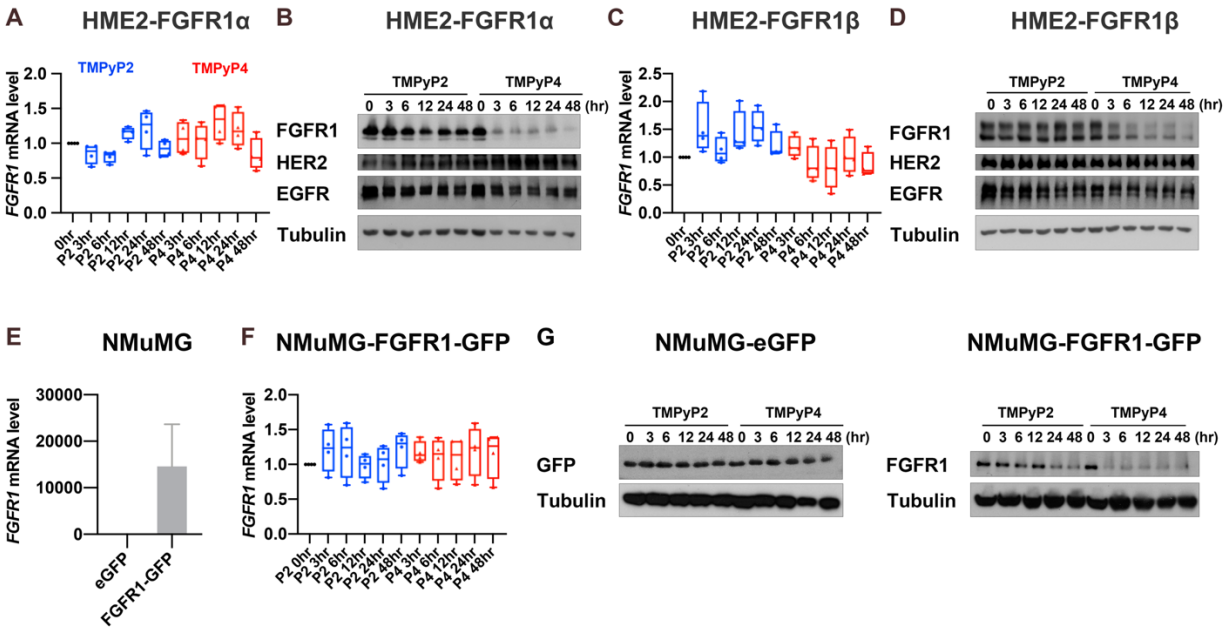

Figure 4.6 TMPyP4 reduces the ectopic FGFR1 expression. A. RT-PCR for the FGFR1α transcript levels upon treatment with TMPyP2 or TMPyP4 for the indicated amounts of time. Data are normalized to FGFR1 levels in the control (0 hour) cells and are the mean ± s.e.m. (n=4). B. Immunoblot analyses for FGFR1, HER2 and EGFR protein levels upon treatment with TMPyP2 and TMPyP4. C-D. Identical approaches as described in panels A and B were used to analyze cells expression of the FGFR1β isoform. E. RT-PCR for FGFR1 transcript levels in NMuMG overexpressing FGFR1-GFP fusion construct as compared to the eGFP control cells. Data are normalized to FGFR1 levels in the control cells (n=4). F. RT-PCR for FGFR1 mRNA levels upon treatment with TMPyP2 or TMPyP4 for the indicated amounts of time points. Data are normalized to FGFR1 levels in the control (0 hour) cells for each treatment and are the mean ± s.e.m. (n=4). G. Immunoblot analyses for GFP in control and FGFR1-GFP fusion expressing cells upon treatment with TMPyP2 or TMPyP4 for the indicated amounts of time. All immunoblots are representative of at least three independent analyses.

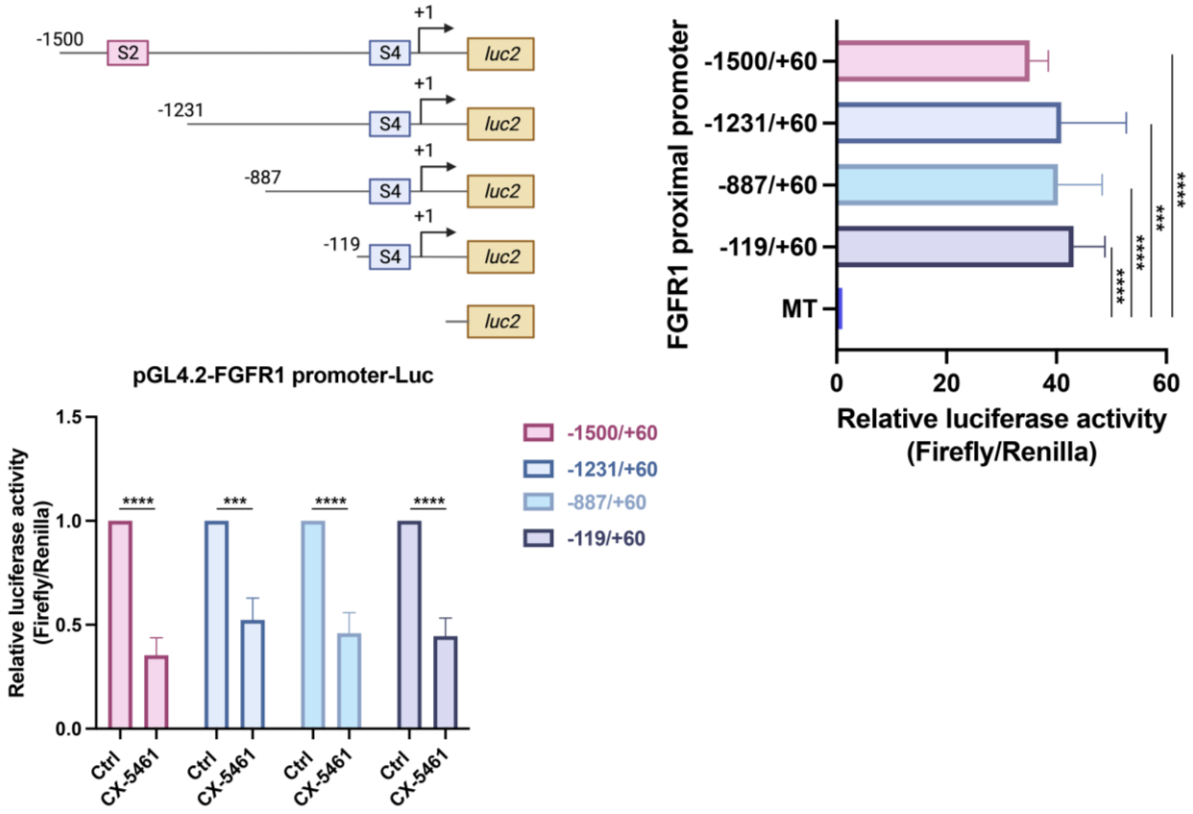

Figure 4.7 CX-5461 suppresses FGFR1 proximal promoter activity. A series of truncated FGFR1 promoter regions were cloned into the pGL4.2 luciferase reporter vector. B. Dual-Glo luciferase assay showing different lengths of truncated FGFR1 proximal promoter activities in HEK293T cell. Data are normalized to the ratio of firefly luciferase to renilla from pGL4.2 empty vector and are the mean ± s.e.m. (n=3), where *p<0.05. C. Dual-Glo luciferase assay showing FGFR1 proximal promoter activity in HEK293T cells in the presence or absence of 1 μM CX-5461 for 72 hours. Data are normalized to the ratio of firefly luciferase to renilla luciferase in control cells and are the mean ± s.e.m. (n=3), where *p<0.05.

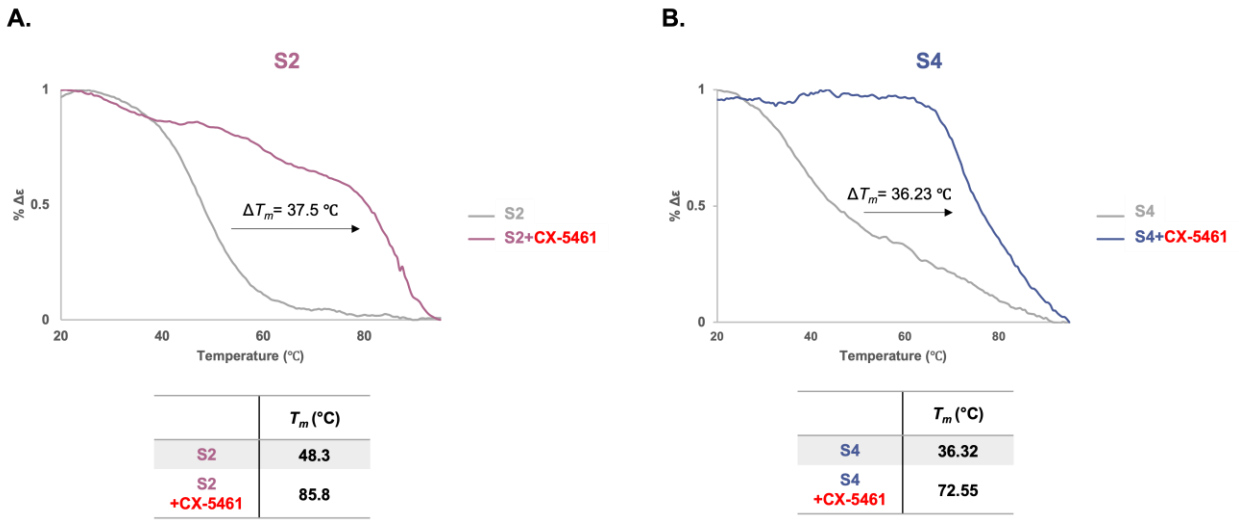

	T_m (°C)
S2	48.3
S2 +CX-5461	85.8

	T_m (°C)
S4	36.32
S4 +CX-5461	72.55

Figure 4.8 CD melting curve for FGFR1 potential G4 forming sequences in the absence and presence of CX-5461. A, B. CD analyses of the melting temperature change of S2 and S4 FGFR1 potential G4 forming sequences in the presence and absence of CX-5461 with a 5:1 ligand: DNA ratio.

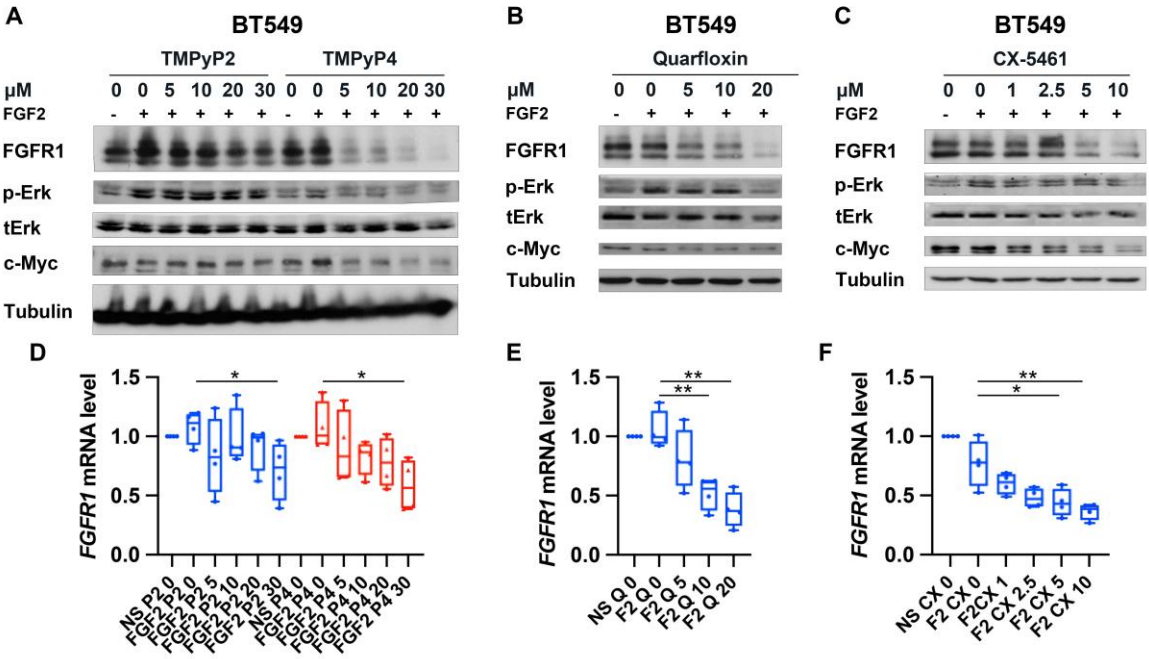

Figure 4.9 G-quadruplex stabilization can block FGF-induced growth and eliminate dormant cells. A. Immunoblot analyses for FGFR1 BT549 cells upon treatment with the indicated concentrations of TMPyP2 or TMPyP4 for 24 hours. Phosphorylation of ERK1/2 (pErk) induced upon FGF2 stimulation (20 ng/ml for 10 minutes) was also analyzed upon TMPyP2 or TMPyP4 pre-treatment. Expression of total ERK1/2 (tErk) served as a loading control. B-C. Immunoblot analyses for FGFR1 expression and FGF2-induced ERK1/2 phosphorylation upon treatment with the G4 stabilizers quarfloxin (B) or CX-5461 (C) for 24 hours. D-F. RT-PCR for FGFR1 transcript levels after treatment with the indicated G4 stabilizers, TMPyP2 and TMPyP4 (D), Quarfloxin (E) and CX-5461(F), for 24 hours in BT549 cells. F2 means 20ng/ml FGF2 treatment. Data are normalized to FGFR1 levels in the control cells for each treatment and are the mean ± s.e.m. of four independent experiments.

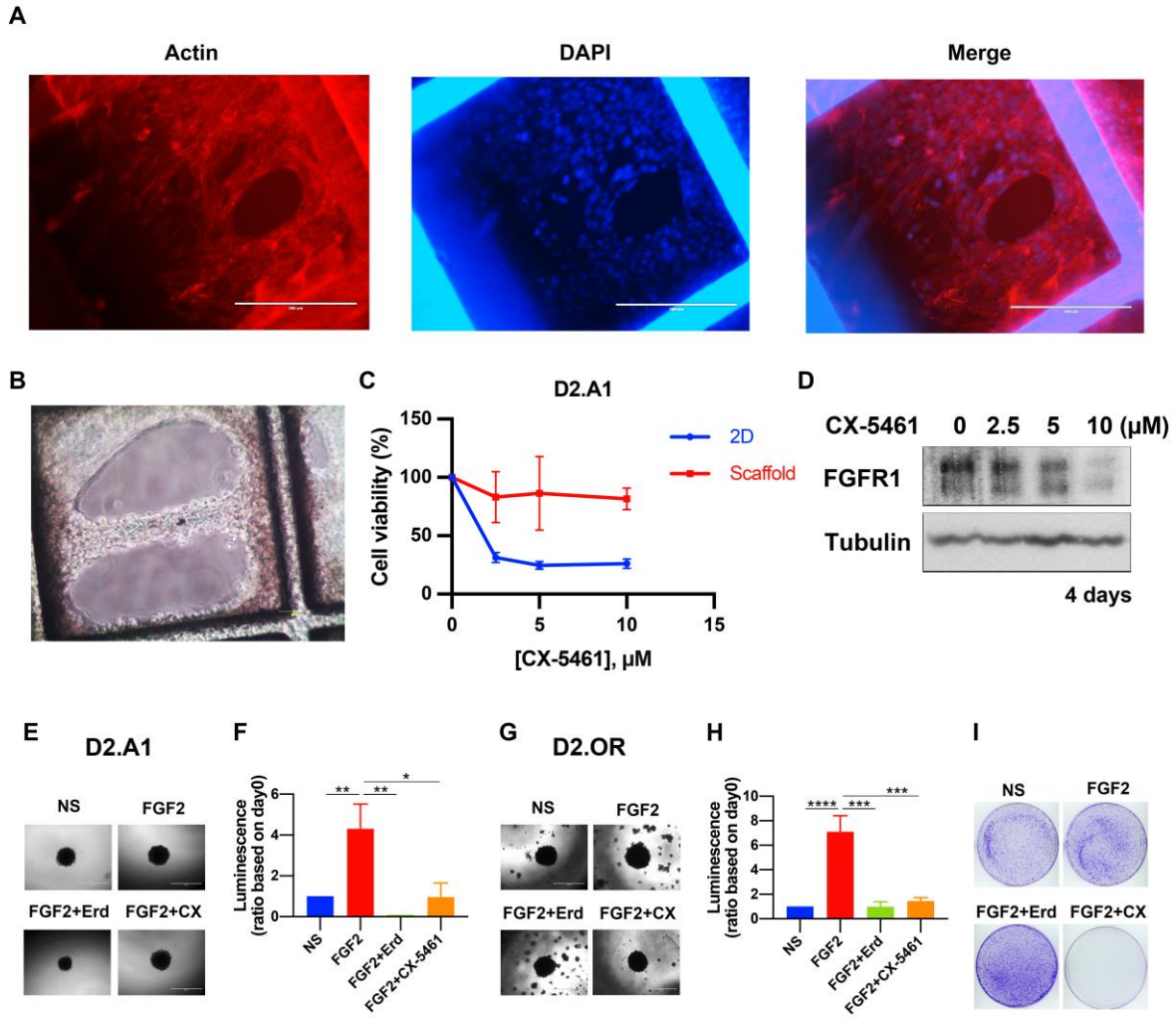

Figure 4.10 CX-5461 targets FGFR1 expression in 3D FN-coated scaffold culture and eliminates dormant breast cancer cells. A. D2.A1 cells were cultured on FN-coated scaffolds for 4 days and counterstained with phalloidin (red) and dapi (blue) to visualize actin skeleton and the nucleus, respectively. B. D2.A1 cells were cultured on FN-coated scaffolds for 4 days. C. D2.A1 cells were cultured on FN-coated scaffolds for 6 days, treated CX-5461 for 4 days and measured the cell viability. D. Immunoblot analyses for FGFR1 upon treatment with the CX-5461 for 4 days. E-F. D2.A1 spheroids expressing firefly luciferase were formed in a round bottom plate and then transferred to a bed of matrix in the presence or absence of 20 ng/ml FGF2, 100 nM Erdafitinib or 100 nM CX-5461. Bioluminescence was measured and these values were normalized to control (NS). Data are the mean ± s.e.m. (n=3) where *p<0.05. G-H As in panel D firefly luciferase expressing D2.OR cells were used in a spheroid growth assay. I. Following 3D culture, D2.OR spheroids were trypsinized and single cells were plated on tissue culture plastic. Colony formation was visualized by crystal violet staining 14 days later.

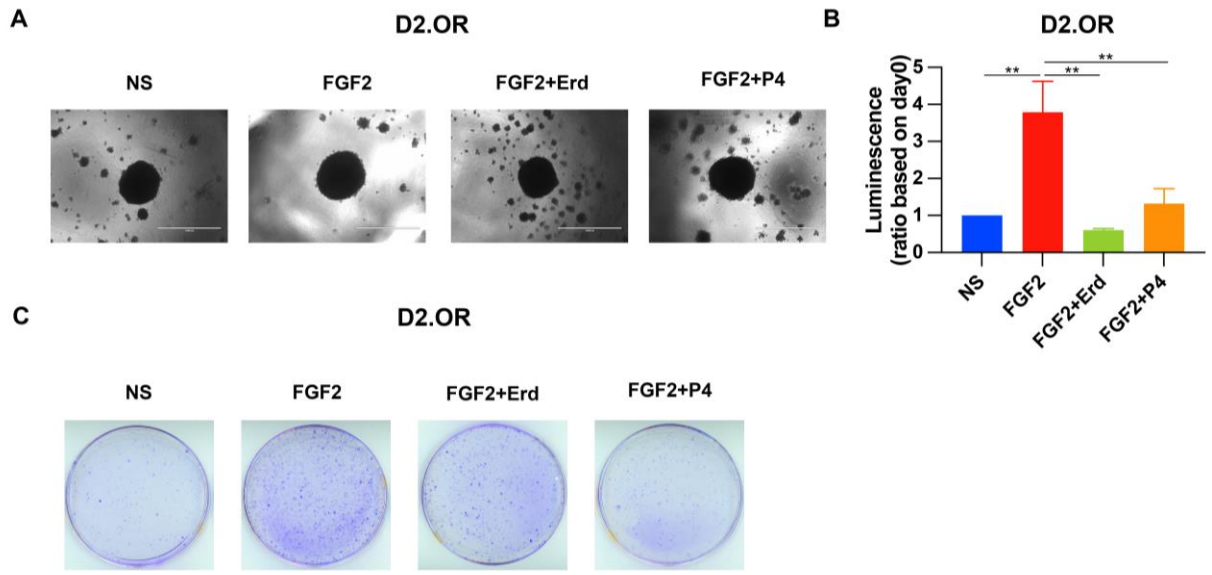

Figure 4.11 TMPyP4 suppresses spheroid growth and eliminates dormant breast cancer cells. A, B. D2.OR spheroids expressing firefly luciferase were formed in a round bottom plate and then transferred to a bed of matrix in the presence or absence of 20 ng/ml FGF2, 100 nM Erdafitinib or 20 μM . Bioluminescence was measured and these values were normalized to control (NS). Data are the mean ± s.e.m. (n=3) where *p<0.05. C. Following 3D culture, D2.OR spheroids were trypsinized and single cells were plated on tissue culture plastic. Colony formation was visualized by crystal violet staining 14 days later.

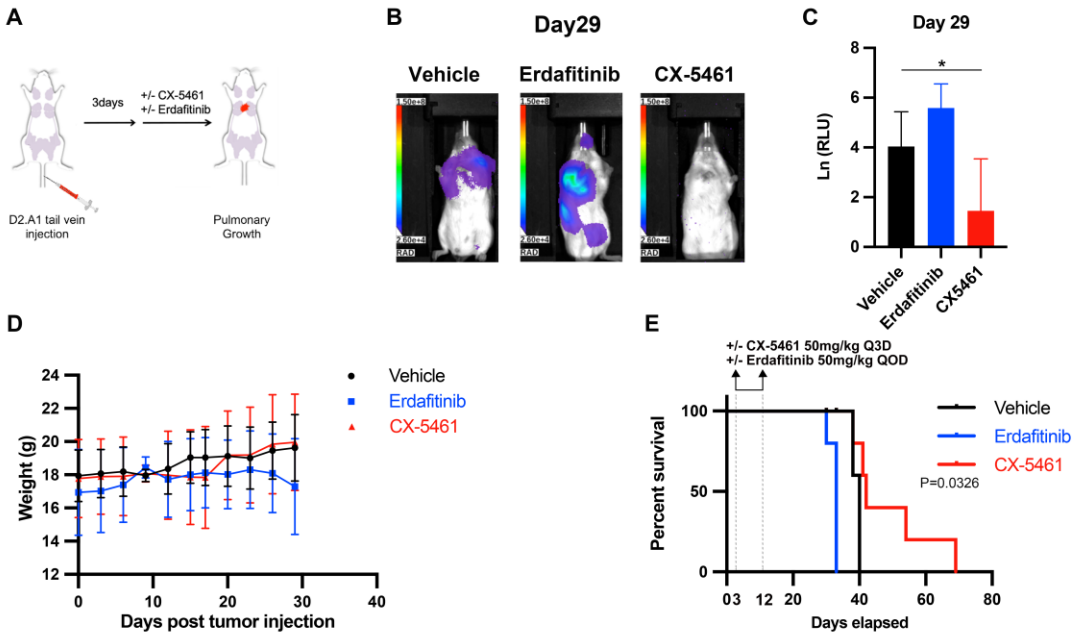

Figure 4.12 Transient G4 ligand treatment prolongs survival. A. Schematic representation of pulmonary delivery of D2.A1 cells followed by treatment with CX-5461or erdafitinib. B. Representative BLI images after delivery of D2.A1 cells 29 days post tumor inoculation for control animals (vehicle) and those that received erdafitinib or CX-5461. C. Bioluminescent values from pulmonary ROI were normalized to the values at the initial day of injection. Data are the mean of 5 mice per treatment group ± s.e.m. where *p<0.05. D. Body weights of mice from vehicle, erdafitinib and CX-5461 treated groups (n=5). E. Survival analyses of mice bearing D2.A1 pulmonary tumors. Mice received the vehicle as a control or were treated with erdafitinib or CX-5461 for the indicated amount of time. Kaplan-Meier analysis comparing the vehicle and CX-5461 treatment groups (n=5 mice per group) resulted in the indicated P value.

Figure 4.13 The G4 stabilizer, CX-5461, reduces FGFR1 expression and blocks pulmonary tumor formation. A. Schematic representation of pulmonary delivery of D2.A1 cells followed by treatment with CX-5461. B. Representative BLI images immediately after delivery of D2.A1 cells (day 0) and 24 days post tumor inoculation for control animals (vehicle) and those that received CX-5461. C. Bioluminescent values from pulmonary ROI were normalized to the values at the initial day of injection. Data are the mean of 5 mice per treatment group ± s.e.m resulting in the indicated P-value. D. Body weights of mice from vehicle and CX-5461 treated groups (n=5). E. Photos of fixed lungs harvested from control (vehicle) and CX-5461 treated animals. Pulmonary tumor nodules are indicated by arrow heads. F. Quantification of pulmonary tumor nodules identified in vehicle and CX-5461 groups. n=5 mice per group resulting in the indicated P value. G. Representative pulmonary H&E staining from 2 mice in the control (vehicle) and CX-5461 treated groups. H. IHC staining FGFR1 and CD8 in pulmonary histological sections from vehicle and CX-5461 treated mice. I. Immunoblot analyses of FGFR1 protein levels in isolated lung nodules from vehicle and CX-5461 treated mice (n=3).

Figure 4.13 continued

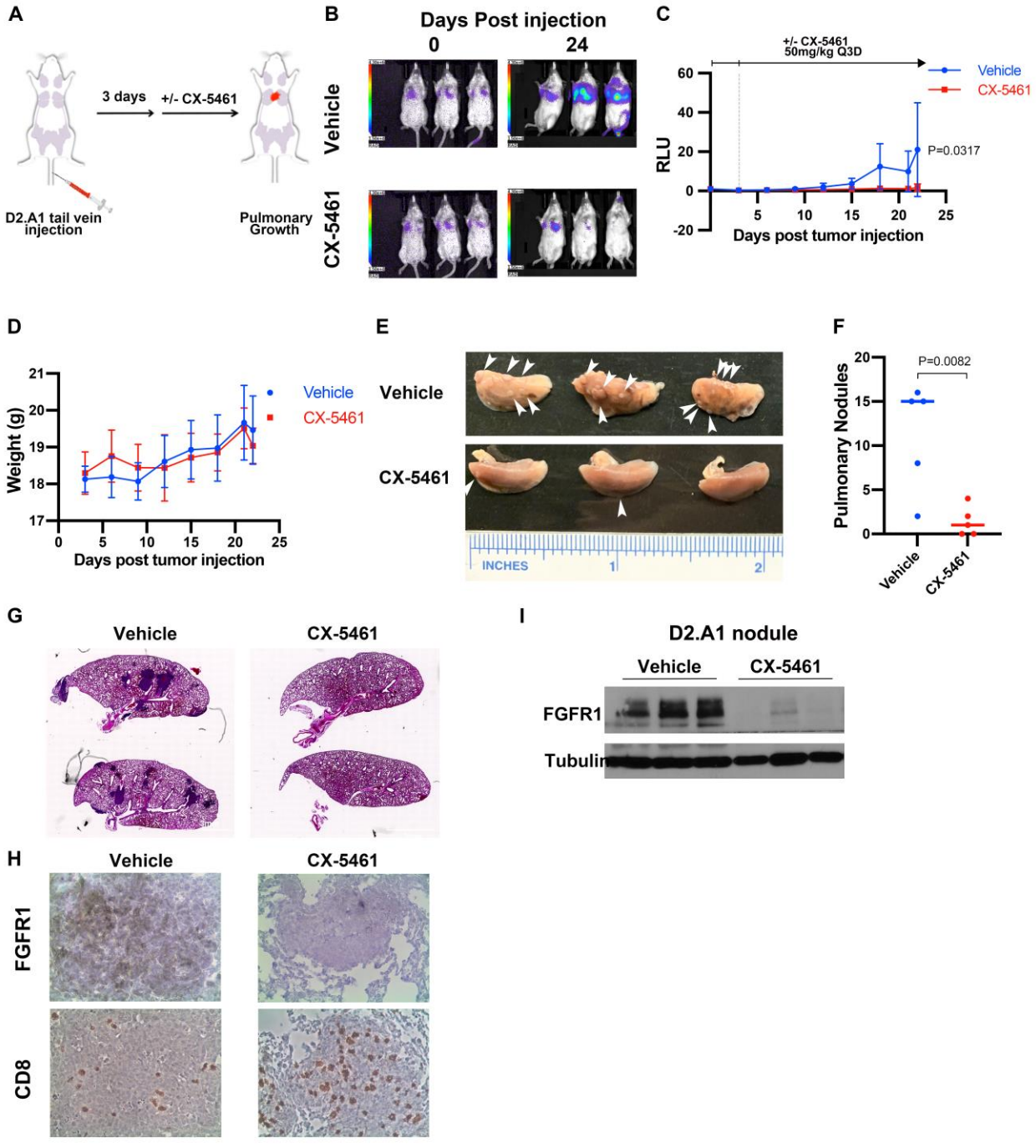

4.5 Conclusion

Though FGFR TKIs have been effective in a variety of cancer types harboring FGFR mutation, BC patients with FGFR1 amplification showed limited responses to FGFR TKI therapies (Nogova et al., 2017). From our 3D spheroid results, we also identified that FGFR TKIs can't eradicate dormant BC cells. This finding implicated that FGFR1 kinase-independent function may contribute to the FGFR TKI resistance in BC. Therefore, we explored different therapeutic avenues to overcome this resistance. G4 ligands have attracted great attention in research for cancer therapies due to their success in targeting oncogene expression via stabilizing G4 structure in promoter regions (Chen et al., 2012; Siddiqui-Jain et al., 2002). After analyzing FGFR1 promoter region, we determined potential G4 forming sequences in FGFR1 promoter. Therefore, we hypothesize that G4 ligands are able to target FGFR1 expression and thus cause sustained signaling inhibition and hinder FGFR1 kinase-independent function. Here, we presented data showing G4 stabilizer treatment as a promising therapeutic approach for targeting MBC.

In this study, using the CD analyses, we determined two sequences, S2 and S4, forming G4 secondary structures *in vitro*. Therefore, we applied different G4 ligands in FGFR1 expressing, metastatic and drug-resistant cell lines. This approach resulted in dramatic downregulation of FGFR1 at the protein level after treatment of TMPyP4 which is a G4 ligand. TMPyP4 also interfered with ectopic FGFR1 expression and EMT-driven FGFR1 expression. However, TMPyP4 only affects FGFR1 protein expression but not FGFR1 mRNA level. We further performed the luciferase reporter assay to investigate if TMPyP4 regulates the activity of FGFR1 proximal promoter region containing G4 forming sequence S4 in MCF-10A overexpressing Twist cells. The results showed that TMPyP4 had no effect on Twist-induced FGFR1 promoter activity. Overall, these data suggested that downregulation of FGFR1 expression caused by TMPyP4 is not due to transcriptional regulation.

Due to the limitation of TMPyP4 in animal studies, we next explored G4 stabilizers which have been entering clinical trials. CX-5461 is the G4 ligand which is under evaluation in phase I clinical trial. We first determined if CX-5461 affects the activities of FGFR1 promoter regions containing S2 or S4. The data showed that CX-5461 constantly suppressed FGFR1 promoter region with S4, which implied that CX-5461 stabilizes G4 structures in S4 sequences. Moreover, CX-5461 effectively blocked FGFR1 expression and inhibited FGFR1 downstream signaling,

resulting in eradication of dormant breast cancer cells. Finally, in vivo application of CX-5461 reduced FGFR1 expression, blocked pulmonary tumor formation, and prolonged animal survival.

In sum, our findings indicated that targeting FGFR1 expression through G4 stabilization may represent an improved therapeutic strategy for MBC. Furthermore, the results also implicated that the combination therapy of G4 ligands and ICB would be a promising therapy for MBC patients. Moreover, we have demonstrated the potential G4 forming sequences in FGFR1 promoter regions. For detailed G4 structures in FGFR1 promoter region, biophysical analyses will be critical to uncover the precise structures and this finding will benefit the advanced development of G4 stabilizers.

CHAPTER 5. DISCUSSION AND FUTURE DIRECTIONS

5.1 Limitation of FGFR TKIs in metastatic breast cancer

FGFR1 plays various roles in breast cancer progression, leading to cell survival, angiogenesis, migration and invasion (Sobhani, Fan, O. Flores-Villanueva, Generali, & Li, 2020). Amplification of the *FGFR1* gene locus correlates with decreased breast cancer patient survival. Hence, FGFR-targeted kinase inhibitors have been evaluated in MBC (Perez-Garcia, Muñoz-Couselo, Soberino, Racca, & Cortes, 2018). However, unlike other cancers that demonstrate robust responses to these drugs, MBC patient response to FGFR kinase inhibitors is limited (Nogova et al., 2017). Consistent with these clinical data our examination of different FGFR kinase inhibitors in mouse models of MBC, indicates that disseminated tumors can quickly overcome FGFR kinase inhibition leading to disease progression.

Intrinsic and acquired resistance to kinase inhibitors is a major clinical challenge in cancer (Santolla & Maggiolini, 2020). FGFR seems to be no exception as studies indicate that mutation of the active site and other epigenetic mechanisms are at play in resistance to FGFR-targeted therapies (Y. Li et al., 2021; Yue et al., 2021). Herein, we demonstrate that FGFR kinase inhibitors can temporarily suppress MBC growth, but more prolonged effects are not achievable and higher dosages are limited by toxicity. Indeed, FGFR kinase inhibitors, AZD4547 and erdafitinib, cause weight reduction of mice, and numerous toxicities have been reported in human patients (Akhand et al., 2020). Furthermore, our lab has identified that some FGFR kinase inhibitors can also have inhibitory effects on T-cell function, limiting anti-tumor immunity (Akhand et al., 2020). In this study, we also show that FGFR kinase inhibitors fail to target dormant tumor cells leaving a population of cells capable of reestablishing disease upon cessation of treatment. While the mechanistic explanations for these shortcomings of FGFR kinase targeting are not definitively defined, FGFR1 nuclear translocation can contribute to oncotherapy resistance (Y. Zhou et al., 2020). Hence, developing a therapeutic approach which can overcome FGFR-TKI resistance could benefit MBC patients.

5.2 Mechanisms of G-quadruplex ligands targeting FGFR1 expression

Through our screening of various G-quadruplex stabilizers, we found that TMPyP4, but not its structural analogue, effectively abrogates FGFR1 protein expression without affecting FGFR1 transcription. Therefore, we conclude that G4s are forming in the FGFR1 ORF and stabilization of these structures limits translation. Indeed, regulation of translation via stabilization of mRNA G4 is a known mechanism of TMPyP4-mediated gene repression (Dabral, Babu, Zareie, & Verma, 2019). Consistent with this notion, TMPyP4 not only reduces endogenous FGFR1 expression but also impedes FGFR1 expression from ectopic expression constructs. Despite these findings, direct evidence of G4 formation by FGFR1 ORF RNA sequence remains to be demonstrated. We also demonstrated the G4 stabilization reduces EMT-driven FGFR1 expression. Extensive studies from our group demonstrate the importance of EMT in facilitating FGFR translocation and the feedback of FGFR on stabilization of a mesenchymal, drug-resistant cell population (Abdullah et al., 2020; W. S. Brown, L. Tan, et al., 2016). Therefore, use of G4 stabilizing ligands presents a potent strategy to target both the kinase-dependent and kinase-independent functions of FGFR1.

CX-5461 is a clinical G4 stabilizer with minimal toxicities (Xu et al., 2017). CX-5461 has also been reported as an RNA polymerase I inhibitor through binding ribosomal DNA, interfering the binding affinity of the SL1 pre-initiation complex and RNA polymerase I complex toward rDNA promoters (Drygin et al., 2011; Khot et al., 2019). However, G4s are enriched in rDNA (Datta, Pollock, Kormuth, & Brosh Jr, 2021). CX-5461 also has been shown to stabilize G4 structures which presumably that CX-5461 exerts its G4 stabilization function to interact with rDNA that is prone to from G4, and then inhibits RNA polymerase I activity (Xu et al., 2017). Our findings demonstrate that CX-5461 suppresses the activity of FGFR1 promoter with G4 forming sequences. Furthermore, the results indicating that enhanced inhibition of FGFR1 expression as compared to other TKIs both *in vitro* and *in vivo* suggest the impact of CX-5461 on FGFR1 expression is driven via G4 binding, but this conclusion remains to be definitively determined. Here, we identified that there are two G4 forming sequences in FGFR1 promoter region interacting with CX-5461, S2 and S4. S2 is the sequence only specific in human FGFR1 promoter region. However, S4 is the conserved sequence in both human and mouse FGFR1 promoter regions. The results also determine that CX-5461 significantly reduces the activities of FGFR1 promoter regions including S4 G4 forming sequence. CX-5461 targets FGFR1 in both human and mouse

breast cancer cell lines. Hence, CX-5461 is highly likely to stabilize the S4 G4 motif and hinder FGFR1 expression.

Similar to targeted inhibition of kinase activity, reduction of FGFR1 expression by G4 stabilizers suppressed ligand-induced downstream signaling. However, we found that D2.OR spheroids treated FGFR kinase inhibitors grow robustly after they are returned to a 2D culture environment. This suggests that restricted inhibition of FGFR kinase activity is not sufficient to eliminate dormant cells. In contrast, abrogating FGFR1 expression via CX-5461 effectively blocked spheroid growth and reduced dormant cell viability. The detailed of mechanism how FGFR kinase-independent function facilitates drug resistance and MBC progression still needs to be clarified. However, previous studies suggest synergy in targeting MYC in combination with FGFR (Hu et al., 2018). The well-established role of G4 in regulating MYC expression could provide a mechanistic basis for the use of CX-5461 or other G4-targeted compounds in FGFR-driven MBC (Chaudhuri, Bhattacharya, Dash, & Bhattacharya, 2021).

5.3 A combination therapy of G-quadruplex stabilizer and immune checkpoint blockade to metastatic tumors

FGFR has been identified to play a key role in modulating the immune microenvironment in various primary cancers (Palakurthi et al., 2019; T. Ye et al., 2014). Recent research has started to determine the critical mechanisms by which TKIs, which originally developed to target tumor cells, can have an impact on immune cell recruitment and function (Goel et al., 2017). However, the detailed mechanism how FGFR signaling modulates the metastatic microenvironment, especially the pulmonary region which is the common site of BC metastasis, is not fully elucidated (Jin et al., 2018). Previously we have reported that the systemically dormant phenotype of the 4T07 cell model only manifested in immune competent BALB/c mice and is under control of the function $CD8^+$ cells (Akhand et al., 2020). Therefore, the systemically dormant immune-excluded 4T07 tumors serve as an ideal model to investigate the immune regulation of the pulmonary metastatic niche following the inhibition of FGFR signaling.

Our lab has identified that mice having competent immune system show prolonged survival with the inhibition of FGFR kinase activity in 4T07 pulmonary tumor models. This result implicated the impact of FGFR signaling on the constitution of the tumor surrounding immune microenvironments in the pulmonary sites. Furthermore, the data showed that inhibition of FGFR

kinase activity gives rise to the increased $CD8^+$ T cells numbers within the metastasis niche. However, FIIN4, a covalent FGFR TKI, presented potential off-target inhibitions of T cell receptor (TCR) signaling (Akhand et al., 2020). Hence, there is a critical need to optimize the combination therapy of FGFR targeted therapy and ICB in MBC.

Here we showed that reduction of FGFR1 expression through G-quadruplex ligand, CX-5461, lead to an elevated level of $CD8^+$ T cells in lung nodules. Consistent with our previous result, genetic depletion of FGFR1 expression via shRNA also increase $CD8^+$ T cell infiltration in pulmonary region (Akhand et al., 2020). Though the impact of CX5461 on T cell function still needs to be validated, our study reveals the potential of promising combination therapy of G4 ligands and ICB which could benefit patients with MBC.

5.4 Summary

In this dissertation work, our study presents a novel therapeutic approach of targeting FGFR1. Consistent with clinical observations our evaluation of FGFR kinase inhibitors validates FGFR-TKI resistance in MBC. Furthermore, we present G4 stabilization as an effective epigenetic approach to block both constitutive and EMT-driven FGFR1 expression. Moreover, we identify potential G4 forming sequences in FGFR1 promoter region which can be stabilized via the G4 ligand, CX-5461. The use of biochemical and functional assays indicates that suppression of FGFR1 expression limits downstream signaling and abrogates dormant cell survival. Our study strongly supports evaluation of CX-5461 or similar G4-targeting agents as therapeutics for treatment of MBC patients, particularly those harboring FGFR1 amplification.

APPENDIX: SUPPLEMENTARY TABLES & FIGURES

Appendix Table 1 Drug and Reagent

Drug/Reagent	Supplier	Catalog No / formulation
AZD4547	Selleckchem	S2801
Erdafitinib	Selleckchem	S8401 Formulation: 0.5% Hydroxypropyl Methylcellulose
FIIN4	Achemtek	0107-000063
Futibatinib	Medkoo	1448169-71-8 Formulation: 0.5% Carboxymethylcellulose
TMPyP2	Frontier	T40846
TMPyP4	Cayman	18474
CX-5461	AdooQ	A11065
Quarfloxin	MCE	HY-14776
Berberine GQC-5 Quindoline	Professor Danzhou Yang at Purdue University	
Basic FGF (FGF2), Human	GoldBio	1140-02-10
Cultrex® RGF BME PathClear®	Sigma	3433-005-01 Concentration: 17.05 mg/ml
D-Luciferin, Potassium Salt	GoldBio	LUCK-100

Appendix Table 2 Primers

Target	Application	Sequence (5' to 3')
mFGFR1	Real time PCR-Sense	5'- CACCGCTCTACCTGGAGATCATTA
mFGFR1	Real time PCR-Antisense	5'- TTGGTGCCGCTCTTCATCTT
hFGFR1	Real time PCR-Sense	5'- CGCCCCTGTACCTGGAGATCATCA
hFGFR1	Real time PCR-Antisense	5'- TTGGTACCACTCTTCATCTT
FGFR1α	Real time PCR-Sense	5'- GACTCCGGCCTCTATGCTTG
FGFR1α	Real time PCR-Antisense	5'- CTACGGGCATACGGTTTGGT
FGFR1β	Real time PCR-Sense	5'- ACCTTGCCTGAACAAGATGCT
FGFR1β	Real time PCR-Antisense	5'- CTACGGGCATACGGTTTGGT
hFGFR1 Promoter	PCR for cloning-Sense	5'-CTCGGCGGCCAAGCTGCTCTTGGC TCCTTCCTGG
hFGFR1 Promoter	PCR for cloning-Antisense	5'-CCGGATTGCCAAGCTGCTGCCGCC CGC
mGAPDH	Real time PCR-Sense	5'-CAACTTTGGCATTGTGGAAGGGCTC
mGAPDH	Real time PCR-Antisense	5'-GCAGGGATGATGTTCTGGGCAGC
hGAPDH	Real time PCR-Sense	5'-TGCACCACCAACTGCTTAGC
hGAPDH	Real time PCR-Antisense	5'-GGCATGGACTGTGGTCATGAG

Appendix Figure 1 Inhibition of FGFR1 glycosylation

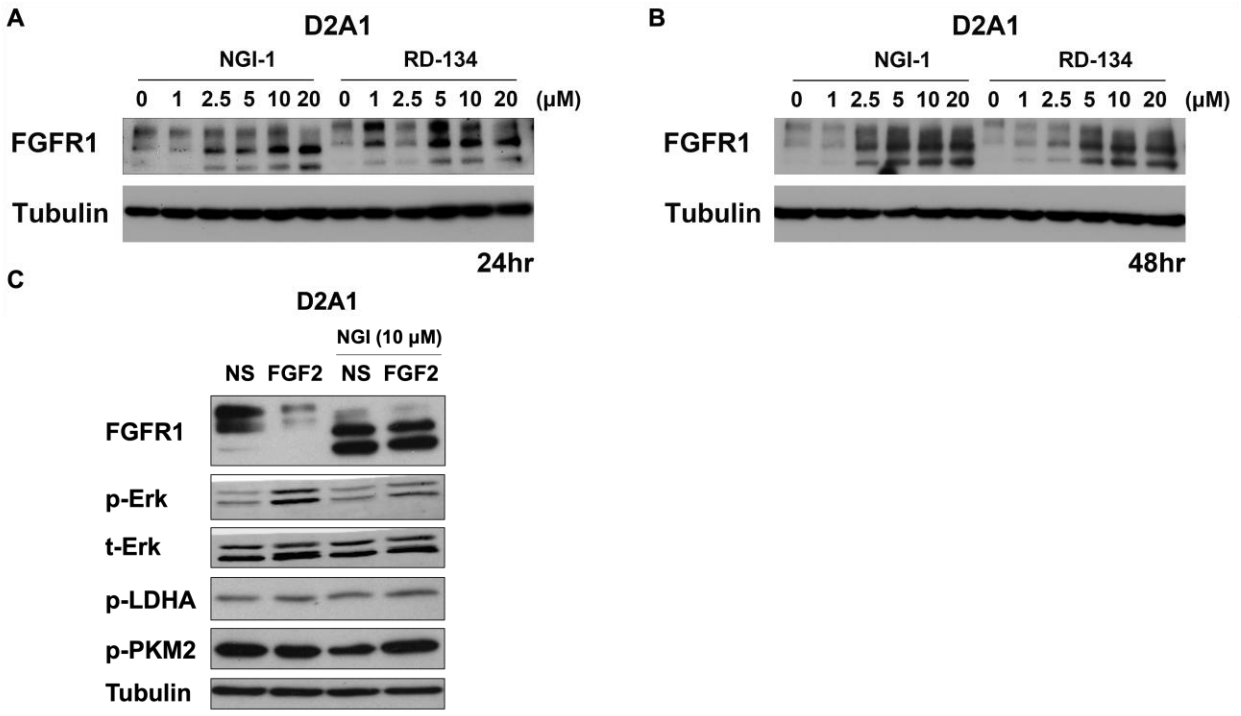

Pharmacological inhibition of FGFR1 glycosylation suppresses FGFR1 downstream signaling. A, B. Immunoblot analyses for FGFR1 in D2.A1 cells upon treatment with the indicated concentrations of NGI and RD-134 which is an NGI derivate with higher solubility for 24 and 48 hours. C. Phosphorylation of ERK1/2 (pErk) induced upon FGF2 stimulation (20 ng/ml for 10 minutes) was also analyzed upon NGI pre-treatment. Expression of total ERK1/2 (tErk) served as a loading control.

Appendix Figure 2 Dox-inducible Snail expression in NMuMG cells

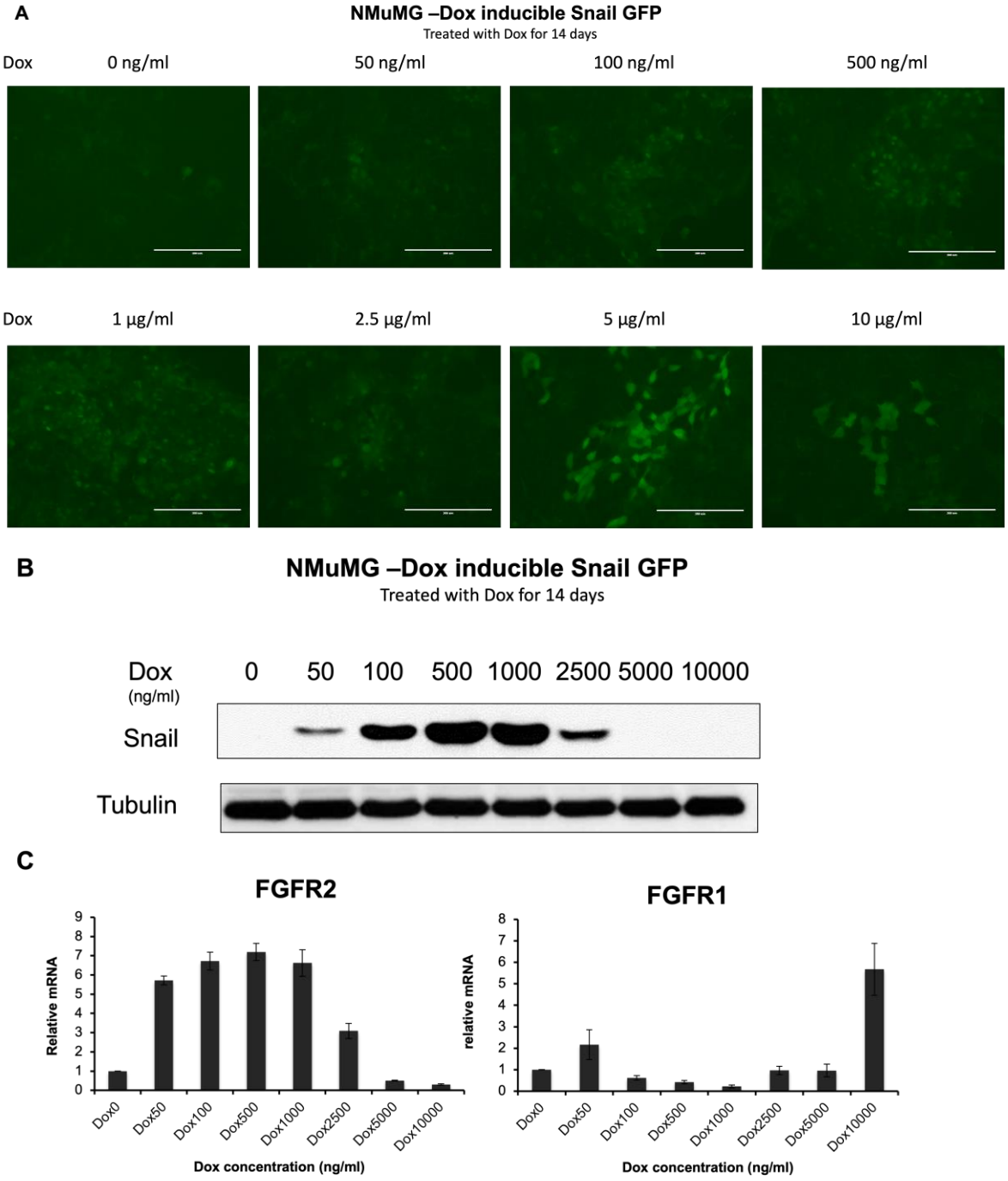

Dox-inducible Snail-GFP expression in NMuMG cells.
A. Snail-GFP expression with different concentration of Dox treatment for 14 days. B. Immunoblot analyses for Snail expression in NMuMG cells upon treatment with the indicated concentrations of Dox for 14 days. C. RT-PCR for FGFR1 and FGFR2 transcript levels after stimulation with the indicated concentration of Dox for 14 days. Data are normalized to FGFR1 or FGFR2 levels in the control cells for each treatment and are the mean ± s.e.m. of three independent experiments.

Appendix Figure 3 Dox-inducible hZeb-1 expression in NMuMG cells

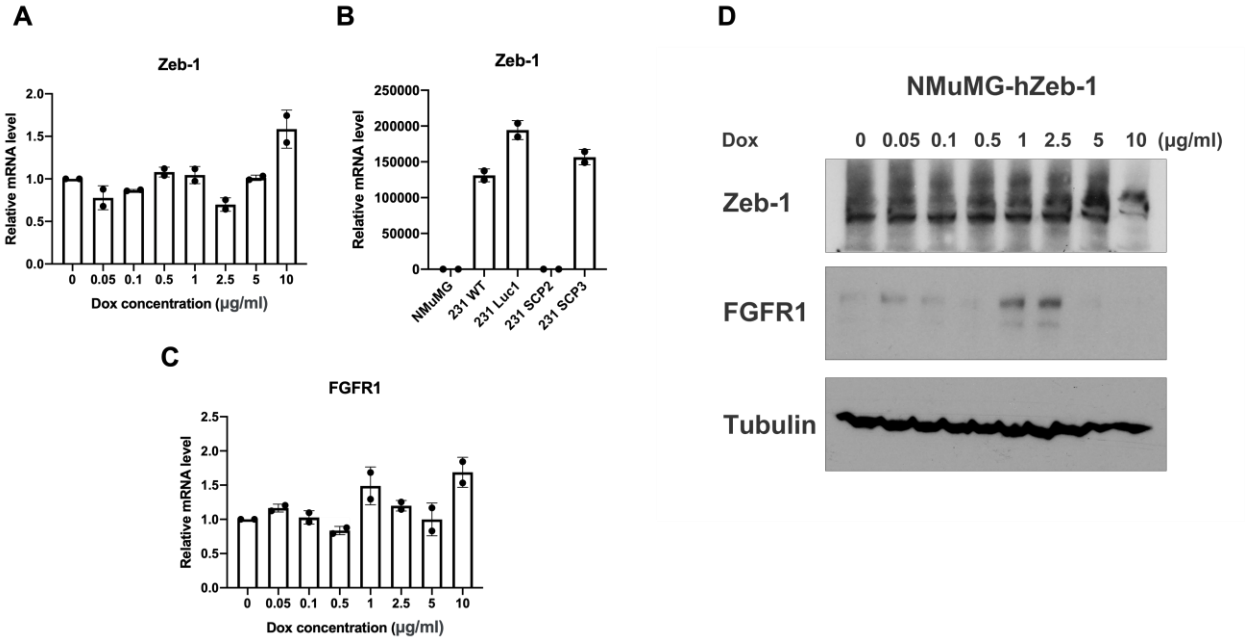

Dox-inducible hZeb-1 expression in NMuMG cells.

A, C. RT-PCR for Zeb-1 and FGFR1 transcript levels after stimulation with the indicated concentration of Dox for 14 days. Data are normalized to Zeb-1 or FGFR1 levels in the control cells for each treatment and are the mean ± s.e.m. of two independent experiments. B. RT-PCR for Zeb-1 transcript levels in different cell lines. Data are normalized to Zeb-1 levels in the NMuMG cells and are the mean ± s.e.m. of two independent experiments. D. Immunoblot analyses for Zeb-1 and FGFR1 expression in NMuMG cells upon treatment with the indicated concentrations of Dox for 14 days.

REFERENCES

Abdullah, A., Akhand, S. S., Paez, J. S. P., Brown, W., Pan, L., Libring, S., . . . Wendt, M. K. (2020). Epigenetic targeting of neuropilin-1 prevents bypass signaling in drug-resistant breast cancer. *Oncogene*. doi:10.1038/s41388-020-01530-6

Abou-Alfa, G. K., Sahai, V., Hollebecque, A., Vaccaro, G. M., Melisi, D., Al-Rajabi, R. M. d. T., . . . Vogel, A. (2021). Pemigatinib for previously treated locally advanced/metastatic cholangiocarcinoma (CCA): Update of FIGHT-202. *Journal of Clinical Oncology, 39*(15_suppl), 4086-4086. doi:10.1200/JCO.2021.39.15_suppl.4086

Akhand, S. S., Liu, Z., Purdy, S. C., Abdullah, A., Lin, H., Cresswell, G. M., . . . Wendt, M. (2020). Pharmacologic Inhibition of FGFR Modulates the Metastatic Immune Microenvironment and Promotes Response to Immune Checkpoint Blockade. *Cancer Immunology Research*, canimm.0235.0202. doi:10.1158/2326-6066.cir-20-0235

Ali, R., Brown, W., Purdy, S. C., Davisson, V. J., & Wendt, M. K. (2018). Biased signaling downstream of epidermal growth factor receptor regulates proliferative versus apoptotic response to ligand. *Cell Death & Disease, 9*(10). doi:10.1038/s41419-018-1034-7

Amato, J., Miglietta, G., Morigi, R., Iaccarino, N., Locatelli, A., Leoni, A., . . . Randazzo, A. (2020). Monohydrazone Based G-Quadruplex Selective Ligands Induce DNA Damage and Genome Instability in Human Cancer Cells. *Journal of Medicinal Chemistry, 63*(6), 3090-3103. doi:10.1021/acs.jmedchem.9b01866

Asamitsu, S., Obata, S., Yu, Z., Bando, T., & Sugiyama, H. (2019). Recent Progress of Targeted G-Quadruplex-Preferred Ligands Toward Cancer Therapy. *Molecules, 24*(3), 429. doi:10.3390/molecules24030429

Belov, A. A., & Mohammadi, M. (2013). Molecular Mechanisms of Fibroblast Growth Factor Signaling in Physiology and Pathology. *Cold Spring Harbor Perspectives in Biology, 5*(6), a015958-a015958. doi:10.1101/cshperspect.a015958

Bockhorn, M., Jain, R. K., & Munn, L. L. (2007). Active versus passive mechanisms in metastasis: do cancer cells crawl into vessels, or are they pushed? *The Lancet Oncology, 8*(5), 444-448. doi:10.1016/s1470-2045(07)70140-7

Brown, W. S., Akhand, S. S., & Wendt, M. K. (2016). FGFR signaling maintains a drug persistent cell population following epithelial-mesenchymal transition. *Oncotarget, 7*(50), 83424-83436. doi:10.18632/oncotarget.13117

Brown, W. S., Akhand, S. S., & Wendt, M. K. (2016). FGFR signaling maintains a drug persistent cell population following epithelial-mesenchymal transition. *Oncotarget, 7*(50). doi:10.18632/oncotarget.13117

Brown, W. S., Tan, L., Smith, A., Gray, N. S., & Wendt, M. K. (2016). Covalent Targeting of Fibroblast Growth Factor Receptor Inhibits Metastatic Breast Cancer. *Molecular Cancer Therapeutics, 15*(9), 2096-2106. doi:10.1158/1535-7163.mct-16-0136

Burslem, G. M., Smith, B. E., Lai, A. C., Jaime-Figueroa, S., McQuaid, D. C., Bondeson, D. P., . . . Crews, C. M. (2018). The Advantages of Targeted Protein Degradation Over Inhibition: An RTK Case Study. *Cell Chemical Biology, 25*(1), 67-77.e63. doi:10.1016/j.chembiol.2017.09.009

Chae, Y. K., Ranganath, K., Hammerman, P. S., Vaklavas, C., Mohindra, N., Kalyan, A., . . . Giles, F. J. (2017). Inhibition of the fibroblast growth factor receptor (FGFR) pathway: the current landscape and barriers to clinical application. *Oncotarget, 8*(9). doi:10.18632/oncotarget.14109

Chambers, V. S., Marsico, G., Boutell, J. M., Di Antonio, M., Smith, G. P., & Balasubramanian, S. (2015). High-throughput sequencing of DNA G-quadruplex structures in the human genome. *Nature Biotechnology, 33*(8), 877-881. doi:10.1038/nbt.3295

Chaudhuri, R., Bhattacharya, S., Dash, J., & Bhattacharya, S. (2021). Recent Update on Targeting c-MYC G-Quadruplexes by Small Molecules for Anticancer Therapeutics. *Journal of Medicinal Chemistry, 64*(1), 42-70. doi:10.1021/acs.jmedchem.0c01145

Chen, Y., Agrawal, P., Brown, R. V., Hatzakis, E., Hurley, L., & Yang, D. (2012). The Major G-Quadruplex Formed in the Human Platelet-Derived Growth Factor Receptor β Promoter Adopts a Novel Broken-Strand Structure in K+ Solution. *Journal of the American Chemical Society, 134*(32), 13220-13223. doi:10.1021/ja305764d

Cheng, C. L., Thike, A. A., Tan, S. Y. J., Chua, P. J., Bay, B. H., & Tan, P. H. (2015). Expression of FGFR1 is an independent prognostic factor in triple-negative breast cancer. *Breast Cancer Research and Treatment, 151*(1), 99-111. doi:10.1007/s10549-015-3371-x

Chioni, A.-M., & Grose, R. (2012). FGFR1 cleavage and nuclear translocation regulates breast cancer cell behavior. *197*(6), 801-817. doi:10.1083/jcb.201108077

Cogoi, S., & Xodo, L. E. (2006). G-quadruplex formation within the promoter of the KRAS proto-oncogene and its effect on transcription. *Nucleic Acids Research, 34*(9), 2536-2549. doi:10.1093/nar/gkl286

Coleman, S. J., Chioni, A. M., Ghallab, M., Anderson, R. K., Lemoine, N. R., Kocher, H. M., & Grose, R. P. (2014). Nuclear translocation of FGFR1 and FGF2 in pancreatic stellate cells facilitates pancreatic cancer cell invasion. *6*(4), 467-481. doi:10.1002/emmm.201302698

Cromm, P. M., Samarasinghe, K. T. G., Hines, J., & Crews, C. M. (2018). Addressing Kinase-Independent Functions of Fak via PROTAC-Mediated Degradation. *J Am Chem Soc*. doi:10.1021/jacs.8b08008

Dabral, P., Babu, J., Zareie, A., & Verma, S. C. (2019). LANA and hnRNP A1 Regulate the Translation of LANA mRNA through G-Quadruplexes. *Journal of Virology, 94*(3). doi:10.1128/jvi.01508-19

Dai, S., Zhou, Z., Chen, Z., Xu, G., & Chen, Y. (2019). Fibroblast Growth Factor Receptors (FGFRs): Structures and Small Molecule Inhibitors. *Cells, 8*(6), 614. doi:10.3390/cells8060614

Datta, A., Pollock, K. J., Kormuth, K. A., & Brosh Jr, R. M. (2021). G-Quadruplex Assembly by Ribosomal DNA: Emerging Roles in Disease Pathogenesis and Cancer Biology. *Cytogenetic and Genome Research, 161*(6-7), 285-296. doi:10.1159/000516394

Del Villar-Guerra, R., Trent, J. O., & Chaires, J. B. (2018). G-Quadruplex Secondary Structure Obtained from Circular Dichroism Spectroscopy. *Angewandte Chemie International Edition, 57*(24), 7171-7175. doi:10.1002/anie.201709184

Dillekås, H., Rogers, M. S., & Straume, O. (2019). Are 90% of deaths from cancer caused by metastases? *Cancer Medicine, 8*(12), 5574-5576. doi:10.1002/cam4.2474

Drago, J. Z., Formisano, L., Juric, D., Niemierko, A., Servetto, A., Wander, S. A., . . . Bardia, A. (2019). FGFR1 Amplification Mediates Endocrine Resistance but Retains TORC Sensitivity in Metastatic Hormone Receptor–Positive (HR+) Breast Cancer. *Clinical Cancer Research, 25*(21), 6443-6451. doi:10.1158/1078-0432.ccr-19-0138

Drygin, D., Lin, A., Bliesath, J., Ho, C. B., O'Brien, S. E., Proffitt, C., . . . Rice, W. G. (2011). Targeting RNA Polymerase I with an Oral Small Molecule CX-5461 Inhibits Ribosomal RNA Synthesis and Solid Tumor Growth. *Cancer Research, 71*(4), 1418-1430. doi:10.1158/0008-5472.can-10-1728

Drygin, D., Siddiqui-Jain, A., O'Brien, S., Schwaebe, M., Lin, A., Bliesath, J., . . . Rice, W. G. (2009). Anticancer Activity of CX-3543: A Direct Inhibitor of rRNA Biogenesis. *Cancer Research, 69*(19), 7653-7661. doi:10.1158/0008-5472.can-09-1304

Eddy, J., & Maizels, N. (2008). Conserved elements with potential to form polymorphic G-quadruplex structures in the first intron of human genes. *Nucleic Acids Research, 36*(4), 1321-1333. doi:10.1093/nar/gkm1138

Elbauomy Elsheikh, S., Green, A. R., Lambros, M. B., Turner, N. C., Grainge, M. J., Powe, D., . . . Reis-Filho, J. S. (2007). FGFR1 amplification in breast carcinomas: a chromogenic in situhybridisation analysis. *Breast Cancer Research, 9*(2), R23. doi:10.1186/bcr1665

Endoh, T., Kawasaki, Y., & Sugimoto, N. (2013). Stability of RNA quadruplex in open reading frame determines proteolysis of human estrogen receptor. *41*(12), 6222-6231. doi:10.1093/nar/gkt286

Fares, J., Fares, M. Y., Khachfe, H. H., Salhab, H. A., & Fares, Y. (2020). Molecular principles of metastasis: a hallmark of cancer revisited. *Signal Transduction and Targeted Therapy, 5*(1). doi:10.1038/s41392-020-0134-x

Fay, M. M., Lyons, S. M., & Ivanov, P. (2017). RNA G-Quadruplexes in Biology: Principles and Molecular Mechanisms. *J Mol Biol, 429*(14), 2127-2147. doi:10.1016/j.jmb.2017.05.017

Fouquerel, E., Parikh, D., & Opresko, P. (2016). DNA damage processing at telomeres: The ends justify the means. *DNA Repair (Amst), 44*, 159-168. doi:10.1016/j.dnarep.2016.05.022

Fujiwara, N., Mazzola, M., Cai, E., Wang, M., & Cave, J. W. (2015). TMPyP4, a Stabilizer of Nucleic Acid Secondary Structure, Is a Novel Acetylcholinesterase Inhibitor. *10*(9), e0139167. doi:10.1371/journal.pone.0139167

The global challenge of cancer. (2020). *Nature Cancer, 1*(1), 1-2. doi:10.1038/s43018-019-0023-9

Goel, S., Decristo, M. J., Watt, A. C., Brinjones, H., Sceneay, J., Li, B. B., . . . Zhao, J. J. (2017). CDK4/6 inhibition triggers anti-tumour immunity. *Nature, 548*(7668), 471-475. doi:10.1038/nature23465

Gomis, R. R., & Gawrzak, S. (2017). Tumor cell dormancy. *Molecular Oncology, 11*(1), 62-78. doi:10.1016/j.molonc.2016.09.009

Goyal, L., Shi, L., Liu, L. Y., Fece De La Cruz, F., Lennerz, J. K., Raghavan, S., . . . Bardeesy, N. (2019). TAS-120 Overcomes Resistance to ATP-Competitive FGFR Inhibitors in Patients with FGFR2 Fusion–Positive Intrahepatic Cholangiocarcinoma. *Cancer Discovery, 9*(8), 1064-1079. doi:10.1158/2159-8290.cd-19-0182

Grand, C. L., Han, H., Munoz, R. M., Weitman, S., Von Hoff, D. D., Hurley, L. H., & Bearss, D. J. (2002). The cationic porphyrin TMPyP4 down-regulates c-MYC and human telomerase reverse transcriptase expression and inhibits tumor growth in vivo. *Mol Cancer Ther, 1*(8), 565-573. Retrieved from https://www.ncbi.nlm.nih.gov/pubmed/12479216

Grand, C. L., Powell, T. J., Nagle, R. B., Bearss, D. J., Tye, D., Gleason-Guzman, M., & Hurley, L. H. (2005). Mutations in the G-quadruplex silencer element and their relationship to c-MYC overexpression, NM23 repression, and therapeutic rescue. *Proc Natl Acad Sci U S A, 102*(2), 516. doi:10.1073/pnas.0408999101

Gu, S., Cui, D., Chen, X., Xiong, X., & Zhao, Y. (2018). PROTACs: An Emerging Targeting Technique for Protein Degradation in Drug Discovery. *BioEssays, 40*(4), 1700247. doi:10.1002/bies.201700247

Guilbaud, G., Murat, P., Recolin, B., Campbell, B. C., Maiter, A., Sale, J. E., & Balasubramanian, S. (2017). Local epigenetic reprogramming induced by G-quadruplex ligands. *Nature Chemistry, 9*(11), 1110-1117. doi:10.1038/nchem.2828

Han, F. X., Wheelhouse, R. T., & Hurley, L. H. (1999). Interactions of TMPyP4 and TMPyP2 with Quadruplex DNA. Structural Basis for the Differential Effects on Telomerase Inhibition. *Journal of the American Chemical Society, 121*(15), 3561-3570. doi:10.1021/ja984153m

Hanahan, D., & Robert. (2011). Hallmarks of Cancer: The Next Generation. *Cell, 144*(5), 646-674. doi:10.1016/j.cell.2011.02.013

Hanahan, D., & Weinberg, R. A. (2000). The Hallmarks of Cancer. *Cell, 100*(1), 57-70. doi:10.1016/s0092-8674(00)81683-9

Harding, T. C., Long, L., Palencia, S., Zhang, H., Sadra, A., Hestir, K., . . . Baker, K. P. (2013). Blockade of nonhormonal fibroblast growth factors by FP-1039 inhibits growth of multiple types of cancer. *Sci Transl Med, 5*(178), 178ra139. doi:10.1126/scitranslmed.3005414

Heerboth, S., Housman, G., Leary, M., Longacre, M., Byler, S., Lapinska, K., . . . Sarkar, S. (2015). EMT and tumor metastasis. *Clinical and Translational Medicine, 4*(1), 6. doi:10.1186/s40169-015-0048-3

Hoy, S. M. (2020). Pemigatinib: First Approval. *Drugs, 80*(9), 923-929. doi:10.1007/s40265-020-01330-y

Hu, T., Wu, Q., Chong, Y., Qin, H., Poole, C. J., Van Riggelen, J., . . . Cowell, J. K. (2018). FGFR1 fusion kinase regulation of MYC expression drives development of stem cell leukemia/lymphoma syndrome. *Leukemia, 32*(11), 2363-2373. doi:10.1038/s41375-018-0124-y

Huang, L., & Fu, L. (2015). Mechanisms of resistance to EGFR tyrosine kinase inhibitors. *Acta Pharm Sin B, 5*(5), 390-401. doi:10.1016/j.apsb.2015.07.001

Huppert, J. L., & Balasubramanian, S. (2007). G-quadruplexes in promoters throughout the human genome. *Nucleic Acids Research, 35*(2), 406-413. doi:10.1093/nar/gkl1057

Itoh, N., & Ornitz, D. M. (2004). Evolution of the Fgf and Fgfr gene families. *Trends Genet, 20*(11), 563-569. doi:10.1016/j.tig.2004.08.007

Jang, M. H., Kim, E. J., Choi, Y., Lee, H. E., Kim, Y. J., Kim, J. H., . . . Park, S. Y. (2012). FGFR1 is amplified during the progression of in situto invasive breast carcinoma. *Breast Cancer Research, 14*(4), R115. doi:10.1186/bcr3239

Jin, L., Han, B., Siegel, E., Cui, Y., Giuliano, A., & Cui, X. (2018). Breast cancer lung metastasis: Molecular biology and therapeutic implications. *Cancer Biology & Therapy, 19*(10), 858-868. doi:10.1080/15384047.2018.1456599

Julien, S., Puig, I., Caretti, E., Bonaventure, J., Nelles, L., Van Roy, F., . . . Larue, L. (2007). Activation of NF-κB by Akt upregulates Snail expression and induces epithelium mesenchyme transition. *Oncogene, 26*(53), 7445-7456. doi:10.1038/sj.onc.1210546

Kalyukina, M., Yosaatmadja, Y., Middleditch, M. J., Patterson, A. V., Smaill, J. B., & Squire, C. J. (2019). TAS-120 Cancer Target Binding: Defining Reactivity and Revealing the First Fibroblast Growth Factor Receptor 1 (FGFR1) Irreversible Structure. *ChemMedChem, 14*(4), 494-500. doi:10.1002/cmdc.201800719

Khot, A., Brajanovski, N., Cameron, D. P., Hein, N., Maclachlan, K. H., Sanij, E., . . . Harrison, S. J. (2019). First-in-Human RNA Polymerase I Transcription Inhibitor CX-5461 in Patients with Advanced Hematologic Cancers: Results of a Phase I Dose-Escalation Study. *Cancer Discovery, 9*(8), 1036-1049. doi:10.1158/2159-8290.cd-18-1455

Kim, N. (2019). The Interplay between G-quadruplex and Transcription. *Curr Med Chem, 26*(16), 2898-2917. doi:10.2174/0929867325666171229132619

Kosiol, N., Juranek, S., Brossart, P., Heine, A., & Paeschke, K. (2021). G-quadruplexes: a promising target for cancer therapy. *Molecular Cancer, 20*(1). doi:10.1186/s12943-021-01328-4

Li, Q., Jiang, B., Guo, J., Shao, H., Del Priore, I. S., Chang, Q., . . . Chandarlapaty, S. (2021). INK4 tumor suppressor proteins mediate resistance to CDK4/6 kinase inhibitors. *Cancer Discovery*, candisc.1726.1720. doi:10.1158/2159-8290.cd-20-1726

Li, Q., Xiang, J., Li, X., Chen, L., Xu, X., Tang, Y., . . . Xu, G. (2009). Stabilizing parallel G-quadruplex DNA by a new class of ligands: two non-planar alkaloids through interaction in lateral grooves. *Biochimie, 91*(7), 811-819. doi:10.1016/j.biochi.2009.03.007

Li, Q., Xiang, J.-F., Yang, Q.-F., Sun, H.-X., Guan, A.-J., & Tang, Y.-L. (2013). G4LDB: a database for discovering and studying G-quadruplex ligands. *Nucleic Acids Research, 41*(D1), D1115-D1123. doi:10.1093/nar/gks1101

Li, Y., Qiu, X., Wang, X., Liu, H., Geck, R. C., Tewari, A. K., . . . Brown, M. (2021). *FGFR inhibitor mediated dismissal of SWI/SNF complexes from YAP-dependent enhancers induces adaptive therapeutic resistance*. Cold Spring Harbor Laboratory. Retrieved from https://dx.doi.org/10.1101/2021.03.02.433446

Liu, L., Ye, T. H., Han, Y. P., Song, H., Zhang, Y. K., Xia, Y., . . . Yu, L. T. (2014). Reductions in Myeloid-Derived Suppressor Cells and Lung Metastases using AZD4547 Treatment of a Metastatic Murine Breast Tumor Model. *Cellular Physiology and Biochemistry, 33*(3), 633-645. doi:10.1159/000358640

Lopes, J., Piazza, A., Bermejo, R., Kriegsman, B., Colosio, A., Teulade-Fichou, M.-P., . . . Nicolas, A. (2011). G-quadruplex-induced instability during leading-strand replication. *The EMBO Journal, 30*(19), 4033-4046. doi:10.1038/emboj.2011.316

Loriot, Y., Necchi, A., Park, S. H., Garcia-Donas, J., Huddart, R., Burgess, E., . . . Siefker-Radtke, A. O. (2019). Erdafitinib in Locally Advanced or Metastatic Urothelial Carcinoma. *New England Journal of Medicine, 381*(4), 338-348. doi:10.1056/nejmoa1817323

M, Ruby, Rebecca, & Jean. (2016). EMT: 2016. *Cell, 166*(1), 21-45. doi:10.1016/j.cell.2016.06.028

Marcel, V., Tran, P. L. T., Sagne, C., Martel-Planche, G., Vaslin, L., Teulade-Fichou, M.-P., . . . Van Dyck, E. (2011). G-quadruplex structures in TP53 intron 3: role in alternative splicing and in production of p53 mRNA isoforms. *Carcinogenesis*, *32*(3), 271-278. doi:10.1093/carcin/bgq253

Markham, A. (2019). Erdafitinib: First Global Approval. *Drugs*, *79*(9), 1017-1021. doi:10.1007/s40265-019-01142-9

Meric, F., Lee, W.-P., Sahin, A., Zhang, H., Kung, H.-J., & Hung, M.-C. (2002). Expression Profile of Tyrosine Kinases in Breast Cancer. *Clinical Cancer Research*, *8*(2), 361-367. Retrieved from https://clincancerres.aacrjournals.org/content/clincanres/8/2/361.full.pdf

Montoya, J. J., Turnidge, M. A., Wai, D. H., Patel, A. R., Lee, D. W., Gokhale, V., . . . Azorsa, D. O. (2019). In vitro activity of a G-quadruplex-stabilizing small molecule that synergizes with Navitoclax to induce cytotoxicity in acute myeloid leukemia cells. *BMC Cancer*, *19*(1). doi:10.1186/s12885-019-6464-9

Muench, D., Rezzoug, F., Thomas, S. D., Xiao, J., Islam, A., Miller, D. M., & Sedoris, K. C. (2019). Quadruplex-forming oligonucleotide targeted to the VEGF promoter inhibits growth of non-small cell lung cancer cells. *PLOS ONE*, *14*(1), e0211046. doi:10.1371/journal.pone.0211046

Nogova, L., Sequist, L. V., Perez Garcia, J. M., Andre, F., Delord, J.-P., Hidalgo, M., . . . Wolf, J. (2017). Evaluation of BGJ398, a Fibroblast Growth Factor Receptor 1-3 Kinase Inhibitor, in Patients With Advanced Solid Tumors Harboring Genetic Alterations in Fibroblast Growth Factor Receptors: Results of a Global Phase I, Dose-Escalation and Dose-Expansion Stu. *Journal of Clinical Oncology*, *35*(2), 157-165. doi:10.1200/jco.2016.67.2048

Odonnell, P., Goldman, J. W., Gordon, M. S., Shih, K., Choi, Y. J., Lu, D., . . . Lam, E. T. (2012). 621 A Phase I Dose-escalation Study of MFGR1877S, a Human Monoclonal Anti-fibroblast Growth Factor Receptor 3 (FGFR3) Antibody, in Patients (pts) with Advanced Solid Tumors. *European Journal of Cancer*, *48*, 191-192. doi:10.1016/s0959-8049(12)72418-8

Ohnstad, H. O., Borgen, E., Falk, R. S., Lien, T. G., Aaserud, M., Sveli, M. A. T., . . . Naume, B. (2017). Prognostic value of PAM50 and risk of recurrence score in patients with early-stage breast cancer with long-term follow-up. *Breast Cancer Research*, *19*(1). doi:10.1186/s13058-017-0911-9

Onel, B., Lin, C., & Yang, D. (2014). DNA G-quadruplex and its potential as anticancer drug target. *Science China Chemistry*, *57*(12), 1605-1614. doi:10.1007/s11426-014-5235-3

Ornitz, D. M., & Itoh, N. (2015). The Fibroblast Growth Factor signaling pathway. *Wiley Interdisciplinary Reviews: Developmental Biology*, *4*(3), 215-266. doi:10.1002/wdev.176

Paeschke, K., Bochman, M. L., Garcia, P. D., Cejka, P., Friedman, K. L., Kowalczykowski, S. C., & Zakian, V. A. (2013). Pif1 family helicases suppress genome instability at G-quadruplex motifs. *Nature, 497*(7450), 458-462. doi:10.1038/nature12149

Palakurthi, S., Kuraguchi, M., Zacharek, S. J., Zudaire, E., Huang, W., Bonal, D. M., . . . Lorenzi, M. V. (2019). The Combined Effect of FGFR Inhibition and PD-1 Blockade Promotes Tumor-Intrinsic Induction of Antitumor Immunity. *Cancer Immunology Research, 7*(9), 1457-1471. doi:10.1158/2326-6066.cir-18-0595

Park, J., Kim, S., Joh, J., Remick, S. C., Miller, D. M., Yan, J., . . . Tse, W. (2016). MLLT11/AF1q boosts oncogenic STAT3 activity through Src-PDGFR tyrosine kinase signaling. *Oncotarget, 7*(28), 43960-43973. doi:10.18632/oncotarget.9759

Pastushenko, I., Brisebarre, A., Sifrim, A., Fioramonti, M., Revenco, T., Boumahdi, S., . . . Blanpain, C. (2018). Identification of the tumour transition states occurring during EMT. *Nature, 556*(7702), 463-468. doi:10.1038/s41586-018-0040-3

Perez-Garcia, J., Muñoz-Couselo, E., Soberino, J., Racca, F., & Cortes, J. (2018). Targeting FGFR pathway in breast cancer. *The Breast, 37*, 126-133. doi:10.1016/j.breast.2017.10.014

Pottier, C., Fresnais, M., Gilon, M., Jérusalem, G., Longuespée, R., & Sounni, N. E. (2020). Tyrosine Kinase Inhibitors in Cancer: Breakthrough and Challenges of Targeted Therapy. *Cancers, 12*(3), 731. doi:10.3390/cancers12030731

Presta, M., Chiodelli, P., Giacomini, A., Rusnati, M., & Ronca, R. (2017). Fibroblast growth factors (FGFs) in cancer: FGF traps as a new therapeutic approach. *Pharmacol Ther, 179*, 171-187. doi:10.1016/j.pharmthera.2017.05.013

Qian, B.-Z., Zhang, H., Li, J., He, T., Yeo, E.-J., Soong, D. Y. H., . . . Pollard, J. W. (2015). FLT1 signaling in metastasis-associated macrophages activates an inflammatory signature that promotes breast cancer metastasis. *Journal of Experimental Medicine, 212*(9), 1433-1448. doi:10.1084/jem.20141555

Raina, K., Lu, J., Qian, Y., Altieri, M., Gordon, D., Rossi, A. M. K., . . . Coleman, K. G. (2016). PROTAC-induced BET protein degradation as a therapy for castration-resistant prostate cancer. *Proceedings of the National Academy of Sciences, 113*(26), 7124-7129. doi:10.1073/pnas.1521738113

Rao, S. S., Kondapaneni, R. V., & Narkhede, A. A. (2019). Bioengineered models to study tumor dormancy. *Journal of Biological Engineering, 13*(1). doi:10.1186/s13036-018-0137-0

Razavi, P., Chang, M. T., Xu, G., Bandlamudi, C., Ross, D. S., Vasan, N., . . . Baselga, J. (2018). The Genomic Landscape of Endocrine-Resistant Advanced Breast Cancers. *Cancer Cell, 34*(3), 427-438 e426. doi:10.1016/j.ccell.2018.08.008

Redig, A. J., & McAllister, S. S. (2013). Breast cancer as a systemic disease: a view of metastasis. *J Intern Med, 274*(2), 113-126. doi:10.1111/joim.12084

Reymond, N., D'Água, B. B., & Ridley, A. J. (2013). Crossing the endothelial barrier during metastasis. *Nature Reviews Cancer, 13*(12), 858-870. doi:10.1038/nrc3628

Ruggiero, E., & Richter, S. N. (2018). G-quadruplexes and G-quadruplex ligands: targets and tools in antiviral therapy. *Nucleic Acids Research, 46*(7), 3270-3283. doi:10.1093/nar/gky187

Russnes, H. G., Lingjærde, O. C., Børresen-Dale, A.-L., & Caldas, C. (2017). Breast Cancer Molecular Stratification. *The American Journal of Pathology, 187*(10), 2152-2162. doi:10.1016/j.ajpath.2017.04.022

Santolla, M. F., & Maggiolini, M. (2020). The FGF/FGFR System in Breast Cancer: Oncogenic Features and Therapeutic Perspectives. *Cancers, 12*(10), 3029. doi:10.3390/cancers12103029

Santolla, M. F., Vivacqua, A., Lappano, R., Rigiracciolo, D. C., Cirillo, F., Galli, G. R., . . . Maggiolini, M. (2019). GPER Mediates a Feedforward FGF2/FGFR1 Paracrine Activation Coupling CAFs to Cancer Cells Toward Breast Tumor Progression. *Cells, 8*(3), 223. doi:10.3390/cells8030223

Sen, D., & Gilbert, W. (1988). Formation of parallel four-stranded complexes by guanine-rich motifs in DNA and its implications for meiosis. *Nature, 334*(6180), 364-366. doi:10.1038/334364a0

Sen, D., & Gilbert, W. (1990). A sodium-potassium switch in the formation of four-stranded G4-DNA. *Nature, 344*(6265), 410-414. doi:10.1038/344410a0

Servetto, A., Kollipara, R., Formisano, L., Lin, C.-C., Lee, K.-M., Sudhan, D. R., . . . Arteaga, C. L. (2021). Nuclear FGFR1 Regulates Gene Transcription and Promotes Antiestrogen Resistance in ER+ Breast Cancer. *Clinical Cancer Research, 27*(15), 4379-4396. doi:10.1158/1078-0432.ccr-20-3905

Sharma, S. V., Lee, D. Y., Li, B., Quinlan, M. P., Takahashi, F., Maheswaran, S., . . . Settleman, J. (2010). A Chromatin-Mediated Reversible Drug-Tolerant State in Cancer Cell Subpopulations. *Cell, 141*(1), 69-80. doi:10.1016/j.cell.2010.02.027

Shinde, A., Libring, S., Alpsoy, A., Abdullah, A., Schaber, J. A., Solorio, L., & Wendt, M. K. (2018). Autocrine Fibronectin Inhibits Breast Cancer Metastasis. *Molecular Cancer Research, 16*(10), 1579-1589. doi:10.1158/1541-7786.mcr-18-0151

Siddiqui-Jain, A., Grand, C. L., Bearss, D. J., & Hurley, L. H. (2002). Direct evidence for a G-quadruplex in a promoter region and its targeting with a small molecule to repress c-MYC transcription. *Proceedings of the National Academy of Sciences, 99*(18), 11593-11598. doi:10.1073/pnas.182256799

Singh, A., & Settleman, J. (2010). EMT, cancer stem cells and drug resistance: an emerging axis of evil in the war on cancer. *Oncogene, 29*(34), 4741-4751. doi:10.1038/onc.2010.215

Singh, J., Petter, R. C., Baillie, T. A., & Whitty, A. (2011). The resurgence of covalent drugs. *Nature Reviews Drug Discovery, 10*(4), 307-317. doi:10.1038/nrd3410

Smith, B. E., Wang, S. L., Jaime-Figueroa, S., Harbin, A., Wang, J., Hamman, B. D., & Crews, C. M. (2019). Differential PROTAC substrate specificity dictated by orientation of recruited E3 ligase. *Nature Communications, 10*(1). doi:10.1038/s41467-018-08027-7

Sobhani, N., Fan, C., O. Flores-Villanueva, P., Generali, D., & Li, Y. (2020). The Fibroblast Growth Factor Receptors in Breast Cancer: from Oncogenesis to Better Treatments. *International Journal of Molecular Sciences, 21*(6), 2011. doi:10.3390/ijms21062011

Song, J., Perreault, J.-P., Topisirovic, I., & Richard, S. (2016). RNA G-quadruplexes and their potential regulatory roles in translation. *Translation, 4*(2), e1244031. doi:10.1080/21690731.2016.1244031

Stemmler, M. P., Eccles, R. L., Brabletz, S., & Brabletz, T. (2019). Non-redundant functions of EMT transcription factors. *Nature Cell Biology, 21*(1), 102-112. doi:10.1038/s41556-018-0196-y

Sung, H., Ferlay, J., Siegel, R. L., Laversanne, M., Soerjomataram, I., Jemal, A., & Bray, F. (2021). Global Cancer Statistics 2020: GLOBOCAN Estimates of Incidence and Mortality Worldwide for 36 Cancers in 185 Countries. *CA: A Cancer Journal for Clinicians, 71*(3), 209-249. doi:10.3322/caac.21660

Tan, L., Wang, J., Tanizaki, J., Huang, Z., Aref, A. R., Rusan, M., . . . Gray, N. S. (2014). Development of covalent inhibitors that can overcome resistance to first-generation FGFR kinase inhibitors. *Proceedings of the National Academy of Sciences, 111*(45), E4869-E4877. doi:10.1073/pnas.1403438111

Templeton, A. J., Diez-Gonzalez, L., Ace, O., Vera-Badillo, F., Šeruga, B., Jordán, J., . . . Ocaña, A. (2014). Prognostic relevance of receptor tyrosine kinase expression in breast cancer: A meta-analysis. *Cancer Treatment Reviews, 40*(9), 1048-1055. doi:10.1016/j.ctrv.2014.08.003

Todd, A. K. (2005). Highly prevalent putative quadruplex sequence motifs in human DNA. *Nucleic Acids Research, 33*(9), 2901-2907. doi:10.1093/nar/gki553

Touat, M., Ileana, E., Postel-Vinay, S., André, F., & Soria, J.-C. (2015). Targeting FGFR Signaling in Cancer. *Clinical Cancer Research, 21*(12), 2684-2694. doi:10.1158/1078-0432.ccr-14-2329

Turner, N., Pearson, A., Sharpe, R., Lambros, M., Geyer, F., Lopez-Garcia, M. A., . . . Ashworth, A. (2010). FGFR1 Amplification Drives Endocrine Therapy Resistance and Is a Therapeutic Target in Breast Cancer. *Cancer Research, 70*(5), 2085-2094. doi:10.1158/0008-5472.can-09-3746

Valastyan, S., & Robert. (2011). Tumor Metastasis: Molecular Insights and Evolving Paradigms. *Cell, 147*(2), 275-292. doi:10.1016/j.cell.2011.09.024

Valton, A. L., & Prioleau, M. N. (2016). G-Quadruplexes in DNA Replication: A Problem or a Necessity? *Trends Genet, 32*(11), 697-706. doi:10.1016/j.tig.2016.09.004

Wainberg, Z. A., Enzinger, P. C., Kang, Y.-K., Yamaguchi, K., Qin, S., Lee, K.-W., . . . Catenacci, D. V. T. (2021). Randomized double-blind placebo-controlled phase 2 study of bemarituzumab combined with modified FOLFOX6 (mFOLFOX6) in first-line (1L) treatment of advanced gastric/gastroesophageal junction adenocarcinoma (FIGHT). *Journal of Clinical Oncology, 39*(3_suppl), 160-160. doi:10.1200/JCO.2021.39.3_suppl.160

Wang, K.-B., Elsayed, M. S. A., Wu, G., Deng, N., Cushman, M., & Yang, D. (2019). Indenoisoquinoline Topoisomerase Inhibitors Strongly Bind and Stabilize theMYCPromoter G-Quadruplex and DownregulateMYC. *Journal of the American Chemical Society, 141*(28), 11059-11070. doi:10.1021/jacs.9b02679

Wang, W., Meng, Y., Dong, B., Dong, J., Ittmann, M. M., Creighton, C. J., . . . Yang, F. (2017). A Versatile Tumor Gene Deletion System Reveals a Crucial Role for FGFR1 in Breast Cancer Metastasis. *Neoplasia, 19*(5), 421-428. doi:10.1016/j.neo.2017.03.003

Wang, Y., Yang, J., Wild, A. T., Wu, W. H., Shah, R., Danussi, C., . . . Huse, J. T. (2019). G-quadruplex DNA drives genomic instability and represents a targetable molecular abnormality in ATRX-deficient malignant glioma. *Nature Communications, 10*(1). doi:10.1038/s41467-019-08905-8

Wendt, M. K., Allington, T. M., & Schiemann, W. P. (2009). Mechanisms of the epithelial–mesenchymal transition by TGF-β. *Future Oncology, 5*(8), 1145-1168. doi:10.2217/fon.09.90

Wendt, M. K., Taylor, M. A., Schiemann, B. J., & Schiemann, W. P. (2011). Down-regulation of epithelial cadherin is required to initiate metastatic outgrowth of breast cancer. *22*(14), 2423-2435. doi:10.1091/mbc.e11-04-0306

Wendt, M. K., Taylor, M. A., Schiemann, B. J., Sossey-Alaoui, K., & Schiemann, W. P. (2014). Fibroblast growth factor receptor splice variants are stable markers of oncogenic transforming growth factor β1 signaling in metastatic breast cancers. *Breast Cancer Research, 16*(2), R24. doi:10.1186/bcr3623

Wise, R., & Zolkiewska, A. (2017). Metalloprotease-dependent activation of EGFR modulates CD44+/CD24− populations in triple negative breast cancer cells through the MEK/ERK pathway. *Breast Cancer Research and Treatment, 166*(2), 421-433. doi:10.1007/s10549-017-4440-0

Xie, Y., Su, N., Yang, J., Tan, Q., Huang, S., Jin, M., . . . Chen, L. (2020). FGF/FGFR signaling in health and disease. *Signal Transduction and Targeted Therapy, 5*(1). doi:10.1038/s41392-020-00222-7

Xu, H., Di Antonio, M., McKinney, S., Mathew, V., Ho, B., O'Neil, N. J., . . . Aparicio, S. (2017). CX-5461 is a DNA G-quadruplex stabilizer with selective lethality in BRCA1/2 deficient tumours. *Nature Communications, 8*(1), 14432. doi:10.1038/ncomms14432

Ye, T., Wei, X., Yin, T., Xia, Y., Li, D., Shao, B., . . . Wei, Y. (2014). Inhibition of FGFR signaling by PD173074 improves antitumor immunity and impairs breast cancer metastasis. *Breast Cancer Research and Treatment, 143*(3), 435-446. doi:10.1007/s10549-013-2829-y

Ye, X., & Weinberg, R. A. (2015). Epithelial–Mesenchymal Plasticity: A Central Regulator of Cancer Progression. *Trends in Cell Biology, 25*(11), 675-686. doi:10.1016/j.tcb.2015.07.012

Yue, S., Li, Y., Chen, X., Wang, J., Li, M., Chen, Y., & Wu, D. (2021). FGFR-TKI resistance in cancer: current status and perspectives. *Journal of Hematology & Oncology, 14*(1). doi:10.1186/s13045-021-01040-2

Zhao, M., Zhuo, M. L., Zheng, X., Su, X., & Meric-Bernstam, F. (2019). FGFR1beta is a driver isoform of FGFR1 alternative splicing in breast cancer cells. *Oncotarget, 10*(1), 30-44. doi:10.18632/oncotarget.26530

Zhou, W., Hur, W., McDermott, U., Dutt, A., Xian, W., Ficarro, S. B., . . . Gray, N. S. (2010). A Structure-Guided Approach to Creating Covalent FGFR Inhibitors. *Chemistry & Biology, 17*(3), 285-295. doi:10.1016/j.chembiol.2010.02.007

Zhou, Y., Wu, C., Lu, G., Hu, Z., Chen, Q., & Du, X. (2020). FGF/FGFR signaling pathway involved resistance in various cancer types. *Journal of Cancer, 11*(8), 2000-2007. doi:10.7150/jca.40531